Channel flow of electrorheological fluids under an inhomogeneous electric field

Vom Fachbereich Mechanik
der Technischen Universität Darmstadt
zur Erlangung des akademischen Grades eines
Doktors der Naturwissenschaften (Dr. rer. nat.)
genehmigte Dissertation

vorgelgt von

Ana Ursescu, M. Sc.

aus Câmpina, Romania

Referent:	Prof. K. Hutter, Ph.D.
Korreferent:	Prof. Dr. M. Růžička
Tag der Einreichung:	16. September 2004
Tag der mündlichen Prüfung:	21. Januar 2005

D 17

Aknowledgments

This work was done during my stay at the Institute of Mechanics of the Darmstadt University of Technology within the framework of the Graduiertenkolleg "Modelling and Numerical Description of Technical Flows" with the financial support of DFG.

I express my sincere gratitude to my supervisor, Professor Kolumban Hutter, for his instructive guidance, for his generous advice, for his constant encouragement and his continuous care to provide me everything I need for my research work, especially for the financial support for conferences and graduate schools and also for his prompt effort and his precious time spent to correct my manuscripts. Thank you for the fresh spirit which made the work at the University to be sunny.

I would like to thank my co-referee, Professor Michael Růžička for his interest in my work, for his kind invitation at his department for discussing the modeling of the ER-fluids under inhomogeneous electric fields. I gained a lot of insight from these meetings. I am grateful to him for accepting to be co-referee and for the effort to come in Darmstadt for my examination.

I am very much thankful to Dr. Winfried Eckart for initiating me in the domain of electrorheological fluids, for introducing me in this fascinating subject and for helpful discussions and suggestions during my study. He offered me valuable support to find a flat and to go through all the formalities at the beginning of my stay in Darmstadt.

I am grateful to Dr. Hubert Marschall for fruitful discussions concerning the analytical solution of the electrical problem, for helping me to get rid of the difficulties I encountered in applying the Wiener-Hopf technique and for providing me access to a Femlab license.

The author is indebted also to Prof. Dr. J. Boersma from Eindhoven University of Technology (The Netherlands) for his careful examination and constructive criticism as a referee of a paper containing an earlier version of the actual Chapter 3 which have resulted in the removal of several inaccuracies.

Special thanks go to my colleagues: Dr. Bernd Muegge, Dr. Shiva Prasad Pudasaini, Dr. Angelika Humbert, Mahmoud Reza Maneshkarimi, Dr. Sergio Faria, Dr. Nina Kirchner, Dr. Harald Ehrentraut, Dr. Ralf Greve, Dr. Yongqi Wang, Dr. Agnieszka Chrzanowska, Niklas Mellgren, Timo Schary, Dr. Vasily Vlasenko and the whole AG3 for their constant help. I will always remember the stimulating working atmosphere from our group and the nice time spent together.

I want to thank further Dr. Steffen Eckert and his colleagues from AG4 for answering my questions about Matlab and related stuff, Dr. Magnus Weiss and Dr. Thomas

Zwinger for providing me useful references about Finite Element Method. I express my appreciation to Dr. Thomas Wunderlich for providing me his doctoral work.

Thanks are due also to Professor Corneliu Balan for sharing me his experience as a former PhD student in the same department, for teaching me important notions of rheology and giving me the opportunity to visit a laboratory of rheology and to see interesting experiments, for his instructive guidance during the European Rheology Conferences I attended twice and for the useful advice he gave me during my stay here in Darmstadt.

I am grateful to my friend, Dr. Agnieszka Swierczewska for her constant help, especially in understanding some matters of not standard mathematics and to her colleagues from the Mathematics Department, AG6, Dr. Andreas Frohlich, Dr. Piotr Gwiazda and Dr. Stefan Ebenfeld for the fruitful discussions we had about the formulation of the electrical problem.

I must thank Dr. Amsini Sadiki for his interest in my work and for valuable discussions.

Special thanks go to Professor Paul Flondor and Dr. Laurentiu Leustean for contributing to the demonstration from Appendix C.2.

I gratefully appreciate the help gained in numerous discussions from Dr. Ioana Luca, guest scientist in our group.

Besides, I would like to thank the people who taught me and encouraged me before I started the doctoral work: Dr. Victor Tigoiu, Professor Cristian Dascalu and all my colleagues from the Applied Mathematical Institute from Bucharest. Special thanks go to the directorate of the institute who allowed me to interrupt my research activity there and to accomplish these doctoral studies.

I am extremely grateful to my husband Daniel for his support, but also for helpful discussions and suggestions. Further I want to thank my two mothers (who left their duties in Romania in order to come here and take care of their granddaughter) and my whole family for helping me in my efforts to finish the thesis and for their encouragement.

Abstract

This thesis is a theoretical study of the steady pressure driven channel flow of electrorheological fluids (ERF) under a space dependent electric field generated by finite electrodes.

Chapter 1 consists in a general description of ERF and their engineering applications and presents also the motivation, the goal and the borders of this work.

Chapter 2 summarizes the governing equations of electrorheology (based on the phenomenological approach presented in [28, 29] with the corresponding jump conditions. It is assumed that the flow does not affect the electric field and consequently, the electrical problem is decoupled from the mechanical one. Both electrical and mechanical boundary value problems are formulated for various configurations of finite electrodes with different potentials placed along the channel walls. The simple case of two infinite electrodes which generate a homogeneous electric field is solved analytically.

In Chapter 3 analytical solutions for different mixed boundary value problems arising from the electrical problem formulated in Chapter 2 are found by use of the Wiener-Hopf method. The solutions are given in terms of infinite series involving Gamma functions. The results can be used to describe the electric field generated between two infinite grounded electrodes by either one long electrode or two long electrodes charged in an anti-symmetric or a non-symmetric way. The electric field in the vicinity of the electrode edges is asymptotically evaluated. Some parametric studies are made with respect to the ratio between the permittivity of the electrorheological fluid and the permittivity of the isolating material outside the channel. We compare the analytical with numerical solutions and find good agreement which is considered as a validation of the numerical method.

Chapter 4 treats the mechanical problem in more detail. First a review of the constitutive models used to describe the ER fluids in the literature is given. Then two-dimensional alternative constitutive laws appropriate for numerical simulations originating from the Casson-like and power law models are introduced using a parameter δ. In the end we non-dimensionalize the problem in both cases.

In the last Chapter, we simulate numerically the flow of the Rheobay TP AI 3565 ER-fluid using the alternative Casson-like model and the EPS 3301 ER-fluid using the alternative power-law model by applying a finite element program. The behaviour of different fields such as velocity, pressure, generalized viscosity and the second invariant of the strain rate tensor near the electrode edges is studied for both fluids. A comparison with the experimental data is performed, validating the simulations. In order to investigate how

the numerical solution depends on the constitutive model we perform a parallel analysis of the two rheological models by applying them to the same material (Rheobay). Then we optimize the configuration of the electrodes by using the inhomogeneities caused by the end effects of the electrodes in order to obtain an enhancement of the ER-effect.

Zusammenfassung

Diese Arbeit ist eine theoretische Studie einer durch stationären Druck angetriebenen ebenen Poiseuille Strömung von elektrorheologischen Flüssigkeiten (ERF) zwischen zwei parallelen Platten in einem räumlich variablen elektrischen Feld, das durch endliche Elektroden generiert wird.

Kapitel 1 besteht aus einer generellen Beschreibung von ERFs und ihren technischen Anwendungen und präsentiert die Motivation, das Ziel und die Grenzen dieser Arbeit.

Kapitel 2 fasst die grundlegenden Gleichungen der Elektrorheologie (basierend auf phänomenologischen Ansätzen, die in [28, 29] präsentiert wurden mit den dazugehörenden Sprungbedingungen) zusammen. Es wurde angenommen, dass die Strömung nicht das elektrische Feld beeinflusst und folglich das elektrische Problem vom mechanischen Problem entkoppelt ist. Beide, elektrische und mechanische Randwertprobleme, sind in verschiedenen Konfigurationen von endlichen Elektroden mit unterschiedlichen Potentialen entlang der Kanalwände formuliert. Der einfache Fall von zwei unendlichen Elektroden, die ein homogenes elektrisches Feld generieren, ist analytisch gelöst.

In Kapitel 3 wurden analytische Lösungen für unterschiedliche gemischte Randwertprobleme, die durch das in Kapitel 2 formulierte elektrische Problem auftreten, durch die Anwendung der Wiener-Hopf Methode gefunden. Die Lösung wurde mittels unendlicher Reihen, die Gamma-Funktionen beinhalten, gegeben. Die Ergebnisse können dazu verwendet werden, elektrische Felder, die zwischen zwei endlichen, geerdeten Elektroden, sowohl durch eine lange, als auch zwei kurze geladene antisymmetrische oder nicht-symmetrische Elektroden erzeugt wurden, zu beschreiben. Das elektrische Feld in der Nähe der Elektrodenenden wurde asymptotisch ausgewertet. Einige Parameterstudien hinsichtlich des Verhältnisses der Permittivität der elektrorheologischen Flüssigkeiten und der Permittivität des Isoliermaterials ausserhalb des Kanals wurden durchgeführt. Wir vergleichen die analytischen und numerischen Simulationen und finden gute Übereinstimmungen, was wir als Validierung der numerischen Methode ansehen.

Kapitel 4 beschreibt das mechanische Problem detaillierter. Zuerst wird ein Überblick über die konstitutiven Modelle, die ER Flüssigkeiten beschreiben, gegeben. Danach werden zweidimensionale alternative konstitutive Gesetze unter der Benutzung des Parameters δ eingeführt, die für numerische Simulationen, die durch Casson-artige und Potenzgesetze entstehen, geeignet sind. Zum Schluss entdimensionalisieren wir das Problem für beide Fälle.

Im letzten Kapitel simulieren wir numerisch den Fluss der Rheobay TP AI 3565

ER-Flüssigkeit mittels des alternativen Casson-artigen Modells und der EPS 3301 ER-Flüssigkeit mittels des Potenzgesetzes, unter Anwendung eines Finite-Elemente Programms. Das Verhalten der verschiedenen Felder, wie die Geschwindigkeit, der Druck, die generalisierte Viskosität und die zweite Invariante des Verzerrungsratentensors nahe den Elektrodenenden wurde für beide Flüssigkeiten studiert. Ein Vergleich mit experimentellen Daten wurde durchgeführt, der die Simulationen validiert. Für die Untersuchung der Abhängigkeit der numerische Lösung vom konstitutiven Modell, führen wir zwei parallele Analysen zweier rheologischer Modelle durch und wenden sie auf das gleiche Material an (Rheobay). Dann optimieren wir die Konfiguration der Elektroden unter Benutzung der Inhomogenitäten, die durch die Effekte der Elektrodenenden verursacht wurden, mit dem Ziel einer Verstärkung des ER-Effekts.

Contents

Chapter 1

Introduction

1.1 Electrorheological fluids

"Smart" materials can adaptively change or respond to an external stimulus producing a useful effect. Mechanical stresses, temperature, an electric or magnetic field, photon radiation or chemicals are typical examples of stimuli. A useful effect usually means a dramatic change of either one physical property (mechanical, electrical, appearance), the structure or the composition, which can be monitored and used in certain applications. A useful effect may be completely reversed when the stimulus is removed and this important feature permits an easy control through simply changing the environmental conditions. A variety of smart materials exist, and are being researched extensively. These include piezoelectric and thermoelectric materials, magnetorheological and electrorheological fluids, photochromic and thermochromic materials, electroluminiscent, fluorescent and phosphorescent materials and shape memory alloys.

Electrorheological fluids (often abbreviated as ERF) are such intelligent materials which exhibit drastic changes in their rheological properties upon the application of an outer electric field on the order of 1 kV/mm. The ER phenomenon is characterized by full reversibility and a very fast response (often quoted in milliseconds). Upon removal of the field, the corresponding relaxation time is of a comparable scale. The term ER-effect refers to the abrupt change in the apparent viscosity. When the viscosity increases we deal with a positive ER-effect while a decrease in viscosity is called negative ER-effect ([34], [76]). Both the positive and negative ER effect can be enhanced by ultraviolet illumination in some ER systems ([35]). This phenomenon is called the photo-electrorheological (PER) effect.

Most of ERFs are dispersions of polarizable small particles within a non-conducting carrier liquid. The typical range size of the particles entering the structure of an ER-fluid is on the order of 0.10 to 100 μm while the particle volume fraction ranges between 2%-50%. Particles with dimensions below the stated range are liable to execute Brownian motion while larger particles are more liable to sedimentation and also to draw excessive currents. A wide variety of particulate media have been employed in ER suspensions

starting from starch, flour, cellulose, ceramic, glass to complex particles such as polyelectrolytes, composite particles (conducting particles coated with a thin non-conducting outer layer, doubly coated particles with dielectric cores of high strength and lower mass (see [83]). The impact of the particle shape on ER performance was recently investigated experimentally in [63] by using microspheres and micro-rods as the component of the solid phase of an ER fluid. The dispersing phase of an ER fluid is an insulating oil or other non-conductive liquid. Currently silicone oil, vegetable oil, mineral oil, paraffin etc. are used. Besides the suspended particles and the carrier fluid, an ER fluid contains also some additives which could be any polar material that can enhance the ER effect or the stability of the whole suspension. ER fluids that contain a small amount of water are normally called hydrous, in contrast to water-free or anhydrous ER fluids in which no detectable water residue exists. It was demonstrated that the addition of water can enhance the ER-effect. Moreover, the influence of water in connecting together the particles has been used as the basis of a theory to explain the ER mechanism (the water bridging mechanism). However, a big disadvantage of the ER-fluids with moisture content is the limited range of operating temperatures by the freezing and boiling points of water. Fortunately, it was shown that the operating mechanism does not depend on the presence of water and recently, considerable emphasis has been placed on the development of anhydrous particle suspensions. Extensive reviews centred on the material science aspects of ERFs are available [14, 35] and much work continues to be done in order to find optimal combination of material properties (see e.g. [67, 83, 95]).

The explanation for the ER effect can be given with the aid of experimental observations at the microscopic level. Under the influence of an external electric field, the initially unordered particles get oriented and attract each other to form particle chains in the fluid along the field lines. The chains then aggregate to form columns. These chain-like and columnar structures cause significant changes in the resistance to the flow, and the material switches in this way from the liquid state to a solid-like state. In 1949, Winslow [90] reported the ER-effect for certain suspensions and described for the first time the phenomenon of induced fibration even though earlier observations on electroviscous effects were reported since 1896 (reviewed in [46]). The basic mechanism for this behaviour is thought to be the field induced particle polarization which is a consequence of the dielectric mismatch between particles and solvent. It should be pointed out that other mechanisms for the field induced increase in viscosity have been suggested including overlap of the diffuse counter-ion clouds surrounding neighboring particles [46, 47], electrostatic torque preventing particle rotation in the flow field [14], inter-electrode circulation [24] and field induced aggregation due to water bridges between particles [73, 80, 81, 84]. A lot of research has been done to develop theoretical models describing these mechanisms and relating the material properties and microscopic phenomena to the measurable macroscopic properties. Most theories are based on the electrostatic polarization mechanism. For an overview of the fundamental physical mechanisms and strategies in relating the microstructural models to the rheological behaviour we refer the reader to the review papers summarizing the main results in this domain [59, 74].

Besides the particulate ER suspensions (heterogeneous ERF), there have been developments of homogeneous physical systems which also show dramatic changes in rheological properties upon application of an external electric field. Oil-in-oil emulsions and liquid-crystal polymer/oil immiscible systems display a relatively strong ER-effect [42, 44, 45, 69, 85, 94]. This is explained by the increase of domain interactions due to the orientation of elongated molecules. In [27, 56, 57] it is shown that also simple dielectric liquids (insulating oils) the viscosity of which hardly changes in uniform fields can be ER-active when subjected to non-uniform electric fields (the ER effect is attributed to the electrohydrodynamic convection enhanced by the use of electrodes with flocked fabrics). At last we can mention the delicious study of the milk chocolate which also displays an ER behaviour [23].

ERFs can be modeled in several different ways. The ERFs may be analysed by means of molecular dynamic simulations by using different models (such as the dipole model, conduction model, equivalent plate conduction model) to establish the equation of the motion of particles. ([96], [97]). Another possibility consists in the investigation of their microstructure in order to obtain a macroscopic description of the material [37, 60, 69, 75, 87, 88].

A different approach is pursued in the context of continuum mechanics. There are descriptions of ERFs as mixtures of two constituents (the particulate medium and the fluid) [65]. However many researchers adopted the approach in which the ER fluids are treated in a homogenized sense [9, 10, 31, 64, 72] etc. Rajagopal and Růžička in [66] and W. Eckart in [28] formulated independently governing equations of ER fluids. These formulations have the advantage that they take into account the interactions between the electro-magnetic and the mechanical fields. After assuming the constitutive law characterizing a certain fluid (see Chapter 4 of the present thesis) this approach permits mathematical modeling of the ER behaviour [17, 25, 70]. In our study we also assume ER-fluids to be homogeneous and continuous liquids and we apply a phenomenological modeling in order to predict their macroscopic behaviour.

Recently, continuum models which try to reflect (at the macroscopic level) field induced effects of the ERFs' microstructure and mesostructure were developed. In [26] a thermodynamical continuum modeling is pursued and the influence of the field generated microstructure is described with the aid of an internal variable theory. We mention the works of Brunn and Abu-Jdayil [15, 16] who carried out a phenomenological study by considering ERF as fluids with transverse isotropy. This assumption is based on the experimental observations according to which fibers are formed upon the application of an electric field. In their approach the extra stress tensor of an ERF depends on the strain rate but also on a vector which characterizes the orientation and size of the field induced fibers. In this way it is possible to describe normal stress effects appearing in viscometric flows. In [30] Eckart and Sadiki applied the polar theory to electrorheological fluids in the context of extended thermodynamics. They succeeded to obtain a model which accounts for different material responses, if the applied electric field (assumed to be constant) is either perpendicular or parallel to the flow direction. This fact was expected but the

previous models were not capable to reflect it.

ER-fluids are potentially useful in numerous technical applications. Many of them belong to the automotive industry: shock absorbers, clutches, valves, brakes, dampers, actuators [18, 77]. A good review of the engineering application of ERFs' in vibration control can be found in [82]. Non-conventional and advanced actuators may be built using ERFs [32, 50]. Another technological area in which ER fluids offer large promises is virtual reality and telepresence enhanced with haptic (tactile and force) feedback systems [48, 49, 61]. A haptic feedback is a modality for interacting with remote and virtual worlds compared with visual and auditory feedback. ER fluids can be used as smart inks, or to produce photonic crystals or in the polishing industry [35].

Despite the rich research literature about ERFs and the gained progress in this subject, the application in real-life problems and commercialization of devices based on ERFs have been very limited. The need for high voltage creates safety problems for the operators especially for the devices that are designed to be in contact with humans. Besides the problem of their feedback (closed-loop) is difficult to solve because of their complex behaviour. Other obstacles in the development of ERF technologies are related to the composition of the ER fluids (e.g. the instabilities caused by the sedimentation tendency of the particles or the limited range of operational temperature). Nevertheless, recent advanced studies led to significant improvements in the fluid formulation.

It can be foreseen that the big interest concerning these materials and the multitude of research studies focused on their potential applications will finally improve the capabilities of ER fluids on the one hand and lead to an optimal design for the ER devices on the other hand.

1.2 Motivation and goal

As we mentioned above, an impediment to overcome and make an industrial exploitation of ER-effect on a large scale possible is the very high voltage requirements necessary to obtain the desired increase in viscosity. There are attempts to increase the electrorheological effect by modifying either the surface or the shape and position of the electrodes relative to the flow geometry in such a way that inhomogeneities in the electric field are introduced [2]–[7], [15, 33, 43, 51, 55, 92, 93]. All these experimental investigations demonstrated that application of non-uniform electric fields may lead to more efficient effects on the flow (than with homogeneous electric fields).

The necessity of models which reproduce the ER behaviour for varying electric fields was formulated in the application area [18, 48] for an accurate description of the experiments performed in order to improve the performance of ER devices. Nevertheless, in most theoretical approaches of ERF flows the electric field is only a constant parameter. In channel flow this is an analytical consequence of the fact that the electrodes are considered to be infinite while in cylindrical configurations this is an assumption that can be made when the fluid channel is small compared with the radius of the inner cylinder. Exceptions are the theoretical results for a radial configuration obtained by Atkin et al.

[9, 10] where the electric field is slightly inhomogeneous in the radial direction. Rajagopal and Růžička in [66] and Eckart in [28] developed a theoretical framework which allows for variable field strength in which the electric field has to be determined from the Maxwell equations.

In general, the working behaviour of devices using ER fluids is classified in three fundamental modes: shear, flow and squeeze [82]. In the flow mode, which is called also Poiseuille flow (the flow occurs under the effect of the axial pressure), it is assumed that the two electrodes are fixed. The present work is focused on a special case of the flow mode, the steady pressure-driven channel flow of electrorheological fluids under an inhomogeneous electric field produced by finite electrodes. A number of ER equipment including valves, dampers and actuators is based on this configuration. Our approach is formulated within the framework of continuum mechanics and the electrorheological fluids are considered here to be homogeneous single constituent materials.

The aim of this study is twofold. On the one hand, we consider it important to give a more realistic modeling by taking into account the inhomogeneity effects which appear in the vicinity of the electrode edges. To our present knowledge these were not yet modeled. Comparing this with the case of plane shear flow subject to infinite electrodes, where the electric field is simply a constant, here the non-uniform electric field will cause inhomogeneities in the flow too which will be non-viscometric. Consequently, we will have two components of the velocity depending on both coordinates. On the other hand, our intention is to examine numerically how the ER-effect can be enhanced by a space-dependent electric field.

The inhomogeneities of the electric field are introduced here by changing the boundary conditions namely by arranging the electrodes in several different ways. The configuration geometry remains unchanged. However, thanks to its generality, the formulation of the problem permits its application and numerical implementation also for modified geometries of the channel (e.g. with oblique electrodes, grooved electrodes or with electrodes separated by a gap smaller/larger than the channel height), by simply adapting the respective boundary conditions.

1.3 Borders of the present study

For analyzing the reality, any theory makes use of two procedures: idealization and simplification. Idealization consists in a careful but also convenient approximation of the real situation which allows its modeling. Eliminating step by step different idealizations one gets more and more accurate descriptions of the real phenomena. Simplification means to take into account some simpler cases which can be employed further as bricks to build more sophisticated systems.

In the present work we also apply a couple of idealizations and simplifications. One main assumption in our macroscopic approach is that the flow does not affect the electric field. We made a further idealization by considering isothermal conditions. Moreover our model does not take into account the effect of the direction of the electric field. The

reason for doing this is the lack of quantitative experimental data which one needs to accurately model such effects. In the end we mention that we generate inhomogeneities in the electric field using electrodes of zero thickness in the numerical modeling. We proceed in this way since we calculated analytically this case and any numerical computation needs an analytical benchmark.

In order to suggest a possible extension of the study we precise also the simplifications adopted here. We focused on the modeling of the inhomogeneities of the electric field and of the end effects of the electrodes under steady state conditions and, consequently, only in stationary electric field. However, differences between measurements under alternating and direct currents were reported for the shear mode, flow mode and torsional flow [2]–[7]. To study the ERFs under alternating currents means to examine also the instationary case which leads to a very complicated and numerically challenging approach.

An important motivation of our study consists in the experimental work done in [4, 92]. The ER-fluids investigated in measurements are viscous. This is a reason why we did not take into account viscoelastic effects.

We mention finally that even if two-dimensional modeling gives a good qualitative and quantitative description of the ERF behaviour under inhomogeneous electric fields, it is nevertheless limited to simple geometrical configurations. Three-dimensional modeling (including radial geometries) has to be further performed in order to obtain also quantitative results for more sophisticated experimental set-ups than those in [4, 92].

Chapter 2

Formulation of the problem

We use in our work a continuum mechanical model in which ERFs are considered as homogeneous single constituent materials. Following [28] and [29] we will summarize in this Chapter the main steps of the phenomenological approach, conducted in order to obtain the governing equations of electrorheology with the corresponding jump conditions and the assumptions made for the decoupling of the electrical problem from the mechanical problem. Then, by using the general equations and jump conditions we will formulate that problem which corresponds to the geometry of the case we wish to study. In the end, the particular case of the flow under an uniform electric field produced by infinite electrodes is described.

2.1 Governing equations of electrorheology

The starting point in deriving the system of equations that characterize the electrorheological fluids consists in recording the balance laws of thermodynamics of fluids in electromagnetic fields (see [28, 38]). We will state them here in a local form and within an inertial frame. The balances of mass, momentum, moment of momentum, internal energy and entropy are

$$\frac{D\rho}{Dt} + \rho v_{j,j} = 0\,, \tag{2.1}$$

$$\rho\frac{Dv_i}{Dt} - \sigma^{me}_{ij,j} - f^{me}_i - f^{el}_i = 0_i\,, \tag{2.2}$$

$$\varepsilon_{ijk}\sigma^{me}_{kj} = 0_i\,, \tag{2.3}$$

$$\frac{D\epsilon}{Dt} + \epsilon v_{j,j} + q_{j,j} - \sigma^{me}_{ij}v_{i,j} - h^{me} - h^{el} = 0\,, \tag{2.4}$$

$$\frac{D\eta}{Dt} + \eta v_{j,j} + \phi_{j,j} - s_\eta \geq 0\,, \tag{2.5}$$

where ρ denotes the mass density, v_j the velocity, σ_{ij}^{me} the Cauchy stress tensor, f_i^{me} and f_i^{el} the non-electromagnetic and the electromagnetic force densities, respectively. Furthermore $\frac{D}{Dt}$ is the material derivative and ε_{ijk} denotes the permutation tensor

$$\varepsilon_{ijk} := \begin{cases} +1 & \text{if } i,j,k \text{ cyclic } 1,2,3\,, \\ -1 & \text{if } i,j,k \text{ cyclic } 1,3,2\,, \\ 0 & \text{otherwise}\,. \end{cases} \tag{2.6}$$

ϵ is the density of the internal energy, q_j the heat flux while h^{me} and h^{el} denote the non-electromagnetic and the electromagnetic energy supply densities, respectively. η is the entropy density, ϕ_j the entropy flux and s_η the entropy supply density. To complete the physical picture we have to add the conservation laws of charge and magnetic flux commonly known as Maxwell's equations. We give them here in the Maxwell-Minkowski formulation, namely

$$\varepsilon_{klm}\mathcal{E}_{m,l} = -\overset{*}{B}_k\,, \tag{2.7}$$

$$\varepsilon_{jlm}\mathcal{H}_{m,l} = \overset{*}{D}{}_k^e + \mathcal{J}_j\,, \tag{2.8}$$

$$D^e_{i,i} = \rho_{el}\,, \tag{2.9}$$

$$B_{i,i} = 0\,. \tag{2.10}$$

$\mathcal{E}_m$ denotes the effective electric field strength, B_k the magnetic flux density, $\mathcal{H}_m$ the effective magnetic field strength, D_j^e the electric displacement, $\mathcal{J}_j$ the conductive current density and ρ_{el} the density of the free electric charges. The effective electric and magnetic field strengths and the conductive current density are defined by

$$\mathcal{E}_m := E_m + \varepsilon_{mpq}v_pB_q\,, \tag{2.11}$$

$$\mathcal{H}_m := H_m - \varepsilon_{mpq}v_pD^e_q\,, \tag{2.12}$$

$$\mathcal{J}_j := J_i - \rho_{el}v_j\,, \tag{2.13}$$

where E_m denotes the electric field strength, while H_m is the magnetic field strength and J_j is the electric current density (or non-conductive current density). Introducing the electric polarization P_i and the magnetization M_i we have the relations

$$D^e_i := \varepsilon_0E_i + P_i\,, \quad D^e_i := \varepsilon_0(\mathcal{E}_m - \varepsilon_{ijk}v_jB_k) + P_i\,, \tag{2.14}$$

$$H_i := \mu_0^{-1}B_i - M_i\,, \quad \mathcal{H}_i := \mu_0^{-1}B_i - \varepsilon_0\varepsilon_{ijk}v_jE_k - \mathcal{M}_i\,, \tag{2.15}$$

where $\mathcal{M}_i$ denotes the effective magnetization

$$\mathcal{M}_i := M_i + \varepsilon_{ijk}v_jP_k\,, \tag{2.16}$$

and ε_0 and μ_0 are the dielectric constant in vacuo and the corresponding magnetic permeability, respectively

$$\varepsilon_0 = 8,85419\cdot 10^{-12}\frac{As}{Vm}\,, \quad \mu_0 = 4\pi\cdot 10^{-7}AsVm\,, \quad \text{with} \quad \varepsilon_0\mu_0 = c^{-2}\,. \tag{2.17}$$

c denotes the speed of electromagnetic waves in vacuo.

Further, we will eliminate the electromagnetic force and energy supply densities f^{el} and h^{el} from the general equations by using the fact that they must be consistent with the Maxwell equations. The procedure for finding these quantities consists in deriving two identities from (2.7) – (2.10) which might be interpreted as balances of electromagnetic momentum and of electromagnetic energy, respectively (see e.g. [38])

$$\frac{Dg_i^{el}}{Dt} + v_{l,l} g_i^{el} = \sigma_{ij,j}^{el} - f_i^{el} \,, \tag{2.18}$$

$$\frac{De^{el}}{Dt} + v_{l,l} e^{el} + (\varepsilon_{ijk} \mathcal{E}_j \mathcal{H}_k)_{,i} = \sigma_{ij}^{el} v_{i,j} - h^{el} \,. \tag{2.19}$$

In (2.18), g_i^{el}, σ_{ij}^{el} and f_i^{el} denote the density of electromagnetic momentum, the electromagnetic stress tensor and the electromagnetic force density, respectively, which are defined as

$$g_i^{el} := \varepsilon_0 \mu_0 \varepsilon_{ijk} \mathcal{E}_j \mathcal{H}_k \,, \tag{2.20}$$

$$\sigma_{ij}^{el} := \mathcal{E}_i D_j^e + \mathcal{H}_i B_j + \varepsilon_0 \mu_0 \varepsilon_{ilk} \mathcal{E}_l \mathcal{H}_k v_j \,, \tag{2.21}$$

$$f_i^{el} := \rho_{el} \mathcal{E}_i + \varepsilon_{ijk} \left(\overset{*}{D}{}_j^e + \mathcal{J}_j \right) B_k + D_j^e \mathcal{E}_{i,j} + B_k \mathcal{H}_{k,i} - \varepsilon_0 \mu_0 \frac{\partial (\varepsilon_{ijk} \mathcal{E}_j \mathcal{H}_k)}{\partial t} \,, \tag{2.22}$$

while in (2.19) e^{el} and h^{el} denote the electromagnetic energy density and the electromagnetic energy supply density, respectively, which are given as

$$e^{el} := \frac{1}{2} (D_j^e \mathcal{E}_j + B_j \mathcal{H}_j) \,, \tag{2.23}$$

$$\begin{aligned} h^{el} := {} & \mathcal{J}_j \mathcal{E}_j + \frac{1}{2} \left(\mathcal{E}_j \frac{D D_j^e}{Dt} - \frac{D \mathcal{E}_j}{Dt} D_j^e + \frac{D B_j}{Dt} \mathcal{H}_j - B_j \frac{D \mathcal{H}_j}{Dt} \right) \\ & + \varepsilon_0 \mu_0 \varepsilon_{imn} \mathcal{E}_m \mathcal{H}_n v_j v_{i,j} + \frac{1}{2} (\mathcal{E}_k D_k^e + \mathcal{H}_k B_k) v_{j,j} \,. \end{aligned} \tag{2.24}$$

Since equations (2.18)-(2.19) contain some relativistic contributions but equations (2.1)-(2.5) are valid only in the non-relativistic case, the relativistic terms should be removed. To this end, two important assumptions concerning magnetic quantities in electrorheological applications are made:

$$M_k = -\varepsilon_{kmn} v_m P_n \,, \tag{2.25}$$

$$B_i = B_i^{ind} + B_i^{ext} \,, \quad B_i^{ext} = 0 \,. \tag{2.26}$$

The first is called the dielectric assumption and it states that the fluid has no magnetic properties in the rest frame. It follows then that the effective magnetization (2.16) vanishes. In $(2.26)_1$ the magnetic flux density is split into the induced magnetic flux density

B_i^{ind}, which depends on the electric field and the external magnetic flux density B_i^{ext}, that does not depend on E_i. In $(2.26)_2$, it is assumed that in electrorheology there is only an electric field dependent part of the magnetic flux density and no external contribution to it. By dropping all the terms of relativistic order (to identify them we need to non-dimensionalize the equations , see [29] for details), (2.21), (2.22), (2.23) and (2.24) become

$$f_i^{el} = \sigma_{ij,j} = (E_i D_j^e)_{,j} \,, \tag{2.27}$$

$$e^{el} = \frac{1}{2} D_j^e E_j \,, \tag{2.28}$$

$$h^{el} = \mathcal{J}_j E_j - \frac{1}{2}\left(D_j^e \frac{DE_j}{Dt} - \frac{DD_j^e}{Dt} E_j \right) + \frac{1}{2} D_k^e E_k v_{j,j} \,. \tag{2.29}$$

We assume further that ERFs are electrically non-conducting fluids and that their charge density can be neglected. Therefore we set $\mathcal{J}_i = 0_i$ and $\rho_{el} = 0$. Consequently all terms containing the conductive current density and the electric charge density will be dropped from the governing equations and from all the derivations starting from them. Two new quantities are introduced: $\tilde{\epsilon}$, the modified internal energy density, and $\tilde{\Psi}$, the density of the free energy

$$\tilde{\epsilon} := \epsilon + e^{el} \,, \tag{2.30}$$

$$\tilde{\Psi} := \tilde{\epsilon} - \theta\eta - D_j^e E_j \,. \tag{2.31}$$

Due to the assumption (2.25) the following identifications are allowed (see [38])

$$\phi_j = \frac{q_j}{\theta} \,, \quad s_\eta = \frac{h^{el}}{\theta} \,. \tag{2.32}$$

The governing equations of electrorheology now take the forms

$$\frac{D\rho}{Dt} + \rho v_{j,j} = 0 \,, \tag{2.33}$$

$$\rho \frac{Dv_i}{Dt} - (\sigma_{ij}^{me} + E_i D_j^e)_{,j} - f_i^{me} = 0_i \,, \tag{2.34}$$

$$\varepsilon_{ijk} \sigma_{kj}^{me} = 0_i \,, \tag{2.35}$$

$$\frac{D\tilde{\epsilon}}{Dt} + \tilde{\epsilon} v_{j,j} + q_{j,j} - \sigma_{ij}^{me} v_{i,j} - h^{me} - E_j \frac{DD_j^e}{Dt} - E_k D_k^e v_{j,j} = 0 \,, \tag{2.36}$$

$$\frac{D\tilde{\Psi}}{Dt} - \tilde{\Psi} v_{i,i} - \eta \frac{D\Theta}{Dt} - \theta_{,j} \frac{q_j}{\theta} - D_j^e \frac{DE_j}{Dt} + \sigma_{ij}^{me} v_{i,j} \geq 0 \,, \tag{2.37}$$

$$\varepsilon_{klm} E_{m,l} = 0_k \,, \tag{2.38}$$

$$\varepsilon_{jlm} [\mu_0^{-1} B_m + \varepsilon_{mpq} v_p (D_q^e - \varepsilon_0 E_q)]_{,l} - \frac{\partial D_j^e}{\partial t} = 0_j \,, \tag{2.39}$$

$$D_{i,i}^e = 0 \,, \tag{2.40}$$

$$B_{i,i} = 0 \,. \tag{2.41}$$

Equations (2.38)-(2.41) are the Maxwell-Minkowski equations in the electrorheological approximation. They are obtained by dropping the terms of relativistic order, by imposing the assumptions (2.25), (2.26) and by setting $\mathcal{J}_i = 0_i$ and $\rho_{el} = 0$.

2.1.1 Jump Conditions

In order to complete the description of electrorheological materials as continuous media, we should add the jump conditions suffered by the mechanical and electromagnetic quantities across a discontinuity surface. Let Σ be a smooth surface, not necessarily material (e.g. a thin wall or a membrane) which separates one part of the body under consideration from another part and let w_i be its velocity in the positive direction of the unit normal to Σ.

The jump conditions are derived using a standard method (see [53]) from the balance laws formulated in the global form, namely for the whole body. One can regard them as local equations of balance in points on singular surfaces in contrast with the classical local form of balance equations which are given in regular points.

By employing the balances of mass, momentum and energy to a "pillbox" volume embracing the singular surface, and contracting the pillbox height to zero (see e.g. [53]) we obtain

$$[[\rho(v_j - w_j)]]n_j = 0\,, \tag{2.42}$$

$$[[\rho v_i(v_j - w_j) - \sigma^{me}_{ij} - E_i D^e_j]]n_j = 0_i\,, \tag{2.43}$$

$$\begin{aligned}&[[(\epsilon + \frac{\rho}{2}v_i v_i + \frac{E_k D^e_k}{2})(v_j - w_j) + q_j + \mu_0^{-1}\varepsilon_{ijk}E_i B_k\\ &+\varepsilon_0(E_i E_j v_i - E_i E_i v_j) - (\sigma^{me}_{ij} + E_i D^e_j)(v_i - w_i)]]n_j = 0\,,\end{aligned} \tag{2.44}$$

while the entropy inequality yields

$$[[\eta(v_j - w_j) + \frac{q_j}{\theta}]]n_j \geq 0\,. \tag{2.45}$$

Here $[[\phi]] := \phi^+ - \phi^-$ denotes the jump across the surface Σ, w_i is the velocity of the singular surface and n_i is the unit normal vector at a point on the singular surface pointing into the positive side of Σ.

The Maxwell-Minkowski equations lead to the following jump conditions

$$\varepsilon_{ijk}n_j[[E_k]] = 0_i\,, \tag{2.46}$$

$$\varepsilon_{ijk}n_j[[\mu_0^{-1}B_i - \varepsilon_0\varepsilon_{ijk}v_j E_k + \varepsilon_{klm}(v_l - w_l)D^e_m]] = 0_i\,, \tag{2.47}$$

$$[[D^e_j]]n_j = 0\,, \tag{2.48}$$

$$[[B_j]]n_j = 0\,. \tag{2.49}$$

2.1.2 Constitutive Equations

Equations (2.33)-(2.41) are not sufficient to determine all the unknowns of the problem; so additional relations reflecting the specific properties of the studied material must be postulated. First, it must be decided which physical variables are supposed to be the independent fields. Then we have to establish the appropriate constitutive equations for the remaining variables. In [29], the independent variables are chosen to be (after applying the principle of material frame indifference)

$$\rho\,,\ \theta\,,\ \ E_j\,,\ D_{ij}\,, \tag{2.50}$$

where D_{ij} denotes the strain rate tensor

$$D_{ij} := \frac{1}{2}(v_{i,j} + v_{j,i})\,. \tag{2.51}$$

The fact that $\theta_{,i}$ is not among the variables (2.50) implies that effects of heat conduction are not considered. It is important to note that the magnetic flux density B_i can not be an independent variable since it can be computed from (2.39) and (2.41) if the electric field strength and the velocity are known. It then follows that B_i will not influence the mechanical equations and it will intervene neither in the electrical problem as it will be seen later. Although the characteristic feature of our problem is that the electric field is space-dependent, the gradient of the electric field is not considered as an independent variable, in a first approximation. This means that we will extrapolate the general constitutive model chosen in [28] (work in which the investigations are restricted to homogeneous electric fields) also to the case of inhomogeneous electric fields. Now let us enumerate the dependent quantities of the problem

$$\sigma_{ij}^{me} = \sigma_{ij}^{me}(\rho, \theta, E_j, D_{ij})\,,\ D_j^e = D_j^e(\rho, \theta, E_j, D_{ij})\,, \tag{2.52}$$

$$\epsilon = \epsilon(\rho, \theta, E_j, D_{ij})\,,\ \tilde{\Psi} = \tilde{\Psi}(\rho, \theta, E_j, D_{ij})\,,\ q_j = q_j(\rho, \theta, E_j, D_{ij})\,. \tag{2.53}$$

2.1.3 Separation of the electric field from the mechanical fields

The evaluation of the entropy inequality will bring the constitutive equations to their ultimate form. We assume this procedure is familiar to the reader (from [38, 53]) and we will give here only a short outline. Substituting $(2.53)_2$ in (2.37) and performing the differentiation according to the chain rule results in

$$-\left(\eta + \frac{\partial\tilde{\Psi}}{\partial\theta}\right)\frac{D\theta}{Dt} - \left(D_j^e + \frac{\partial\tilde{\Psi}}{\partial E_j}\right)\frac{DE_j}{Dt} - \frac{\partial\tilde{\Psi}}{\partial D_{kl}}\frac{DD_{kl}}{Dt} - \theta_{,j}\frac{q_j}{\theta}$$

$$+\left[\sigma_{ij}^{me} + \left(\rho\frac{\partial\tilde{\Psi}}{\partial\rho} - \tilde{\Psi}\right)\delta_{ij}\right]D_{ij} \geq 0\,. \tag{2.54}$$

The inequality is explicitly linear in

$$\frac{D\theta}{Dt}, \frac{DE_j}{Dt}, \frac{DD_{kl}}{Dt}, \theta_{,j}. \tag{2.55}$$

Since all these terms may have any arbitrarily assigned values it follows that each of the coefficients of these variables must be identically zero. This implies the relations

$$\eta = -\frac{\partial \tilde{\Psi}}{\partial \theta}, \tag{2.56}$$

$$D_j^e = -\frac{\partial \tilde{\Psi}}{\partial E_j}, \tag{2.57}$$

$$0_{kl} = -\frac{\partial \tilde{\Psi}}{\partial D_{kl}}, \tag{2.58}$$

$$\frac{q_j}{\theta} = 0_j, \tag{2.59}$$

and the residual inequality

$$\left[\sigma_{ij}^{me} + \left(\rho\frac{\partial \tilde{\Psi}}{\partial \rho} - \tilde{\Psi}\right)\delta_{ij}\right] D_{ij} \geq 0. \tag{2.60}$$

Differentiating again (2.57) and (2.58) gives

$$\frac{\partial D_j^e}{\partial D_{kl}} = 0_{jkl}, \tag{2.61}$$

which means that the only pure electromagnetic dependent quantity, D_j^e cannot depend on the strain rate tensor that is, apart from ρ the only independent mechanical quantity.

(2.61) substituted in $(2.52)_2$ agrees with the experimental results presented in [29]. Consequently, we will choose a constitutive equation for D_j^e corresponding to a linear, isotropic and homogeneous dielectricum

$$D_j^e = \varepsilon(\rho, \theta) E_j, \tag{2.62}$$

where ε denotes the effective permittivity of the fluid which could also depend on E_j. Now substituting this relation in (2.40) and in the jump conditions (2.46) and (2.48) we can formulate a boundary value problem for the electric field which (in the case of constant density and under isothermal conditions) is independent of the mechanical and magnetic problem.

Remark: The fact that the flow does not affect the electric field is not only a consequence of the entropy inequality but also of a number of assumptions made before like the neglect of the time derivatives of the strain rate in the constitutive equations and the non-conductivity of the ER-fluids (a conductive current which would depend on the strain rate would have been a critical quantity in the problem).

In the end of this Section we have to mention two restrictions imposed by the inequality (2.60) (see [28]). If we use the definitions of the thermodynamic pressure and if we decompose the Cauchy stress into a spherical tensor containing the dynamic pressure $-p\delta_{ij}$ and an extra stress tensor σ^e_{ij}, viz,

$$p := \rho\frac{\partial\tilde{\Psi}}{\partial\rho} - \tilde{\Psi}\,, \tag{2.63}$$

$$\sigma^e_{ij} := \sigma^{me}_{ij} + p\delta_{ij}\,, \tag{2.64}$$

(2.60) can be written as

$$\gamma_n := \sigma^e_{ij}D_{ij} \geq 0\,. \tag{2.65}$$

In order to fulfill the thermodynamic equilibrium requirement$\gamma_n = 0$ there is a necessary condition which can be expressed like this

$$\text{If}\quad D_{pq} = 0_{pq}\,,\quad \text{then}\quad \sigma^e_{ij} = 0_{ij}\quad \text{must hold true}\,; \tag{2.66}$$

and a sufficient condition: the following matrix must be positive semi-definite

$$(6\times 6)_E := \left(\frac{\partial^2\gamma_n}{\partial D_A\partial D_B}\right)_E\,, \tag{2.67}$$

where both D_A and D_B denote the 6 independent components of the strain rate tensor

$$(D_{11},\ D_{12},\ D_{13},\ D_{22},\ D_{23},\ D_{33})\,. \tag{2.68}$$

2.2 The flow problem in a plane channel with finite electrodes

As we mentioned in the Introduction we want to study the stationary pressure-driven flow of an ER-fluid in a plane channel under an electric field produced by finite electrodes under isothermal conditions. Let Ox_1x_2 be a Cartesian coordinate system. We consider an infinitely long channel of height $2h$ made by two infinite parallel planes of zero thickness. These planes are situated at $x_2 = -h$, $x_2 = h$, respectively. Along the channel walls, finite electrodes, charged with different potentials are placed. They may be disposed in various configurations as one can see in the examples illustrated in Figures 2.1–2.4.

If the electrodes were of infinite length (as in Figure 2.5), the electric field would be homogeneous. However, in every realistic application the electrodes are finite and the field is inhomogeneous, especially close to the edges of the electrodes. The electrodes are isolated outside the channel with a dielectric material having electric permittivity ε_1. The medium inside the channel has electric permittivity ε_2. Since our problem is two-dimensional the indices i and j used henceforth take only the values 1 and 2.

Equation (2.38) is equivalent with the statement that E_i is the gradient of a scalar function

$$E_i = -\varphi_{,i}\,. \tag{2.69}$$

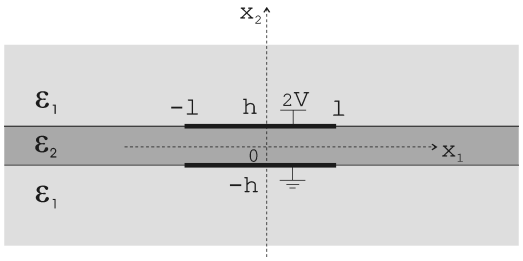

Figure 2.1: Configuration with two finite electrodes of equal lengths ($n_1 = n_2 = 1$, $V_1 = 2V$, $V_2 = 0$)

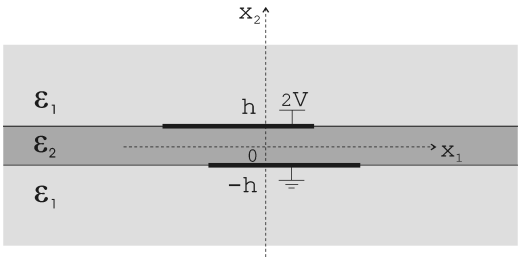

Figure 2.2: Configuration with two equal but shifted finite electrodes ($n_1 = n_2 = 1$, $V_1 = 2V$, $V_2 = 0$)

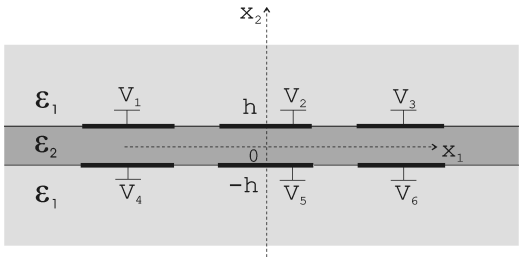

Figure 2.3: Configuration with finite electrodes interrupted by electric neutral walls (periodic structure) ($n_1 = n_2 = 3$)

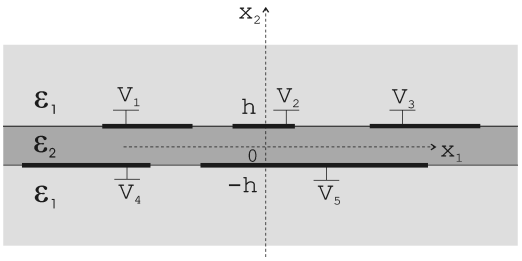

Figure 2.4: Configuration with finite electrodes interrupted by electric neutral walls (general case) ($n_1 = 3$, $n_2 = 2$)

where φ is the electric potential. Substituting this in (2.62) and the resulting equation in (2.40) shows that the potential must fulfill the Laplace equation in the whole domain

$$\nabla^2 \varphi = 0 \quad \text{in} \quad -\infty < x_1 < \infty, \quad -\infty < x_2 < \infty \,. \tag{2.70}$$

We must specify now the boundary conditions. The following Dirichlet boundary conditions are given on the part of the boundary where the electrodes are placed

$$\varphi(x_1, h) = V_{i_1} \,, \; x_1 \in I^{el}_{i_1} \,, \tag{2.71}$$
$$\varphi(x_1, -h) = V_{i_2} \,, \; x_1 \in I^{el}_{i_2} \,, \tag{2.72}$$

where $i_1 = 1, 2, ..., n_1$, $i_2 = n_1 + 1, n_1 + 2, ..., n_1 + n_2$ and n_1, n_2 are the numbers of electrodes placed on the upper and lower walls of the channel respectively. $I^{el}_{i_1}$, $I^{el}_{i_2}$ are the interval domains of the x_1 coordinate of the electrodes placed on the upper and lower walls of the channel, respectively.

Using (2.62) and (2.69) in (2.48) the jump conditions of the electrode-free boundary

parts implies the following equations for the normal derivative of φ:

$$\varepsilon_2\varphi_{,2}\,(x_1,\,h^-) = \varepsilon_1\,\varphi_{,2}\,(x_1,\,h^+), \quad x_1 \in (-\infty,\infty)\setminus\bigcup_{i_1} I^{el}_{i_1}\,, \tag{2.73}$$

$$\varepsilon_2\varphi_{,2}\,(x_1,\,-h^+) = \varepsilon_1\,\varphi_{,2}\,(x_1,\,-h^-), \quad x_1 \in (-\infty,\infty)\setminus\bigcup_{i_2} I^{el}_{i_2}\,, \tag{2.74}$$

while from (2.46) the following continuity conditions in the tangential derivative are obtained

$$\varphi_{,1}\,(x_1,\,h^+) = \varphi_{,1}\,(x_1,\,h^-), \quad x_1 \in (-\infty,\infty)\setminus\bigcup_{i_1} I^{el}_{i_1}\,, \tag{2.75}$$

$$\varphi_{,1}\,(x_1,\,-h^+) = \varphi_{,1}\,(x_1,\,-h^-), \quad x_1 \in (-\infty,\infty)\setminus\bigcup_{i_2} I^{el}_{i_2}\,. \tag{2.76}$$

To specify the jump of the components of the electric field across $x_2 = \pm h$, we use the upper indices "+" and "−" as defined in Appendix E. Moreover we may choose

$$\lim_{x_2\to\pm\infty} \varphi(x_1,x_2) = 0\,. \quad -\infty < x_1 < \infty \tag{2.77}$$

In order to formulate a boundary value problem for the mechanical part we recall the balance of momentum (2.34) for a steady flow

$$\rho v_j v_{i,j} - (\sigma_{ij} + E_i D^e_j)_{,j} - f_i = 0_i\,, \tag{2.78}$$

where we have dropped the upper index "me" from the Cauchy stress and from the body force density. Using (2.62) and (2.64) in the last equation we obtain

$$\rho v_j v_{i,j} - (-p\delta_{ij} + \sigma^e_{ij} + \varepsilon_2 E_i E_j)_{,j} - f_i = 0_i\,. \tag{2.79}$$

Using (2.69) and (2.70) we obtain

$$(E_i E_j)_{,j} = \frac{1}{2}(E_j E_j)_{,i}\,. \tag{2.80}$$

If we suppose that the force density f_i is conservative then we may incorporate it into the pressure. Doing this and substituting (2.80) in the momentum balance it follows

$$-p_{,i} + \sigma^e_{ij,j} + \frac{1}{2}\varepsilon_2(E_j E_j)_{,i} = \rho v_j v_{i,j}\,, \tag{2.81}$$

Our investigations in the remaining part of our study assume incompressible fluids i.e.,

$$D_{kk} = v_{k,k} = 0\,. \tag{2.82}$$

Then the pressure is an unknown that can be determined up to a constant.

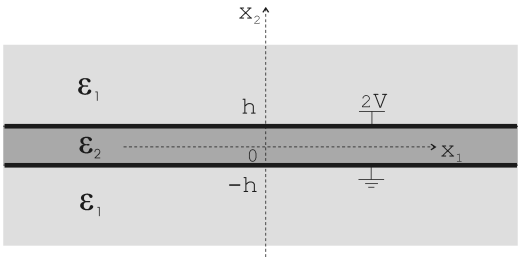

Figure 2.5: Configuration with infinite electrodes

Substituting in (2.81) a constitutive function for the Cauchy stress tensor and the solution for the electric field we obtain in the plain flow case two equations which together with (2.82) may be used to determine the three unknowns: the components of the velocity vector and the pressure. A discussion about the constitutive form of the Cauchy extra stress tensor σ^e_{ij} is postponed until Chapter 4 where the mechanical problem is analysed. Unlike the electrical problem, the domain for the mechanical problem is restricted to the channel. We assume no-slip and impermeability conditions on the channel walls

$$v_1(x_1, \pm h) = 0\,, \quad v_2(x_1, \pm h) = 0\,, \quad -\infty < x_1 < \infty \tag{2.83}$$

Besides, we have to assume boundary conditions at the entrance and the exit of the channel, respectively.

The BVP (2.70)-(2.76) can be solved analytically in a bounded domain in the x_2-direction (condition (2.77) will be changed to a similar condition imposed on the upper and lower boundaries), for the case $n_1 = n_2 = 1$, $I^{el}_1 = I^{el}_2 = [-l, l]$ provided that the electrodes length $2l$ allows a decoupling of the electrode ends. The solution method is presented in detail in Chapter 3 for different ways of charging the electrodes: symmetrically ($V_1 = V$, $V_2 = V$), anti-symmetrically ($V_1 = V$, $V_2 = -V$) and non-symmetrically ($V_1 = 2V$, $V_2 = 0$). The cases of two short electrodes and of the other electrode configurations will be solved numerically together with the mechanical problem. The numerical approach is exposed in Chapter 5.

2.2.1 Particular case – infinite electrodes

If we consider in (2.71), (2.72) that $n_1 = n_2 = 1$, $I^{el}_1 = I^{el}_2 = (-\infty, \infty)$ and $V_1 = 2V$, $V_2 = 0$ we obtain the configuration sketched in Figure (2.5). The solution of the electrical problem in this case is

$$\varphi(x_1, x_2) = \frac{V}{h} x_2 + V\,, \quad -\infty < x_1 < \infty\,, \quad |x_2| \le h\,. \tag{2.84}$$

Consequently, the electric field has the form

$$E_1 = 0\,, \quad E_2 = -\frac{V}{h}\,, \tag{2.85}$$

everywhere in the channel. The dielectric material outside the channel has no influence on the solution. Another consequence of the fact that the electric field is constant is that the flow problem will be one-directional, i.e. the only non-vanishing velocity component only varies in the flow direction, providing, of course, that the inlet and outlet boundary conditions agree with this. We may assume first that $v_{1,1} = 0$, $v_{2,1} = 0$. Then, from the continuity equation it follows that $v_{2,2} = 0$. If we take into account the impermeability condition on the walls, we obtain that the x_2-component of the velocity vanishes in the whole domain. So, we have

$$v_1 = v_1(x_2) \,, \tag{2.86}$$

$$v_2 = 0 \,. \tag{2.87}$$

Consequently, the only non-vanishing components of the strain rate tensor are

$$D_{12} = D_{21} = \frac{v_{1,2}(x_2)}{2} \,, \tag{2.88}$$

and from (2.52) it follows that all the components of the stress tensor are independent of x_1. By applying all these considerations in the momentum balance (2.81) we obtain

$$-p_{,1} = -\sigma^e_{12,2} \,, \tag{2.89}$$

$$-p_{,2} + \sigma^e_{22,2} = 0 \,. \tag{2.90}$$

From the last equation it follows that the quantity $-p + \sigma^e_{22}$ can be only a function of x_1. However, $\sigma^e_{22,1} = 0$, hence also $p_{,1}$ is only a function of x_1. Since the right hand side of (2.89) is not a function of x_1, neither is the left hand side, and therefore $p_{,1} = (p - \sigma^e_{22})_{,1}$ should be constant. If we denote this constant by k, it follows from (2.89) that

$$p = kx_1 + \sigma^e_{22} + c_1 \,. \tag{2.91}$$

The constant k denotes the pressure gradient in the x_1-direction. The constant c_1 can be determined if a boundary condition for p is given. From (2.90) we can write

$$\sigma^e_{12} = kx_2 + c_2 \,, \tag{2.92}$$

where c_2 is the shear stress in the middle of the channel. By assigning certain constitutive functions to σ^e_{ij} one can often determine analytically the solution for the velocity and the pressure (see e.g. [28] and Appendix D).

The model presented in this Subsection was used up to now to describe the flow of an ERF in a channel (see [28]). When interpreting the experimental results in slit flow, it was usually considered that the electric field is constant and that it determines a shear flow in the channel [3, 5, 68, 76, 93]. In other words the model with infinite electrodes was used as an approximation for the real case with finite electrodes. In our view this is not a realistic approximation in all the cases since it neglects the electrode end effects which may considerably affect the flow (see Chapter 5).

Chapter 3

The analytical solution of the inhomogeneous electric field generated by two long electrodes

As one can see from the previous Chapter, the electric field is the key element of our problem since its dependence on the space coordinates determines the kinematical character of the flow. In order to gain a better understanding of the electrode end effects on the electric field inhomogeneity in the channel, we will investigate first the simplest configuration of electrodes. Namely we will study here the distribution of the electric potential around two long electrodes charged with different potentials in a symmetric, an anti-symmetric and a non-symmetric way. The term "long electrode" denotes here either a semi-infinite electrode or a finite electrode of a certain length chosen so that the two far edges of the electrode do not interact.

The solutions are found (semi)-analytically and they are constructed with the use of the Wiener-Hopf (W-H) technique. The reason for doing this is two-fold: on the one hand, the method of constructing allows us to find an entire class of solutions for technically interesting configurations, and, on the other hand, the WH-technique sets the singularities at the tips of the electrodes explicitly in evidence, which in a numerical solution must be approximately accounted for in rather costly mesh refinements. Furthermore, the analytical solution is very useful as a benchmark for the numerical solution obtained using the available numerical program.

In Section 3.1, the mixed boundary value problem for the electric potential is formulated for the case of two semi-infinite electrodes. Continuity conditions in the tangential derivative and jump conditions in the normal derivative are taken into account across the channel walls. Owing to the linearity of the problem, the solution is constructed as a sum of two solutions for two particular problems: with symmetric and anti-symmetric boundary conditions. The Wiener-Hopf procedure which is described in Section 3.2 is successfully applied to solve these problems in Sections 3.3, 3.4 and 3.5. First we deduce the Wiener-Hopf equations, then the factorizations are accomplished and the solution is

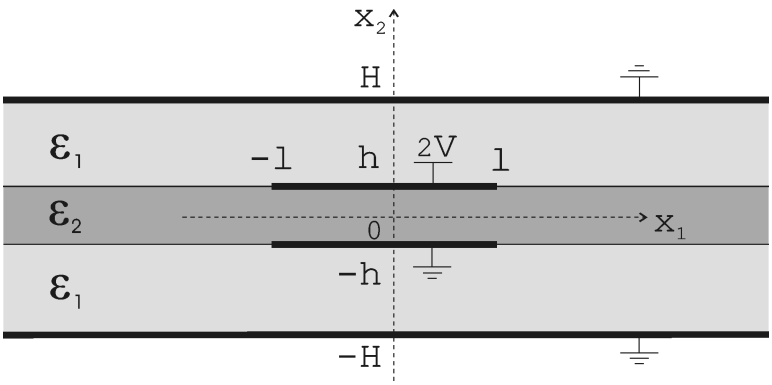

Figure 3.1: Configuration of the electrodes with non-symmetric boundary conditions

calculated. The singular behaviour of the electric field near the ends of the electrodes is determined in Section 3.6. We discuss the extension of the solution to the case of finite electrodes in Section 3.7. In the same Chapter the main results are plotted and some remarks are presented. The final Section is devoted to summarizing the achieved results.

The content of this Chapter should be accessible to anyone who is familiar with the basic concepts of complex variable theory such as regular functions, singularities, poles, multi-valued functions, analytic continuation, integration in the complex plane (the calculus of residues, integration along branch cuts) [20, 89]. Also knowledge about Fourier transforms is required. An appendix A, meant to supplement this knowledge, is added at the end of the thesis. Not frequently used theorems and formulas needed in our Wiener-Hopf approach are also given there. For more details we refer the reader to [1, 54, 71].

3.1 Formulation of the problem

Let Ox_1x_2 be a Cartesian coordinate system. As in Section 2.2 we consider an infinitely long channel of height $2h$ made by two infinite parallel planes of zero thickness (see Figure 3.1) situated at $x_2 = -h$, $x_2 = h$, respectively. Along the channel walls, two electrodes of lengths $2l$, charged with different potentials are placed (at the upper electrode a constant potential $2V$ is applied and the lower electrode is grounded). The electrodes are isolated outside the channel with a dielectric material having electric permittivity ε_1. The medium inside the channel has electric permittivity ε_2. We solve the problem in a bounded domain in the x_2-direction, where the upper and lower boundaries consist of two infinite grounded electrodes situated at a distance $H > h$ from the x_1-axis. If H is sufficiently large, this is equivalent with the usual infinity conditions which means vanishing potential at $x_2 = \pm\infty$. For smaller H, this configuration can still be easily realized in practice. We mention that the two grounding electrodes at $x_2 = \pm H$ are needed for technical reasons when solving the WH-problem, for otherwise, i.e., when no grounding electrodes are present no solution could be found (see Appendix B for a detailed explanation). Physically, this is no restriction because the channel will always be earthed and the system can always be

looked at for large H.

First, we will formulate and solve the problem in the case of semi-infinite electrodes. The origin of the coordinate system is shifted to the left by the amount $x_1 = l$ and the electrodes are prolonged to infinity on the right side. The solution can be used directly to describe the corresponding case with finite electrodes provided that their length allows non-coupling of the left and right electrode ends. From parametric studies we can determine such length values in relation with H, h and $c = \varepsilon_1/\varepsilon_2$ (see Section 3.7). Using the general model from Section 2.2 we can formulate our problem as follows

$$\nabla^2\varphi = 0 \quad \text{in} \quad -\infty < x_1 < \infty, \quad |x_2| \leq H\,, \tag{3.1}$$

with the boundary conditions

$$\varphi\,(x_1, h) = 2V, \quad x_1 \geq 0\,, \tag{3.2}$$
$$\varphi\,(x_1, -h) = 0, \quad x_1 \geq 0\,, \tag{3.3}$$
$$\varphi_{,1}\,(x_1,\, h^+) = \varphi_{,1}\,(x_1,\, h^-), \quad x_1 \leq 0\,, \tag{3.4}$$
$$\varphi_{,1}\,(x_1,\, -h^+) = \varphi_{,1}\,(x_1,\, -h^-), \quad x_1 \leq 0\,, \tag{3.5}$$
$$\varphi_{,2}\,(x_1,\, h^-) = c\,\varphi_{,2}\,(x_1,\, h^+), \quad x_1 \leq 0\,, \tag{3.6}$$
$$\varphi_{,2}\,(x_1,\, -h^+) = c\,\varphi_{,2}\,(x_1,\, -h^-), \quad x_1 \leq 0\,, \tag{3.7}$$
$$\varphi(x_1, \pm H) = 0, \quad -\infty < x_1 < \infty\,. \tag{3.8}$$

Here the quantity φ denotes the electric potential. The electric field is then given by $E = -\text{grad}\,\varphi$. The asymptotic behaviour of φ is given by

$$\lim_{x_1 \to \pm\infty} \varphi(x_1, x_2) = 0\,,\ -H \leq x_2 \leq H\,. \tag{3.9}$$

Since the domain is symmetric with respect to the x_1-axis it is more convenient to split the problem, by applying the principle of superposition, in two easier problems corresponding to the symmetric and anti-symmetric parts φ^s, φ^a of the unknown function φ with respect to x_2 (see Figure 3.2):

$$\varphi^s(x_1, x_2) = \frac{\varphi(x_1, x_2) + \varphi(x_1, -x_2)}{2}\,, \tag{3.10}$$
$$\varphi^a(x_1, x_2) = \frac{\varphi(x_1, x_2) - \varphi(x_1, -x_2)}{2}\,. \tag{3.11}$$

Again, from symmetry considerations, it is sufficient to solve these two problems for $x_2 \geq 0$ (see Figure 3.3). It is easy to prove that the boundary value problem (BVP) for the symmetric part reads

$$\nabla^2\varphi^s = 0 \quad \text{in} \quad -\infty < x_1 < \infty, \quad 0 \leq x_2 \leq H\,, \tag{3.12}$$

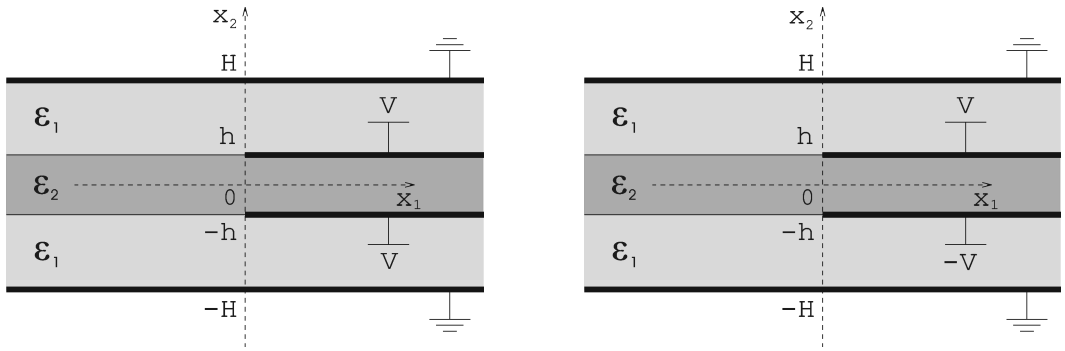

Figure 3.2: Schematic diagram of the electrodes configuration for the particular problems: symmetric case (left) and anti-symmetric case (right)

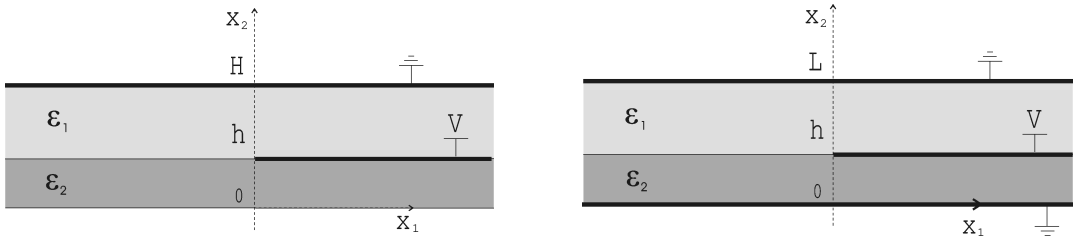

Figure 3.3: Schematic diagram of the upper-half configuration for the particular problems: symmetric case (left) and anti-symmetric case (right)

where φ^s satisfies the boundary conditions

$$\varphi^s\,(x_1, h) = V, \quad x_1 \geq 0\,, \tag{3.13}$$
$$\varphi^s_{,2}\,(x_1,\, 0) = 0, \quad -\infty < x_1 < \infty\,, \tag{3.14}$$
$$\varphi^s_{,1}\,(x_1,\, h^+) = \varphi^s_{,1}\,(x_1,\, h^-), \quad x_1 \leq 0\,, \tag{3.15}$$
$$\varphi^s_{,2}\,(x_1,\, h^-) = c\,\varphi^s_{,2}\,(x_1,\, h^+), \quad x_1 \leq 0\,, \tag{3.16}$$
$$\varphi^s(x_1, H) = 0, \quad -\infty < x_1 < \infty\,, \tag{3.17}$$

while the BVP for the anti-symmetric part is

$$\nabla^2\varphi^a = 0 \quad \text{in} \quad -\infty < x_1 < \infty, \quad 0 \leq x_2 \leq H\,, \tag{3.18}$$

with the boundary conditions

$$\varphi^a\,(x_1, h) = V, \quad x_1 \geq 0\,, \tag{3.19}$$
$$\varphi^a\,(x_1, 0) = 0, \quad -\infty < x_1 < \infty\,, \tag{3.20}$$
$$\varphi^a_{,1}\,(x_1,\, h^+) = \varphi^a_{,1}\,(x_1,\, h^-), \quad x_1 \leq 0\,, \tag{3.21}$$
$$\varphi^a_{,2}\,(x_1,\, h^-) = c\,\varphi^a_{,2}\,(x_1,\, h^+), \quad x_1 \leq 0\,, \tag{3.22}$$
$$\varphi^a(x_1, H) = 0, \quad -\infty < x_1 < \infty\,. \tag{3.23}$$

Let us derive the asymptotic behaviour for the two functions φ^s and φ^a. We have

$$\lim_{x_1 \to -\infty} \varphi^s(x_1, x_2) = 0\,,\ 0 \le x_2 \le H\,, \tag{3.24}$$

while φ^a satisfies the same condition. If we denote by

$$f^s(x_2) = \lim_{x_1 \to \infty} \varphi^s(x_1, x_2)\,, \tag{3.25}$$

$$f^a(x_2) = \lim_{x_1 \to \infty} \varphi^a(x_1, x_2)\,, \tag{3.26}$$

then the function $f^s(x_2)$ satisfies

$$f^{s\prime\prime}(x_2) = 0\,,\ 0 \le x_2 \le H\,, \tag{3.27}$$

and the boundary conditions

$$f^s(H) = 0\,,\ f(h) = V\,,\ f'(0) = 0\,, \tag{3.28}$$

while the function $f^a(x_2)$ satisfies

$$f^{a\prime\prime}(x_2) = 0\,,\ 0 \le x_2 \le H\,, \tag{3.29}$$

and the boundary conditions

$$f^a(H) = 0\,,\ f(h) = V\,,\ f(0) = 0\,. \tag{3.30}$$

The solutions are given by

$$f^s(x_2) = \begin{cases} V\,, & 0 \le x_2 \le h\,, \\ \dfrac{V(H - x_2)}{H - h}\,, & h \le x_2 \le H\,, \end{cases} \tag{3.31}$$

$$f^a(x_2) = \begin{cases} \dfrac{V x_2}{h}\,, & 0 \le x_2 \le h\,, \\ \dfrac{V(H - x_2)}{H - h}\,, & h \le x_2 \le H\,. \end{cases} \tag{3.32}$$

We note that the functions f^s and f^a are no longer symmetric and anti-symmetric, respectively, for $0 \le x_2 \le h$. The asymptotic behaviour of the function φ, namely the function

$$f(x_2) = \lim_{x_1 \to \infty} \varphi(x_1, x_2)\,, \tag{3.33}$$

may be derived in two ways: either by solving the problem

$$f''(x_2) = 0\,,\ |x_2| \le H\,, \tag{3.34}$$

$$f(\pm H) = 0\,,\ f(-h) = 0\,,\ f(h) = 2V\,, \tag{3.35}$$

or by using the formula

$$f(x_2) = f^s(|x_2|) + \text{sign}(x_2) f^a(|x_2|)\,. \tag{3.36}$$

We obtain

$$f(x_2) = \begin{cases} \dfrac{V x_2}{h} + V\,, & |x_2| \le h\,, \\ 0\,, & -H \le x_2 \le -h\,, \\ \dfrac{2V(H - x_2)}{H - h}\,, & h \le x_2 \le H\,. \end{cases} \tag{3.37}$$

These results also follow by taking limits as $x_1 \to \infty$ in (3.107), (3.110) as well as in (3.118), (3.121) and in (3.127). The infinity conditions will not intervene in the subsequent solution method but they are useful for checking the final solution.

We simply remark that, until now, the two problems differ only in their asymptotic behaviour when $x_1 \to \infty$ in the channel and through the conditions (3.14) and (3.20) which are required by symmetry and anti-symmetry, respectively. We continue by solving them in parallel and writing the common relations only once (with double superscript). The solutions will be found by means of the Wiener-Hopf technique which is briefly described in the next Section.

3.2 The Wiener-Hopf method

A remarkable feature of the mathematical description of the natural phenomena by means of partial differential equations is the comparative ease with which the solutions can be obtained for certain geometrical shapes, such as circles and infinite strips, by the method of separation of variables in contrast with the considerable difficulty encountered in finding solutions for shapes not covered by this method. The Wiener-Hopf technique provides a significant extension of the range of problems that can be solved by use of Fourier transforms. A typical problem where it can be applied is the steady-state wave equation in free space when semi-infinite boundaries are present. Many examples can be given from electromagnetic theory, acoustics, hydrodynamics, elasticity and potential theory.

The Wiener-Hopf method consists in a complex variable procedure to find the solution of a functional equation of the form

$$A(\alpha)F_+(\alpha) + B(\alpha)F_-(\alpha) + C(\alpha) = 0\,, \tag{3.38}$$

which is defined in a strip of the complex α-plane $\tau_- < \tau < \tau_+$, $-\infty < \sigma < \infty$, where $\alpha = \sigma + i\tau$; $F_+(\alpha)\,, F_-(\alpha)$ are the unknown functions; $F_+(\alpha)$ should be regular in the half-plane $\tau > \tau_-$ while $F_-(\alpha)$ should be regular in the half-plane $\tau < \tau_+$, so that $\tau_- < \tau < \tau_+$ is the common domain of analyticity for F_+ and F_- as shown in Fig. 3.4. Certain information has to be specified regarding the behaviour of these functions as α tends to ∞ in appropriate half-planes. $A(\alpha)$, $B(\alpha)$, $C(\alpha)$ are given non-zero functions of α, regular in the strip. Functional equations of this type are obtained by the Fourier transformation

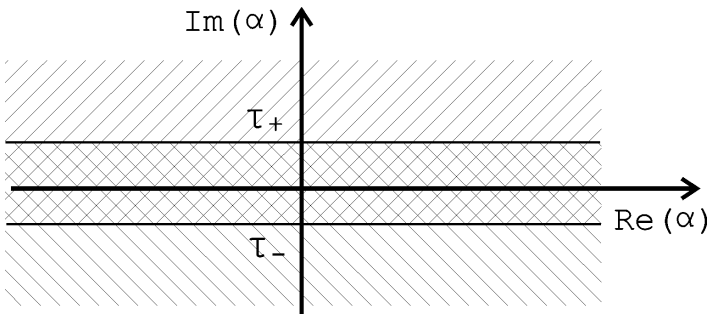

Figure 3.4: Common strip of analyticity of the functions F_+ and F_-

of the partial differential equations or integral equations that have to be solved.

The fundamental step in the Wiener-Hopf procedure for solving this equation is the identification of two functions $K_+(\alpha)$ regular and non-zero in $\tau > \tau_-$ and $K_-(\alpha)$ regular and non-zero in $\tau < \tau_+$, such that

$$K(\alpha) := A(\alpha)/B(\alpha) = K_+(\alpha)/K_-(\alpha)\,. \tag{3.39}$$

Substitution of (3.39) into equation (3.38) and rearranging yield the functional equation

$$K_+(\alpha)F_+(\alpha) + K_-(\alpha)F_-(\alpha) + K_-(\alpha)C(\alpha)/B(\alpha) = 0\,. \tag{3.40}$$

Subsequently we construct two functions $L_+(\alpha)$ and $L_-(\alpha)$ which are regular in the upper-half plane $\tau > \tau_-$ and in the lower-half plane $\tau < \tau_+$, respectively and satisfy the relation

$$L(\alpha) := K_-(\alpha)C(\alpha)/B(\alpha) = L_+(\alpha) + L_-(\alpha)\,. \tag{3.41}$$

With the help of (3.41) one can rearrange (3.40) and so define a function $J(\alpha)$ by

$$J(\alpha) := K_+(\alpha)F_+(\alpha) + L_+(\alpha) = -K_-(\alpha)F_-(\alpha) - L_-(\alpha)\,. \tag{3.42}$$

So far this equation defines $J(\alpha)$ only in the strip $\tau_- < \tau < \tau_+$. But the second part of the equation is defined and is regular in $\tau > \tau_-$, and the third part is defined and is regular in $\tau < \tau_+$. Hence by analytic continuation we can define $J(\alpha)$ over the whole α-plane and $J(\alpha)$ is regular in the whole α-plane. Now if it can be shown that

$$|K_+(\alpha)F_+(\alpha) + L_+(\alpha)| < |\alpha|^p \quad \text{as} \quad \alpha \longrightarrow \infty\,,\ \tau > \tau_-\,, \tag{3.43}$$
$$|K_-(\alpha)F_-(\alpha) + L_-(\alpha)| < |\alpha|^q \quad \text{as} \quad \alpha \longrightarrow \infty\,,\ \tau < \tau_+\,, \tag{3.44}$$

then, by the extended form of the Liouville theorem, $J(\alpha)$ is a polynomial $P(\alpha)$ of degree less than or equal to the integral part of $\min(p, q)$. Once the degree of the polynomial has been determined, its coefficients can be found by means of other mathematical or physical conditions which need be satisfied by the solution of the particular problem. Thus, in

general, the entire function $J(\alpha)$ is well defined and the functions $F_+(\alpha)$ and $F_-(\alpha)$ can be written as

$$F_+(\alpha) = (P(\alpha) - L_+(\alpha))/K_+(\alpha)\,, \tag{3.45}$$
$$F_-(\alpha) = (-P(\alpha) - L_-(\alpha))/K_-(\alpha)\,. \tag{3.46}$$

We note that the successful execution of the Wiener-Hopf technique depends to a large part on the ability to factorize the function $K(\alpha)$ and to decompose the function $L(\alpha)$. In some elementary problems the factorization and decomposition can be accomplished by inspection while in more complicated cases recourse must be sought in known product and sum rules (see Appendix A.3 and [19, 54, 71]).

We should mention that not all the problems solvable by the Wiener-Hopf method involve an equation of the form (3.38). In particular, the approach described above is called Jone's method. Actually, it is said about any method in which the crucial decomposition of form (3.39) is involved at some stage of the solution, that it is based on the Wiener-Hopf technique. In [54] there are also other methods described such as the integral equation method.

3.3 Solution procedure

We will solve the problem formulated in Section 3.1 by following Jone's method described in the foregoing Section. To avoid the difficulties that appear when Fourier transforming a constant function, we will replace $\varphi^{s/a}(x_1, h) = V$ by

$$\varphi^{s/a}(x_1, h) = Ve^{-\varepsilon x_1} =: \varphi_0(x_1)\,, \quad 0 \le x_1 < \infty \quad (\varepsilon > 0). \tag{3.47}$$

We shall ultimately let $\varepsilon \to 0$.* Multiplying the Laplace equation by $e^{i\alpha x_1}$ with α being the Fourier transform variable and integrating the resulting equation with respect to x_1 from $-\infty$ to ∞ gives

$$d^2\Phi^{s/a}(\alpha, x_2)/dx_2^2 - \alpha^2\Phi^{s/a}(\alpha, x_2) = 0\,, \quad 0 \le x_2 \le H\,, \tag{3.48}$$

where

$$\Phi^{s/a}(\alpha, x_2) = \frac{1}{(2\pi)^{1/2}} \int_{-\infty}^{\infty} \varphi^{s/a}\, e^{i\alpha x_1}\, dx_1\,. \tag{3.49}$$

The solution of (3.48) is

$$\Phi^{s/a}(\alpha, x_2) = \begin{cases} A_1^{s/a}(\alpha)\, e^{-\alpha x_2} + B_1^{s/a}(\alpha)\, e^{\alpha x_2}\,, & 0 \le x_2 \le h\,, \\ A_2^{s/a}(\alpha)\, e^{-\alpha x_2} + B_2^{s/a}(\alpha)\, e^{\alpha x_2}\,, & h \le x_2 \le H\,. \end{cases} \tag{3.50}$$

*The idea of 3.47 has been adopted from [54, pp.135].

The Fourier transformed common boundary conditions are

$$\Phi_+^{s/a}(\alpha, h^+) = \Phi_+^{s/a}(\alpha, h^-) = \Phi_0\,, \tag{3.51}$$
$$\Phi_-^{s/a}(\alpha, h^+) = \Phi_-^{s/a}(\alpha, h^-)\,, \tag{3.52}$$
$$(\Phi_-^{s/a})'(\alpha, h^-) = c\,(\Phi_-^{s/a})'(\alpha, h^+)\,, \tag{3.53}$$
$$\Phi_-^{s/a}(\alpha, H) = \Phi_+^{s/a}(\alpha, H) = 0\,, \tag{3.54}$$

where

$$\Phi_+^{s/a}(\alpha, x_2) = \frac{1}{(2\pi)^{1/2}} \int_0^\infty \varphi^{s/a}\, e^{i\alpha x_1}\, dx_1\,, \tag{3.55}$$

$$\Phi_-^{s/a}(\alpha, x_2) = \frac{1}{(2\pi)^{1/2}} \int_{-\infty}^0 \varphi^{s/a}\, e^{i\alpha x_1}\, dx_1\,, \tag{3.56}$$

$$\Phi_0(\alpha) = k/(\varepsilon - i\alpha)\ ,\ \ k = V/\sqrt{2\pi}\,, \tag{3.57}$$

and where the prime is used to denote differentiation with respect to x_2. In addition, (3.14) and (3.20) yield

$$(\Phi_+^s)'(\alpha, 0) = (\Phi_-^s)'(\alpha, 0) = 0\,, \tag{3.58}$$
$$\Phi_+^a(\alpha, 0) = \Phi_-^a(\alpha, 0) = 0\,. \tag{3.59}$$

From now on, the α-argument of the functions will be dropped. Using (3.50), (3.58), (3.54) and $\Phi^s(h^+) = \Phi^s(h^-)$ in view of (3.51) and (3.52) we deduce

$$\Phi^s(x_2) = \begin{cases} +2A_1^s\, \cosh(\alpha x_2)\,, & 0 \le x_2 \le h\,, \\ +2A_1^s \dfrac{\cosh(\alpha h)\sinh(\alpha H - \alpha x_2)}{\sinh(\alpha H - \alpha h)}\,, & h \le x_2 \le H\,. \end{cases} \tag{3.60}$$

After straightforward calculations we obtain from (3.60), on using (3.51)-(3.58), the relations

$$\Phi_0 + \Phi_-^s(h) = 2A_1^s\, \cosh(\alpha h)\,, \tag{3.61}$$
$$(\Phi_+^s)'(h^+) + (\Phi_-^s)'(h^+) = -2\alpha\, A_1^s\, \cosh(\alpha h) \coth(\alpha(H-h))\,, \tag{3.62}$$
$$(\Phi_+^s)'(h^-) + c(\Phi_-^s)'(h^+) = 2\alpha\, A_1^s\, \sinh(\alpha h)\,. \tag{3.63}$$

Analogously, (3.50), (3.59), (3.54) and $\Phi^a(h^+) = \Phi^a(h^-)$, in view of (3.51) and (3.52), yield

$$\Phi^a(x_2) = \begin{cases} -2A_1^a\, \sinh(\alpha x_2)\,, & 0 \le x_2 \le h\,, \\ -2A_1^a \dfrac{\sinh(\alpha h)\sinh(\alpha H - \alpha x_2)}{\sinh(\alpha H - \alpha h)}\,, & h \le x_2 \le H\,. \end{cases} \tag{3.64}$$

Then from (3.64) and (3.51)-(3.59) we have

$$\Phi_0 + \Phi_-^a(h) = -2A_1^a \sinh(\alpha h)\,, \tag{3.65}$$
$$(\Phi_+^a)'(h^+) + (\Phi_-^a)'(h^+) = 2\alpha\, A_1^a \sinh(\alpha h)\coth(\alpha(H-h))\,, \tag{3.66}$$
$$(\Phi_+^a)'(h^-) + c(\Phi_-^a)'(h^+) = -2\alpha\, A_1^a \cosh(\alpha h)\,. \tag{3.67}$$

This puts us now in the position to formulate the Wiener-Hopf equation. To this end, multiply (3.62) and (3.66) by c and subtract the resulting equations from (3.63) and (3.67), respectively. If we introduce $F_+^{s/a} = c\,(\Phi_+^{s/a})'(h^+) - (\Phi_+^{s/a})'(h^-)$ and $F_-^{s/a} = \Phi_-^{s/a}(h)$ we obtain, by eliminating the unknown coefficient $A_1^{s/a}$, the Wiener-Hopf equations for the unknown functions $F_+^{s/a}$ and $F_-^{s/a}$ corresponding to each problem, namely

$$K^{s/a}F_+^{s/a} + F_-^{s/a} = -\Phi_0\,, \tag{3.68}$$

where

$$K^s(\alpha) = \frac{1}{\alpha\,[\,c\coth(\alpha H - \alpha h) + \tanh(\alpha\, h)\,]}\,, \tag{3.69}$$
$$K^a(\alpha) = \frac{1}{\alpha\,[\,c\coth(\alpha H - \alpha h) + \coth(\alpha\, h)\,]}\,. \tag{3.70}$$

If equation (3.68) is solved then the coefficients $A_1^{s/a}$ are found by inserting the functions $F_-^{s/a}$ in (3.61) and in (3.65), respectively. We can obtain the Fourier transforms of the solutions from (3.60) and (3.64) and then, by inverting them, we obtain the final solutions.

3.4 Application of the Wiener-Hopf Technique

In addition to the boundary conditions listed in Section 3.1, some regularity assumptions concerning the potential function are needed in order to ensure the applicability of the Wiener-Hopf technique. Assuming that $\varphi(x_1, h)$ is a bounded function of x_1 for $x_1 \le 0$, the function $F_-^{s/a}$ will be analytic in the half-plane $\tau < 0$, $-\infty < \sigma < \infty$, where $\alpha = \sigma + i\tau$ (see A.1.1). It is also reasonable, because of (3.47), to expect that $\varphi(x_1, x_2)$ decays exponentially to zero as $x_1 \to \infty$, i.e., there exists a $b > 0$ such that $\varphi(x_1, x_2)e^{-bx_1}$ is absolutely integrable over the positive x_1-axis for all x_2. This yields that $(\Phi_+^{s/a})'(h^+)$ and $(\Phi_+^{s/a})'(h^-)$ are analytic for $\tau > -b$ (see A.1.1). We may take $b = \varepsilon$, where ε is the small parameter introduced in (3.47). Now, the functions $F_-^{s/a}$ and $F_+^{s/a}$ are both analytic in the strip $-\varepsilon < \tau < 0$. If a decomposition of the kernel $K^{s/a}$ can be accomplished in the form $K^{s/a}(\alpha) = K_-^{s/a}(\alpha)K_+^{s/a}(\alpha)$ where $K_+^{s/a}$ is analytic and non-zero for $\tau > -\varepsilon$, and $K_-^{s/a}$ is analytic and non-zero for $\tau < 0$, one may rearrange (3.68) as

$$K_+^{s/a}F_+^{s/a} + F_-^{s/a}/K_-^{s/a} = -\Phi_0/K_-^{s/a}\,. \tag{3.71}$$

Writing

$$-\Phi_0/K_-^{s/a} = L_+^{s/a} + L_-^{s/a}\,, \tag{3.72}$$

where $L_-^{s/a}(\alpha)$ and $L_+^{s/a}(\alpha)$ are analytic in $\tau < 0$ and $\tau > -\varepsilon$, respectively, then a new function can be defined,

$$\begin{aligned} J^{s/a}(\alpha): &= K_+^{s/a}(\alpha)F_+^{s/a}(\alpha) - L_+^{s/a}(\alpha) \\ &= -F_-^{s/a}(\alpha)/K_-^{s/a}(\alpha) + L_-^{s/a}(\alpha)\,, \end{aligned} \tag{3.73}$$

in $-\varepsilon < \tau < 0$. Because of the properties of the second and third parts of this equation, by analytic continuation, $J(\alpha)$ can be defined over the whole α-plane as an entire function. Using the order properties of the functions $K_+^{s/a}F_+^{s/a} - L_+^{s/a}$ and $-F_-^{s/a}/K_-^{s/a} + L_-^{s/a}$ for large values of α, one can determine the form of $J^{s/a}(\alpha)$ with the help of the Liouville theorem and then find $F_-^{s/a}(\alpha)$.

The most important step in the solution consists in decomposing the Wiener-Hopf kernel $K^{s/a}(\alpha)$. It can be accomplished by inspection when infinite-product representations of the numerator and denominator are known. We shall derive these representations as follows: first an appropriate form of $K^{s/a}$ is needed,

$$K^s(\alpha) = \frac{[2\sinh(\alpha H - \alpha h)\,\cosh(\alpha h)]/\alpha}{[\,(c+1)\cosh(\alpha H) + (c-1)\cosh(\alpha H - 2\alpha h)\,]}\,, \tag{3.74}$$

$$K^a(\alpha) = \frac{[2\sinh(\alpha H - \alpha h)\,\sinh(\alpha h)]/\alpha^2}{[\,(c+1)\sinh(\alpha H) + (1-c)\sinh(\alpha H - 2\alpha h)\,]/\alpha}\,. \tag{3.75}$$

Now, the numerator and the denominator of $K^{s/a}$ can be decomposed using the infinite product theorem applied for an even function (see Appendix A.3). To do this, the zeros of the functions should be determined. The numerator vanishes for $\alpha = \pm i\kappa_n$ and $\alpha = \pm i\lambda_n$ in the symmetric case, and for $\alpha = \pm i\mu_n$ and $\alpha = \pm i\kappa_n$ in the anti-symmetric case, where $\kappa_n = n\pi/(H-h)$, $\lambda_n = (n-1/2)\pi/h$ and $\mu_n = n\pi/h$, $(n = 1, 2, 3, ...)$. It can be proved that the zeros of the denominator are purely imaginary in both cases (see Appendix C.1). Consequently, the zeros $\alpha = i\tau$ can be found by solving the real equations (with τ as unknown)

$$\cos(\tau H) = c_1\,\cos(\tau(H-2h))\,, \tag{3.76}$$

$$\sin(\tau H) = -c_1\,\sin(\tau(H-2h))\,, \tag{3.77}$$

where $c_1 = (1-c)/(1+c)$, $|c_1| < 1$. There are two special cases when the roots of (3.76) and (3.77) are explicitly known: when $H = 2h$ and when $\varepsilon_1 = \varepsilon_2$ that means $c = 1$ and $c_1 = 0$. Except for these particular situations, equations (3.76) and (3.77) cannot be solved analytically and, consequently, their zeros must be found numerically. Now, let us study the periodicity of the solutions. Suppose that $H > 2h$ and that $H/(H-2h)$ is a rational number written as

$$H/(H-2h) = p/q\,, \tag{3.78}$$

where p, q are positive integers that are mutually prime, with $p > q$. Then it follows that the complete solutions of (3.76) and (3.77) are $\tau = \pm\delta_{nl} = \pm(\delta_l + 2p\pi(n-1)/H)$ and $\tau = 0, \tau = \pm\gamma_{nl} = \pm(\gamma_l + 2p\pi(n-1)/H)$, respectively, $l = 1, 2, ...\, 2p$, $n = 1, 2, 3...$, where δ_l and γ_l are the solutions of these equations only in the interval $(0, 2\pi p/H]$, ordered increasingly (see Appendix C.2). So, the zeros of the denominators are $\alpha = \pm i\,\delta_{nl}$ in the symmetric case and $\alpha = \pm i\,\gamma_{nl}$ in the anti-symmetric one. We note that δ_l is located between $(l-1)\pi/H$ and $l\pi/H$, while γ_l is located between $(2l-1)\pi/2H$ and $(2l+1)\pi/2H$ and $\gamma_{2p} = 2\pi p/H$. Moreover, if δ_l and γ_l are solutions of (3.76) and (3.77), respectively, in the interval $(0, 2\pi p/H]$ then $2\pi p/H - \delta_l$ and $2\pi p/H - \gamma_l$ are also solutions of (3.76) and (3.77), respectively. δ_l and γ_l will be numerically determined with good precision using the MATHEMATICA software [91].

We mention that the choice of H and h as in (3.78) is not restrictive for the concrete model but very advantageous since it reduces the computation only to the interval $(0, 2\pi p/H]$. Moreover, (3.78) provides us the approximate locations of the zeros and this is helpful in evaluating the asymptotic behaviour of the split functions of $K^s(\alpha)$ and $K^a(\alpha)$.

Applying the infinite product theorem we finally arrive at the representations

$$K^s(\alpha) = \frac{2(H-h)\prod\limits_{n=1}^{\infty}\left\{\left[1+\left(\frac{\alpha}{\lambda_n}\right)^2\right]\left[1+\left(\frac{\alpha}{\kappa_n}\right)^2\right]\right\}}{2c\prod\limits_{n=1}^{\infty}\left\{\prod\limits_{l=1}^{2p}\left[1+\left(\frac{\alpha}{\delta_{nl}}\right)^2\right]\right\}}\,, \tag{3.79}$$

$$K^a(\alpha) = \frac{2h(H-h)\prod\limits_{n=1}^{\infty}\left\{\left[1+\left(\frac{\alpha}{\mu_n}\right)^2\right]\left[1+\left(\frac{\alpha}{\kappa_n}\right)^2\right]\right\}}{[\,2H-2h(1-c)\,]\prod\limits_{n=1}^{\infty}\left\{\prod\limits_{l=1}^{2p}\left[1+\left(\frac{\alpha}{\gamma_{nl}}\right)^2\right]\right\}}\,. \tag{3.80}$$

The last two formulas can also be applied to the particular cases $c = 1$ and $H = 2h$. However, in these cases p will not be determined from (3.78); in fact, it can be proved that p can be assigned with any positive integer larger than 1 and so, we will take $p = 2$ if $c = 1$ or $H = 2h$.

We can now write

$$K^{s/a}(\alpha) = K_+^{s/a}(\alpha)K_-^{s/a}(\alpha)\,, \tag{3.81}$$

where

$$K_\pm^s(\alpha) = c_2^s\, e^{\pm\chi^s(\alpha)}\,\frac{\prod\limits_{n=1}^{\infty}\left\{\left(1\mp\frac{i\alpha}{\lambda_n}\right)e^{\pm i\alpha/\lambda_n}\left(1\mp\frac{i\alpha}{\kappa_n}\right)e^{\pm i\alpha/\kappa_n}\right\}}{\prod\limits_{n=1}^{\infty}\left\{\prod\limits_{l=1}^{2p}\left(1\mp\frac{i\alpha}{\delta_{nl}}\right)e^{\pm i\alpha/\frac{2p\pi n}{H}}\right\}}\,, \tag{3.82}$$

$$K_\pm^a(\alpha) = c_2^a\, e^{\pm\chi^a(\alpha)}\,\frac{\prod\limits_{n=1}^{\infty}\left\{\left(1\mp\frac{i\alpha}{\mu_n}\right)e^{\pm i\alpha/\mu_n}\left(1\mp\frac{i\alpha}{\kappa_n}\right)e^{\pm i\alpha/\kappa_n}\right\}}{\prod\limits_{n=1}^{\infty}\left\{\prod\limits_{l=1}^{2p}\left(1\mp\frac{i\alpha}{\gamma_{nl}}\right)e^{\pm i\alpha/\frac{2p\pi n}{H}}\right\}}\,, \tag{3.83}$$

with

$$c_2^s = \sqrt{\frac{H-h}{c}}\,, \quad c_2^a = \sqrt{\frac{h(H-h)}{H-h(1-c)}}\,. \tag{3.84}$$

The functions $\chi^{s/a}(\alpha)$ are arbitrary and have to be chosen to ensure that $K_+^{s/a}$ and $K_-^{s/a}$ exhibit simple asymptotic behaviour as $|\alpha| \to \infty$ in appropriate half-planes. To get rid of the infinite products it is convenient to express the functions $K_+^{s/a}$ and $K_-^{s/a}$ in terms of Γ-functions by use of the formulae (A.16) and (A.17) (see Appendix A.2) which leads to the representations

$$K_\pm^s(\alpha) = \frac{c_2^s}{c_3^s}\,\Gamma\left(\frac{1}{2}\right) \frac{\displaystyle\prod_{l=1}^{2p} \Gamma\left[\mp\frac{i\alpha H}{2p\pi} + \frac{\delta_l H}{2p\pi}\right] \exp[\pm\chi^s(\alpha) \pm i\alpha h\tfrac{2\ln 2}{\pi}]}{\Gamma\left[1 \mp i\dfrac{\alpha(H-h)}{\pi}\right]\Gamma\left(\dfrac{1}{2} \mp i\dfrac{\alpha h}{\pi}\right)}, \tag{3.85}$$

$$K_\pm^a(\alpha) = \frac{c_2^a}{c_3^a} \frac{\displaystyle\prod_{l=1}^{2p} \Gamma\left[\mp\frac{i\alpha H}{2p\pi} + \frac{\gamma_l H}{2p\pi}\right] \exp[\pm\chi^a(\alpha)]}{\Gamma\left[1 \mp i\dfrac{\alpha(H-h)}{\pi}\right]\Gamma\left(1 \mp i\dfrac{\alpha h}{\pi}\right)}, \tag{3.86}$$

where $c_3^s = \displaystyle\prod_{l=1}^{2p} \Gamma\left[\frac{\delta_l H}{2p\pi}\right]$ and $c_3^a = \displaystyle\prod_{l=1}^{2p} \Gamma\left[\frac{\gamma_l H}{2p\pi}\right]$. Employing Stirling's formula (see Appendix A.2) we find the asymptotic forms

$$K_\pm^s(\alpha) \sim B^s \exp[\pm\chi^s(\alpha) \pm i\alpha h\frac{2\ln 2}{\pi}]\,(\mp i\alpha)^{c_4^s}(c_5)^{\mp i\alpha}\,, \tag{3.87}$$
$$\text{as} \quad |\alpha| \to \infty\,,$$

$$K_\pm^a(\alpha) \sim B^a \exp[\pm\chi^a(\alpha)]\,(\mp i\alpha)^{c_4^a}(c_5)^{\mp i\alpha}\,, \quad \text{as} \quad |\alpha| \to \infty\,, \tag{3.88}$$

where $B^{s/a}$ are constants independent of α and

$$c_4^{s/a} = -\frac{1}{2}\,, \tag{3.89}$$

$$c_5 = \left(\frac{H}{2p(H-h)}\right)^{H/\pi} \left(\frac{H-h}{h}\right)^{h/\pi}. \tag{3.90}$$

(3.89) was obtained by using the properties of δ_l and γ_l mentioned after (3.78). To get a simple asymptotic behaviour of $K_\pm^{s/a}(\alpha)$ as $|\alpha| \to \infty$, we choose

$$\chi^s(\alpha) = i\,\alpha\,\ln c_5 - i\,\alpha\,h\frac{2\ln 2}{\pi}\,, \tag{3.91}$$

$$\chi^a(\alpha) = i\,\alpha\,\ln c_5\,. \tag{3.92}$$

By inserting the expressions of $\chi^s(\alpha)$, $\chi^a(\alpha)$ in (3.85), (3.86), respectively, we arrive at the final representations for $K^s_\pm$, $K^a_\pm$.

If, moreover, $\varepsilon < \min(\gamma_1, \delta_1, \kappa_1, \lambda_1)$, it can be easily checked that $K^{s/a}_-(\alpha)$ is analytic for $\tau < \varepsilon$ and $K^{s/a}_+(\alpha)$ is analytic for $\tau > -\varepsilon$, and, consequently, $K^{s/a}(\alpha)$ is analytic for $-\varepsilon < \tau < \varepsilon$.

We decompose the function on the left-hand side of (3.72) as follows

$$\begin{aligned} -\frac{\Phi_0}{K^{s/a}_-(\alpha)} &= \frac{-k}{(\varepsilon - i\alpha)K^{s/a}_-(-i\varepsilon)} + \frac{-k}{\varepsilon - i\alpha}\left[\frac{1}{K^{s/a}_-(\alpha)} - \frac{1}{K^{s/a}_-(-i\varepsilon)}\right] \\ &= L^{s/a}_+(\alpha) + L^{s/a}_-(\alpha)\,, \end{aligned} \tag{3.93}$$

where $L_-(\alpha)$ and $L_+(\alpha)$ are analytic in $\tau < \varepsilon$ and $\tau > -\varepsilon$, respectively. Let us now return to equation (3.73); we wish to determine the functions $J^{s/a}(\alpha)$. We have already shown that $K^{s/a}_-$, $K^{s/a}_+$ are asymptotic to $|\alpha|^{-1/2}$ as $|\alpha| \to \infty$. Next, some specific assumptions about the behaviour of $\varphi^{s/a}(x_1, x_2)$ in the vicinity of $x_1 = 0$ are necessary, in order to be able to use the Abelian theorem for the Fourier transform (see Appendix A.3) for finding the properties of $F^{s/a}_+$ and $F^{s/a}_-$ as $|\alpha| \to \infty$. We assume that $\varphi^{s/a}(x_1, h) = O(1)$, as $x_1 \to 0$ with $x_1 < 0$, and $\partial\varphi^{s/a}/\partial x_2\,(x_1, h^\pm) = O(x_1^{-1/2})$, as $x_1 \to 0$ with $x_1 > 0$. This implies that $F^{s/a}_- = O(|\alpha|^{-1})$ and $F^{s/a}_+ = O(|\alpha|^{-1/2})$ as $|\alpha| \to \infty$. Hence, all terms in equation (3.73) tend to zero as $|\alpha| \to \infty$. On applying Liouville's theorem, $J^{s/a}(\alpha)$ must therefore be identically zero, and so

$$F^{s/a}_-(\alpha) = L^{s/a}_-(\alpha)K^{s/a}_-(\alpha) = \frac{-k}{\varepsilon - i\alpha} + \frac{k\,K^{s/a}_-(\alpha)}{K^{s/a}_-(-i\varepsilon)(\varepsilon - i\alpha)}\,, \tag{3.94}$$

$$F^{s/a}_+(\alpha) = \frac{L^{s/a}_+(\alpha)}{K^{s/a}_+(\alpha)} = -\frac{k}{(\varepsilon - i\alpha)\,K^{s/a}_+(\alpha)\,K^{s/a}_-(-i\varepsilon)}\,. \tag{3.95}$$

3.5 The solution

Now following the steps described at the end of Section 3.3 we obtain, after straightforward calculations,

$$2A^s_1 = \frac{k\,K^s_-(\alpha)}{K^s_-(-i\varepsilon)\,(\varepsilon - i\alpha)\cosh(\alpha h)}\,, \tag{3.96}$$

$$-2A^a_1 = \frac{k\,K^a_-(\alpha)}{K^a_-(-i\varepsilon)\,(\varepsilon - i\alpha)\sinh(\alpha h)}\,, \tag{3.97}$$

$$\varphi^{s/a}(x_1,x_2)=\begin{cases}\dfrac{k\,c_2^{s/a}}{\sqrt{2\pi}\,c_3^{s/a}}\displaystyle\int_{-\infty}^{\infty}\Phi_i^{s/a}(\alpha,x_1,x_2)\,d\alpha\,, & 0\le x_2<h\,,\\[2ex] \dfrac{k\,c_2^{s/a}}{\sqrt{2\pi}\,c_3^{s/a}}\displaystyle\int_{-\infty}^{\infty}\Phi_o^{s/a}(\alpha,x_1,x_2)\,d\alpha\,, & h\le x_2\le H\,,\end{cases} \tag{3.98}$$

where

$$\Phi_i^s(\alpha,x_1,x_2)=\frac{\Gamma(1/2)}{(\varepsilon-i\alpha)\,K_-^s(-i\varepsilon)}\,\frac{\displaystyle\prod_{l=1}^{2p}\Gamma\left[\frac{i\alpha H}{2p\pi}+\frac{\delta_l H}{2p\pi}\right]}{\Gamma\left[1+i\dfrac{\alpha(H-h)}{\pi}\right]}\times \frac{\Gamma\left(\frac{1}{2}-i\dfrac{\alpha h}{\pi}\right)}{\pi}\,\cosh(\alpha x_2)\,e^{-i\alpha(x_1+\ln c_5)}\,, \tag{3.99}$$

$$\Phi_o^s(\alpha,x_1,x_2)=\frac{\Gamma(1/2)}{(\varepsilon-i\alpha)\,K_-^s(-i\varepsilon)}\,\frac{\displaystyle\prod_{l=1}^{2p}\Gamma\left[\frac{i\alpha H}{2p\pi}+\frac{\delta_l H}{2p\pi}\right]}{\Gamma\left[\frac{1}{2}+i\dfrac{\alpha h}{\pi}\right]}\times \frac{\Gamma\left(1-i\dfrac{\alpha(H-h)}{\pi}\right)}{\alpha(H-h)}\,\sinh(\alpha(H-x_2))\,e^{-i\alpha(x_1+\ln c_5)}\,, \tag{3.100}$$

$$\Phi_i^a(\alpha,x_1,x_2)=\frac{1}{(\varepsilon-i\alpha)\,K_-^a(-i\varepsilon)}\,\frac{\displaystyle\prod_{l=1}^{2p}\Gamma\left[\frac{i\alpha H}{2p\pi}+\frac{\gamma_l H}{2p\pi}\right]}{\Gamma\left[1+i\dfrac{\alpha(H-h)}{\pi}\right]}\times \frac{\Gamma\left(1-i\dfrac{\alpha h}{\pi}\right)}{\alpha h}\,\sinh(\alpha x_2)\,e^{-i\alpha(x_1+\ln c_5)}\,, \tag{3.101}$$

$$\Phi_o^a(\alpha,x_1,x_2)=\frac{1}{(\varepsilon-i\alpha)\,K_-^a(-i\varepsilon)}\,\frac{\displaystyle\prod_{l=1}^{2p}\Gamma\left[\frac{i\alpha H}{2p\pi}+\frac{\gamma_l H}{2p\pi}\right]}{\Gamma\left[1+i\dfrac{\alpha h}{\pi}\right]}\times \frac{\Gamma\left(1-i\dfrac{\alpha(H-h)}{\pi}\right)}{\alpha(H-h)}\,\sinh(\alpha(H-x_2))\,e^{-i\alpha(x_1+\ln c_5)}\,. \tag{3.102}$$

The indices 'i' and 'o' are labels for 'inside' and 'outside' the channel. In order to derive (3.99)-(3.102) we have used the formulae (A.13), (A.14). The integrals can be evaluated using the residue theorem (see [89]). We close the contour by a semicircle of radius R and center at $\alpha = 0$. The contour is closed in the lower half-plane when $x_1 > 0$ and in the upper half-plane when $x_1 < 0$ (see Fig. 3.5). We denoted by $z_i^{\mp}$, $i = 1, 2, ...n$, the singularities of the functions to be integrated in the lower half-plane and in the upper half-plane, respectively. Since K_- is asymptotic to $|\alpha|^{-1/2}$ as $|\alpha| \to \infty$ we can prove by

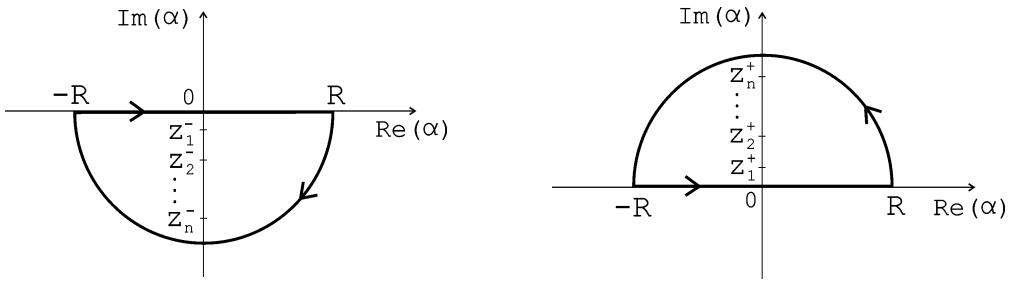

Figure 3.5: Closed contours corresponding to the case $x_1 > 0$ (left) and to the case $x_1 < 0$ (right)

using Jordan's lemma (see Appendix A.3) that the contribution of the semicircle to the integrals vanishes when R tends to infinity. We employ the following

$$\varphi^{s/a}(x_1, x_2) = \begin{cases} \varphi_1^{s/a}(x_1, x_2)\,, & 0 \le x_2 \le h\,,\ 0 \le x_1\,, \\ \varphi_2^{s/a}(x_1, x_2)\,, & 0 \le x_2 \le h\,,\ x_1 \le 0\,, \\ \varphi_3^{s/a}(x_1, x_2)\,, & h < x_2 \le H\,,\ x_1 \le 0\,, \\ \varphi_4^{s/a}(x_1, x_2)\,, & h < x_2 \le H\,,\ 0 \le x_1\,. \end{cases} \tag{3.103}$$

Taking into account that the singularities of Φ_i^s in the lower half-plane are $-i\varepsilon$ and $-i\lambda_n$ and that the singularities of Φ_o^s in the same region are $-i\varepsilon$ and $-i\kappa_n$, for $n = 1, 2, 3, ...$, we can write

$$\varphi_1^s(x_1, x_2) = -2\pi i \frac{kc_2^s}{\sqrt{2\pi}c_3^s}\left[\sum_{n=1}^{\infty} \mathrm{Res}(\Phi_i^s, -i\lambda_n) + \mathrm{Res}(\Phi_i^s, -i\varepsilon)\right]\,, \tag{3.104}$$

$$\varphi_4^s(x_1, x_2) = -2\pi i \frac{kc_2^s}{\sqrt{2\pi}c_3^s}\left[\sum_{n=1}^{\infty} \mathrm{Res}(\Phi_o^s, -i\kappa_n) + \mathrm{Res}(\Phi_o^s, -i\varepsilon)\right]\,, \tag{3.105}$$

where $\mathrm{Res}(f, z_0)$ denotes the residue of the function f in the point z_0 (see [89] for the definition of the residue). In the upper-half plane Φ_i^s and Φ_o^s are both singular in $i\delta_{nl}$, for $l = 1, 2, ...2p$, $n = 1, 2, 3, ...$ so we obtain

$$\varphi_{2/3}^s(x_1, x_2) = 2\pi i \frac{kc_2^s}{\sqrt{2\pi}c_3^s}\left[\sum_{n=1}^{\infty}\sum_{l=1}^{2p} \mathrm{Res}(\Phi_{i/o}^s, i\delta_{nl})\right]\,. \tag{3.106}$$

Straightforward calculations based on the use of the formula (A.12) and invoking the limit $\varepsilon \to 0$ yield

$$\varphi_1^s(x_1,x_2) = V\sum_{n=1}^{\infty}\mathbf{a_{1n}^s}\,\cos(\lambda_n\,x_2)e^{-\lambda_n\,x_1} + V\,, \tag{3.107}$$

$$\varphi_2^s(x_1,x_2) = V\sum_{n=1}^{\infty}\sum_{l=1}^{2p}\mathbf{a_{2\,nl}^s}\,\cos(\delta_{nl}\,x_2)\,e^{\delta_{nl}\,x_1}\,, \tag{3.108}$$

$$\varphi_3^s(x_1,x_2) = V\sum_{n=1}^{\infty}\sum_{l=1}^{2p}\mathbf{a_{3\,nl}^s}\,\sin(\delta_{nl}\,(H-x_2))\,e^{\delta_{nl}\,x_1}\,, \tag{3.109}$$

$$\varphi_4^s(x_1,x_2) = V\sum_{n=1}^{\infty}\mathbf{a_{4n}^s}\sin(\kappa_n(H-x_2))e^{-\kappa_n\,x_1} + \frac{V(H-x_2)}{H-h}\,, \tag{3.110}$$

where

$$\mathbf{a_{1n}^s} = \frac{1}{c_3^s}\,\frac{\prod_{j=1}^{2p}G_j^s(\lambda_n)}{\Gamma(1+\lambda_n\,\frac{H-h}{\pi})}\,\frac{(-1)^n\sqrt{\pi}}{\lambda_n\,(n-1)!\,h}\,e^{-\lambda_n\,\ln c_5}\,, \tag{3.111}$$

$$\mathbf{a_{2nl}^s} = \frac{1}{c_3^s}\,\frac{\prod_{j=1}^{l-1}G_j^s(-\delta_{nl})\prod_{j=l+1}^{2p}G^s(-\delta_{nl})\,\Gamma\left[1/2+\delta_{nl}\,\frac{h}{\pi}\right]}{\Gamma\left(1-\delta_{nl}\,\frac{H-h}{\pi}\right)}\times$$
$$\frac{(-1)^{n-1}\,\sqrt{\pi}\,2p}{\delta_{nl}\,(n-1)!\,H}\,e^{\delta_{nl}\ln c_5}\,, \tag{3.112}$$

$$\mathbf{a_{3nl}^s} = \frac{1}{c_3^s}\,\frac{\prod_{j=1}^{l-1}G_j^s(-\delta_{nl})\prod_{j=l+1}^{2p}G^s(-\delta_{nl})\,\Gamma\left[1+\delta_{nl}\frac{H-h}{\pi}\right]}{\Gamma\left(1/2-\delta_{nl}\,\frac{h}{\pi}\right)}\times$$
$$\frac{(-1)^{n-1}\,\sqrt{\pi}\,\pi\,2p}{\delta_{nl}^2\,(n-1)!\,H\,(H-h)}\,e^{\delta_{nl}\ln c_5}\,, \tag{3.113}$$

$$\mathbf{a_{4n}^s} = \frac{1}{c_3^s}\,\frac{\prod_{j=1}^{2p}G_j^s(\kappa_n)}{\Gamma(1/2+\kappa_n\,\frac{h}{\pi})}\,\frac{(-1)^n\sqrt{\pi}}{\kappa_n\,n!\,(H-h)}\,e^{-\kappa_n\,\ln c_5} \tag{3.114}$$

and where $G_j^s(x) = \Gamma\left[(x+\delta_j)\,\frac{H}{2p\pi}\right]$.

The solution for the anti-symmetric problem is derived in the same manner. The singularities of Φ_i^a in the lower half-plane are $-i\varepsilon$ and $-i\mu_n$ while the the singularities of Φ_o^a in the same region are $-i\varepsilon$ and $-i\kappa_n$, for $n = 1, 2, 3, ...$ Then we can write

$$\varphi_1^a(x_1, x_2) = -2\pi i \frac{k c_2^a}{\sqrt{2\pi} c_3^a} \left[\sum_{n=1}^{\infty} \mathrm{Res}(\Phi_i^a, -i\mu_n) + Rez(\Phi_i^a, -i\varepsilon) \right] , \tag{3.115}$$

$$\varphi_4^a(x_1, x_2) = -2\pi i \frac{k c_2^a}{\sqrt{2\pi} c_3^a} \left[\sum_{n=1}^{\infty} \mathrm{Res}(\Phi_o^a, -i\kappa_n) + Rez(\Phi_o^a, -i\varepsilon) \right] . \tag{3.116}$$

In the upper-half plane Φ_i^a and Φ_o^a are both singular in $i\gamma_{nl}$, for $l = 1, 2, ...2p$, $n = 1, 2, 3, ...$ so we obtain

$$\varphi_{2/3}^a(x_1, x_2) = 2\pi i \frac{k c_2^a}{\sqrt{2\pi} c_3^a} \left[\sum_{n=1}^{\infty} \sum_{l=1}^{2p} \mathrm{Res}(\Phi_{i/o}^a, i\gamma_{nl}) \right] . \tag{3.117}$$

$$\varphi_1^a(x_1, x_2) = V \sum_{n=1}^{\infty} \mathbf{a_{1n}^a} \sin(\mu_n x_2) e^{-\mu_n x_1} + \frac{V x_2}{h} , \tag{3.118}$$

$$\varphi_2^a(x_1, x_2) = V \sum_{n=1}^{\infty} \sum_{l=1}^{2p} \mathbf{a_{2\,nl}^a} \sin(\gamma_{nl} x_2) e^{\gamma_{nl} x_1} , \tag{3.119}$$

$$\varphi_3^a(x_1, x_2) = V \sum_{n=1}^{\infty} \sum_{l=1}^{2p} \mathbf{a_{3\,nl}^a} \sin(\gamma_{nl} (H - x_2)) e^{\gamma_{nl} x_1} , \tag{3.120}$$

$$\varphi_4^a(x_1, x_2) = V \sum_{n=1}^{\infty} \mathbf{a_{4n}^a} \sin(\kappa_n (H - x_2)) e^{-\kappa_n x_1} + \frac{V(H - x_2)}{H - h} , \tag{3.121}$$

where

$$\mathbf{a_{1n}^a} = \frac{1}{c_3^a} \frac{\prod_{j=1}^{2p} G_j^a(\mu_n)}{\Gamma(1 + \mu_n \frac{H-h}{\pi})} \frac{(-1)^n}{\mu_n \, n! \, h} e^{-\mu_n \ln c_5} , \tag{3.122}$$

$$\mathbf{a_{2nl}^a} = \frac{1}{c_3^a} \frac{\prod_{j=1}^{l-1} G_j^a(-\gamma_{nl}) \prod_{j=l+1}^{2p} G^a(-\gamma_{nl}) \, \Gamma\left[1 + \gamma_{nl} \frac{h}{\pi}\right]}{\Gamma\left(1 - \gamma_{nl} \frac{H-h}{\pi}\right)} \times$$

$$\frac{(-1)^{n-1} \pi \, 2p}{\gamma_{nl}^2 \, (n-1)! \, H \, h} e^{\gamma_{nl} \ln c_5} , \tag{3.123}$$

$$\mathbf{a^a_{3nl}} = \frac{1}{c_3^a} \frac{\prod_{j=1}^{l-1} G_j^a(-\gamma_{nl}) \prod_{j=l+1}^{2p} G^a(-\gamma_{nl})\, \Gamma\left[1+\gamma_{nl}\dfrac{H-h}{\pi}\right]}{\Gamma\left(1-\gamma_{nl}\,\dfrac{h}{\pi}\right)} \times$$

$$\frac{(-1)^{n-1}\,\pi\,2p}{\gamma_{nl}^2\,(n-1)!\,H\,(H-h)}\, e^{\gamma_{nl}\ln c_5}\,, \tag{3.124}$$

$$\mathbf{a^a_{4n}} = \frac{1}{c_3^a} \frac{\prod_{j=1}^{2p} G_j^a(\kappa_n)}{\Gamma(1+\kappa_n\,\dfrac{h}{\pi})} \frac{(-1)^n}{\kappa_n\, n!\,(H-h)}\, e^{-\kappa_n\,\ln c_5}\,, \tag{3.125}$$

and where $G_j^a(x) = \Gamma\left[(x+\gamma_j)\,\dfrac{H}{2p\pi}\right]$.

The solution of (3.1)-(3.8) can be written as

$$\varphi(x_1,x_2) = \begin{cases} \varphi_1(x_1,x_2)\,, & |\,x_2\,| \le h\,,\ 0 \le x_1\,, \\ \varphi_2(x_1,x_2)\,, & |\,x_2\,| \le h\,,\ x_1 \le 0\,, \\ \varphi_3(x_1,x_2)\,, & h < |\,x_2\,| \le H\,,\ x_1 \le 0\,, \\ \varphi_4(x_1,x_2)\,, & h < |\,x_2\,| \le H\,,\ 0 \le x_1\,, \end{cases} \tag{3.126}$$

where

$$\varphi_i(x_1,x_2) = \varphi_i^s(x_1,|\,x_2\,|) + \mathrm{sign}(x_2)\,\varphi_i^a(x_1,|\,x_2\,|) \tag{3.127}$$

for $i = 1,2,3,4$.

In the numerical representation of the solution the infinite sums from (3.107)-(3.110) and (3.118)-(3.121) will be truncated after the Nth term.

3.6 Electric field near the electrode edges

In order to determine the behaviour of the electric field at the ends of the electrodes, we need to evaluate the quantities $\varphi_{,1}^{s/a}$ and $\varphi_{,2}^{s/a}$ when $(x_1,x_2) \to (0,h^{\pm})$. Differentiating and using the properties of the Fourier transform yields

$$\varphi_{,1}^{s/a}(x_1,x_2) = \frac{1}{\sqrt{2\pi}} \int_{-\infty}^{\infty} (-i)\alpha\Phi^{s/a}(\alpha,x_2)\, e^{-i\alpha x_1} d\alpha\,, \tag{3.128}$$

$$\varphi_{,2}^{s/a}(x_1,x_2) = \frac{1}{\sqrt{2\pi}} \int_{-\infty}^{\infty} \Phi_{,2}^{s/a}(\alpha,x_2)\, e^{-i\alpha x_1} d\alpha\,, \tag{3.129}$$

where $\Phi^{s/a}(\alpha,x_2)$ are found by inserting (3.96) and (3.97) in (3.60) and (3.64), respectively. Let us consider first the asymptotic evaluation of $\varphi_{,1}^{s/a}$ when $(x_1,x_2) \to (0,h^-)$. The

integral can be written as the sum

$$\varphi_{,1}^{s/a}(x_1,x_2)=\int\limits_{-\infty}^{-M}E(\alpha,x_1,x_2)\,d\alpha+\int\limits_{-M}^{M}E(\alpha,x_1,x_2)\,d\alpha+\int\limits_{M}^{\infty}E(\alpha,x_1,x_2)\,d\alpha\,, \tag{3.130}$$

where $M>0$ and $E(\alpha,x_1,x_2)=\dfrac{k\,K_-^s(\alpha)\cosh(\alpha x_2)(-i)\alpha}{\sqrt{2\pi}K_-^s(-i\varepsilon)\,(\varepsilon-i\alpha)\cosh(\alpha h)(\varepsilon-i\alpha)}\,e^{-i\alpha x_1}$. If we assume that M is sufficiently large, we can replace E in the first and third integrals with its asymptotic expression valid for large arguments. The second term can be neglected because E is a bounded function of α on the interval $[-M,M]$ and, consequently, $\int\limits_{-M}^{M}E\,d\alpha$ will be a continuous function of x_1. By using (3.87) and $\cosh(\alpha x_2)/\cosh(\alpha h)\sim e^{|\alpha|(x_2-h)}$ when $\alpha\to\pm\infty$, we obtain

$$\varphi_{,1}^{s}\sim\frac{k\,B^s}{\sqrt{2\pi}\,K_-^s(-i\varepsilon)}\left[\int\limits_{-\infty}^{-M}\frac{e^{i\alpha x_1+\alpha(x_2-h)}}{\sqrt{-i\alpha}}\,d\alpha+\int\limits_{M}^{\infty}\frac{e^{-i\alpha x_1+\alpha(x_2-h)}}{\sqrt{i\alpha}}\,d\alpha\right]\,, \tag{3.131}$$

as $(x_1,x_2)\to(0,h^-)$. If we take the limit $M\to 0$, we may ignore the resulting finite contributions because they do not alter the singular behaviour. Using the formula [1, pp. 255]

$$\int\limits_0^{\infty}e^{-t\alpha}\,\alpha^{-1/2}d\alpha=\sqrt{\frac{\pi}{t}}\,,\quad \operatorname{Re}t>0\,, \tag{3.132}$$

in (3.131), yields

$$\varphi_{,1}^{s}\sim\frac{\sqrt{2}\,k\,B^s}{K_-^s(-i\varepsilon)}\,\frac{\sin(\theta/2)}{\sqrt{r}}\,,\quad\text{where}\quad re^{i\theta}=x_1+i(x_2-h)\,. \tag{3.133}$$

The other cases are treated analogously and similar expressions are derived. After applying the limit $\varepsilon\to 0$ we readily find

$$\varphi_{,1}^{s/a}\sim\frac{\sqrt{2}\,k\,B^{s/a}}{c_2^{s/a}}\,\frac{\sin(\theta/2)}{\sqrt{r}}\,,\quad \varphi_{,2}^{s/a}\sim\frac{\sqrt{2}\,k\,B^{s/a}}{c_2^{s/a}}\,\frac{\cos(\theta/2)}{\sqrt{r}}\,, \tag{3.134}$$

when $(x_1,x_2)\to(0,h^{\pm})$ and where $x_1\pm i(x_2-h)=re^{i\theta}$. The singular behaviour of the electric field

$$E^{s/a}(x_1,x_2)=\sqrt{(\varphi_{,1}^{s/a})^2+(\varphi_{,x_2}^{s/a})^2} \tag{3.135}$$

is then given by

$$E^{s/a}(x_1,x_2)\sim\frac{\sqrt{2}\,k\,B^{s/a}}{c_2^{s/a}}\,\frac{1}{\sqrt{r}}\quad,r=\sqrt{x_1^2+(x_2-h)^2}\,, \tag{3.136}$$

when $(x_1,x_2)\to(0,h^{\pm})$. Thus, we have established square root singularities of the electric field at the electrode tips.

3.7 Results and discussion

The analytical solution given at the end of Section 3.5 is expressed in terms of infinite series. It can be easily checked that each term of the series satisfies the corresponding boundary value problem but only the limit of the series is a continuous function in $x_1 = 0$. To obtain a better precision in further use of the solution one should take the truncation number N for the infinite series, as large as the used software permits.

It is important to remark that the solution found here has a high degree of generality. First, it can be applied to different configurations of the electrodes (see Table 3.1). Each of these configurations can be extended to the case of finite electrodes in which the far edges of the electrodes do not interact. To determine the appropriate length of the electrodes one can use the following criterion

$$|E_{x_1}(x_1, x_2)| < 0.05\, E_\infty(x_2) \quad \text{for} \quad x_1 > l\,, \ |x_2| \le H \tag{3.137}$$

where l is the half length of the electrodes, $E_{x_1}(x_1, x_2) = \varphi_{,1}(x_1, x_2)$ and $E_\infty(x_2) = \lim\limits_{x_1 \to \infty} \sqrt{(\varphi_{,1}(x_1, x_2))^2 + (\varphi_{,2}(x_1, x_2))^2}$. This means that the electric field becomes approximately uniform for $x_1 > l$. For instance, a parametric study done for an anti-symmetric configuration, for values of H, h and c so that $2 \le H/h \le 100$ and $0.01 < c < 50$, shows that (3.137) holds for $x_1 \ge H - h$ outside the channel and for $x_1 \ge 0.8\, h$ inside the channel. Consequently, one can build the solution for the case of two finite electrodes of length $2\, l$, with $l > H - h$, charged in an anti-symmetric way, by taking the solution (3.118)-(3.121) for $x_1 < l$ and extending it by symmetry with respect to the line $x_1 = l$. Similar studies can be done for each case, and they are very useful for the numerical modeling.

Second, the solution is depending on parameters like H/h and c, each of them having a certain influence on the profile of the electric potential. However, this Chapter will not contain a detailed discussion of all these cases. We consider it more reasonable to do this in connection with the investigations of the flow in order to determine the optimal parameters for the desired effects on the fluid flow. We limit ourselves only to stating a number of configurations in Table 3.1, offering a few comments and postponing further studies of the solution to Chapter 5 in which we will examine the influence of the parameters on the channel flow of an electrorheological fluid.

In all the graphical representations that follow we use the dimensionless quantities

$$\tilde{x_1} = \frac{x_1}{h}\,, \ \ \tilde{x_2} = \frac{x_2}{h}\,, \ \ \tilde{H} = \frac{H}{h}\,, \ \ \tilde{h} = 1\,, \tag{3.138}$$

$$\tilde{\varphi}(\tilde{x_1}, \tilde{x_2}) = \frac{\varphi(x_1, x_2)}{V}\,, \ \ \tilde{E}(\tilde{x_1}, \tilde{x_2}) = E(x_1, x_2)\frac{h}{V}\,. \tag{3.139}$$

All plots are done for the case of semi-infinite electrodes and in the plots from Figures 3.6, 3.7 ,3.8 and 3.9 we use the truncation number $N = 100$. We note that the electric permittivities ε_1 and ε_2 do not appear explicitly in the solution. Only their ratio c influences the results through γ_{nl} and δ_{nl}, which are computed numerically from equations (3.76) and (3.77). Since the ERF (Rheobay for example) can exhibit values of the electric

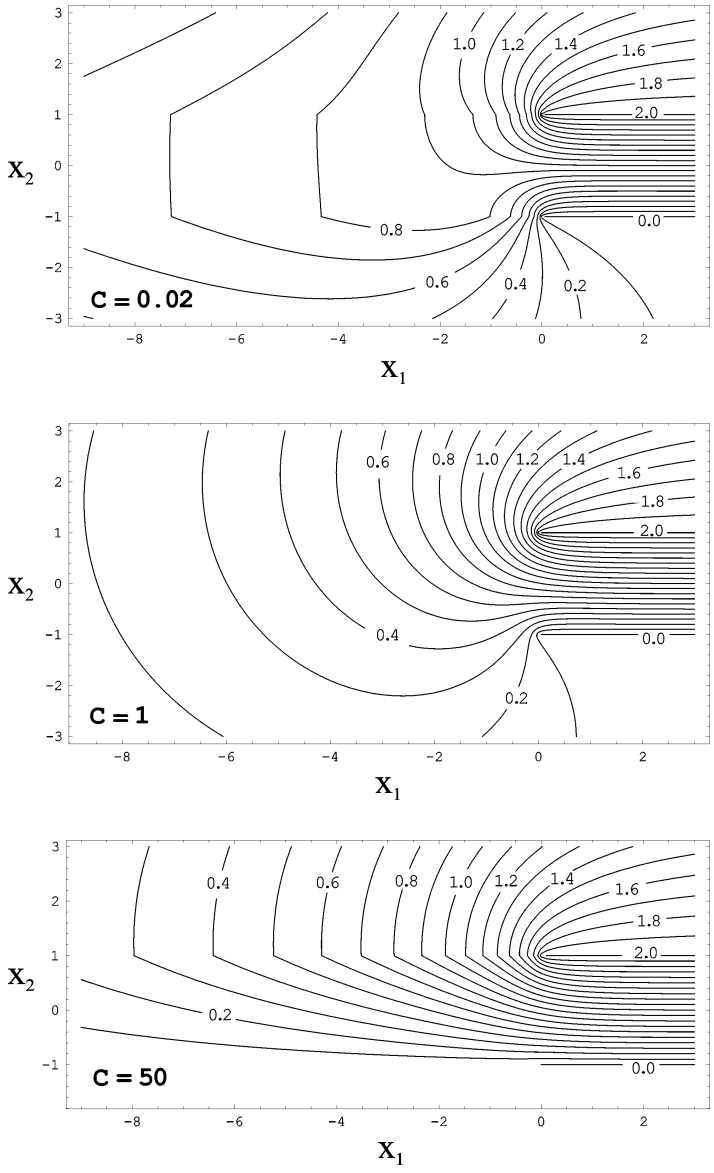

Figure 3.6: Equipotential lines $\tilde{\varphi}(\tilde{x_1}, \tilde{x_2}) = \text{constant}$ for different values of $c = \varepsilon_1/\varepsilon_2$ ($\tilde{H} = 10$)

Table 3.1: Schematic diagrams of the configurations for which the solution is applicable

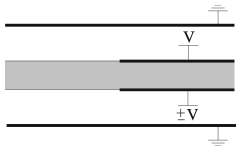	2 semi-infinite electrodes symmetrically or anti-symmetrically charged along the channel walls and 2 infinite grounded electrodes
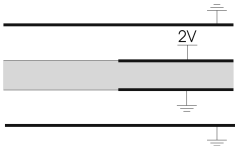	2 semi-infinite electrodes non-symmetrically charged along the channel walls and 2 infinite grounded electrodes
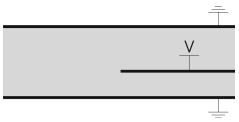	one semi-infinite electrode placed inside the fluid flowing through a grounded channel

permittivity around 10^{-9} As/Vm (see [29, p. 53]) which is quite large, it is reasonable to consider small values of the ratio c and we take $c = 0.02$ as a usual technical value. Nevertheless, we show in Fig. 3.6 what effects are produced by different values of c on the electric potential and, consequently, on the electric field. The potential lines are equidistant, every second contour being marked. The contours are shifted upwards and the non-symmetry becomes more pronounced as c is increased. If $c = 50$ the electric potential in the channel is faster decreasing when x_1 tends to $-\infty$ than if $c = 0.02$. As was to be expected, for $c = 0.02$, the electric field outside the channel is larger than inside and this is reversed for $c = 50$. In particular this means that the insulator surrounding the channel has a significant influence on the flow behaviour of the ERF inside the channel.

Finally, besides the non-symmetric case we want to refer to the other cases, to which our results can be applied (see Table 3.1). One can study the electric field also in the anti-symmetric case. Here the potential in the middle of the channel vanishes. Therefore, one can use the solution (3.118)-(3.125) with $c = 1$ to characterize the case of a single electrode, placed inside the fluid, parallel with the channel walls which are considered to be grounded. To illustrate this case we plotted in Fig. 3.7 the modulus of the electric field, $\tilde{E}(\tilde{x_1}, \tilde{x_2}) = \sqrt{(\tilde{\varphi}_{,1}(\tilde{x_1}, \tilde{x_2}))^2 + (\tilde{\varphi}_{,2}(\tilde{x_1}, \tilde{x_2}))^2}$ produced by an electrode placed at $\tilde{x_2} = \tilde{H}/2$. In Fig. 3.8 the electric field modulus, $\tilde{E}(\tilde{x_1}, \tilde{x_2})$ in the anti-symmetric case is compared with that in the non-symmetric case for $c = 0.02$. It can be seen that the profiles are quite similar near the electrode ends but become very different for $\tilde{x_1} < -0.5$. In Fig. 3.7 and in Fig. 3.8 every second contour is marked, except when the lines are too close to one

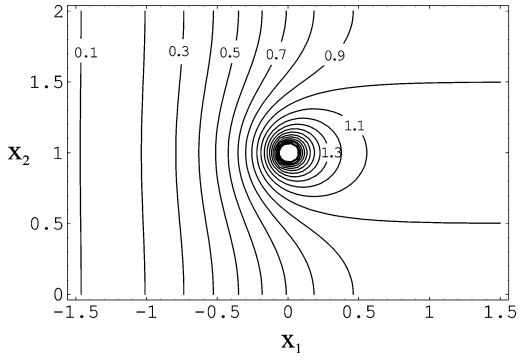

Figure 3.7: Contour lines of the electric field modulus, $\tilde{E}(\tilde{x_1}, \tilde{x_2})$, around the edge of a single electrode placed inside the fluid; the channel walls are placed at $\tilde{x_2} = 0$ and $\tilde{x_2} = \tilde{H}$ and they are grounded ($c = 1$, $\tilde{H} = 2\tilde{h}$)

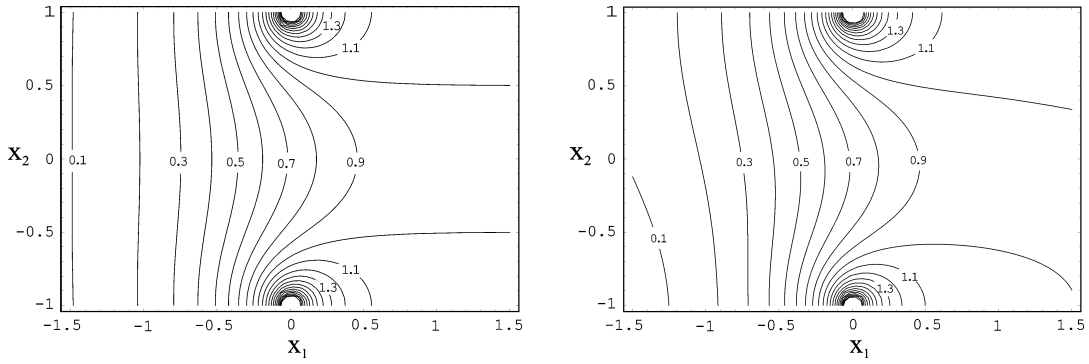

Figure 3.8: Contour lines of $\tilde{E}(\tilde{x_1}, \tilde{x_2})$ inside the channel, in the anti-symmetric (left) and non-symmetric (right) configurations ($c = 0.02$, $\tilde{H} = 10$)

another. In the white regions around the points where the electrode edges are situated, the dimensionless electric field is greater than 3.

3.7.1 Comparison with the numerical results

The analytical solution cannot be employed to determine the electric field in more complex electrode configurations so, as we mentioned already in Chapter 2, we will use a numerical program to do this. For the numerical simulation we consider a bounded domain also in the x_1-direction: $x_1 \leq L$. The inlet and outlet conditions in $x_1 = L$ and $x_1 = -L$, respectively, for the electrical problem are continuity conditions in the derivatives of the electric potential

$$\varphi_{,i}(\pm L^+, x_2) = \varphi_{,i}(\pm L^-, x_2)\ ,\ \ |x_2| \leq H\ ,\ i = 1, 2\ . \tag{3.140}$$

The analytical solution can be used to test and benchmark the numerical program. To do this we compare the analytical solution for one of the configurations treated in this Chapter

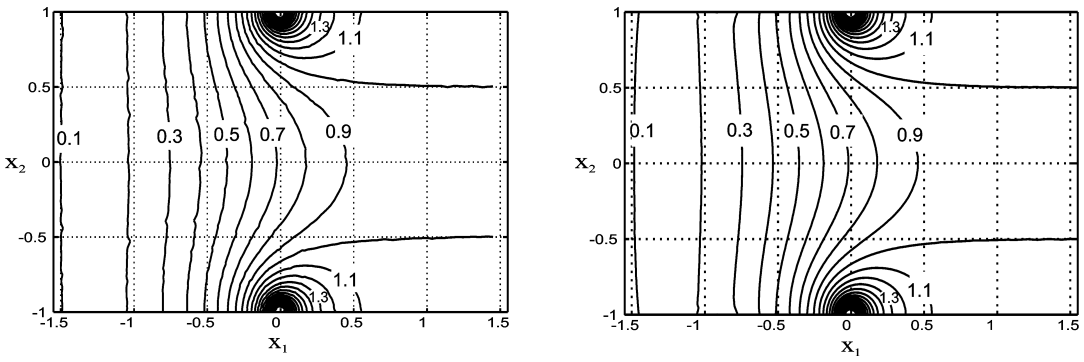

Figure 3.9: Contour lines of $\tilde{E}(\tilde{x_1}, \tilde{x_2})$ inside the channel, in the anti-symmetric case obtained numerically (left) and analytically-numerically (right) ($c = 0.02$, $\tilde{H} = 10$)

with the solution of the same problem but obtained numerically. The software used in our approaches is called FEMLAB [21] and it is a program based on the finite element method. Besides the analytical and numerical way to determine the solution, there is another mixed way, in which we use the analytical solution in the numerical program in order to reduce the domain and consequently, the memory space and computing time. We can do this by imposing in the numerical program the Dirichlet boundary conditions on the whole channel walls deduced from the analytical solution. In this way the domain of the problem is reduced to the channel. Since the expressions of the analytical solutions on the walls are too complicated and create difficulties when trying to introduce them into FEMLAB, we will interpolate them and use polynomials which approximate in a good way the original solution. In Figures 3.9 we plotted the contour lines of the electric field obtained numerically and by using the fore-mentioned analytical-numerical method for the same configuration and values of the parameters as in Fig. 3.8 (left). The good agreement obtained between the analytical plot and the numerical ones provides the validation of the numerical method.

3.7.2 The behaviour of the truncated solution close to the singular points

For further use of the solution in a numerical approach it is important to know how the truncated solutions approximate the singular behaviour of the analytical solution found in Section 3.6. We are interested to find out how large the domain is within which the truncated solutions deviate from the exact singular behaviour and how the values of the electric field differ for different truncation numbers N in this domain. To study this, we compare the electric field modulus $\tilde{E}(\tilde{x_1}, \tilde{x_2})$ in the anti-symmetric case, close to the electrode tip situated at the point $(0, 1)$ (see Fig. 3.10), calculated by taking into account $N = 10, 50, 100$ and 300 terms in the sums (3.118)-(3.121). In Fig. 3.10 we have drawn the lines along which we plot the electric field $\tilde{E}(t) = \tilde{E}(\tilde{x_1}(t), \tilde{x_2}(t))$, t being the curve

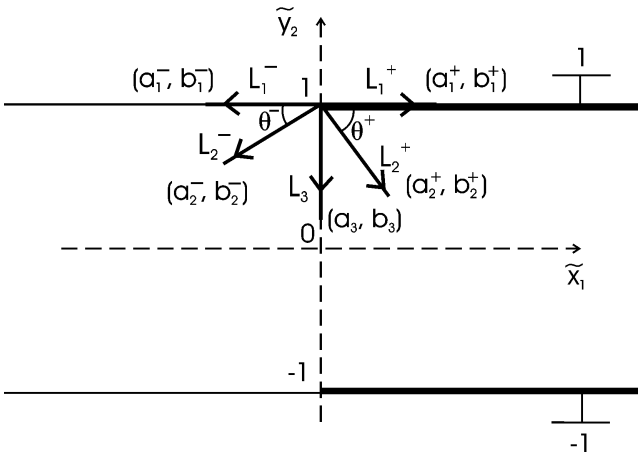

Figure 3.10: Visualisation of the cuts along which the electric field was plotted in Figures 3.11-3.13

parameter

$$L_i^{\pm} \; : \; (\tilde{x_1}(t), \tilde{x_2}(t)) = (a_i^{\pm} t \, , \; t(b_i^{\pm} - 1) + 1) \, , \quad i = 1, 2 \, , \tag{3.141}$$

$$L_3 \; : \; (\tilde{x_1}(t), \tilde{x_2}(t)) = (a_3 t \, , \; t(b_3 - 1) + 1) \, , \tag{3.142}$$

where $t \in [0, 1]$, $a_3 = 0$, $b_1^{\pm} = 1$. The Figures 3.11-3.13 are using $-a_1^- = a_1^+ = 0.3$, $a_2^- = -0.22$, $b_2^- = 0.8$, $a_2^+ = 0.1$, $b_2^+ = 0.71$ and $b_3 = 0.7$. These values are chosen so that the length of the cuts is approximately 0.3. Consequently we will describe the singular behaviour around the electrode end in the channel, in the vicinity of the radius 0.3. The coordinate t is represented on a logarithmic scale.

A first remark concerning all the figures is that the higher the truncation number N is, the higher is the electric field in the singular point. This reflects the singular behaviour found in Section 3.6. From Fig. 3.11 one can see that the behaviour of the truncated functions close to the singularity, along the channel wall is symmetric with respect to the vertical axes. Since L_2^- and L_2^+ are not symmetrically chosen with respect to the vertical axes, there are differences between the two plots. If we denote by E_{Ni} the electric field calculated for the truncation number N_i, where $N_1 = 10$, $N_2 = 50$, $N_3 = 100$, $N_4 = 300$, we can use the criterion

$$\text{Find } t_0 \text{ so that} \quad \frac{E_{Ni} - E_{Ni-1}}{E_{Ni-1}} < \frac{p}{100} \quad \text{for } t > t_0 \, , \tag{3.143}$$

to determine the vicinity diameter outside which the electric field is not affected by the singularity, with a precision given by the number p. We found (for $\theta^{\pm} < 75°$) $p = 1$ and $t_0 = 0.05$ for $i = 4$. Consequently, we can use the truncated solution for $N = 100$ with a good precision for $t > 0.05$. This means that the diameter of the vicinity around the singularity is reduced to 0.015 i.e. 0.75% of the channel height.

As the cut is approaching the vertical axes ($\theta^{\pm} \to 90°$) the curves start to oscillate.

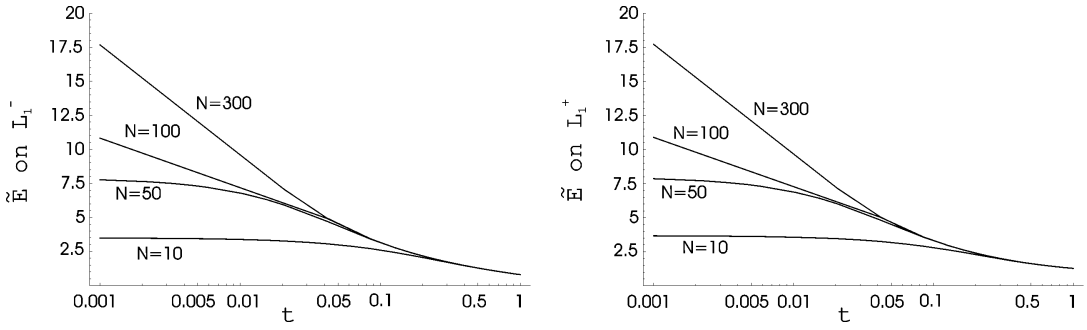

Figure 3.11: Modulus of the electric field along the lines L_1^- (left) and L_1^+ (right) for different truncation numbers N

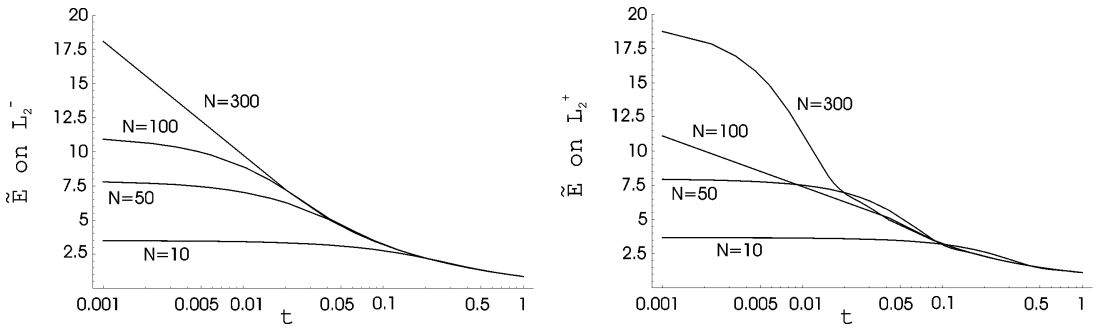

Figure 3.12: Modulus of the electric field along the lines L_2^- (left) and L_2^+ (right) for different truncation numbers N

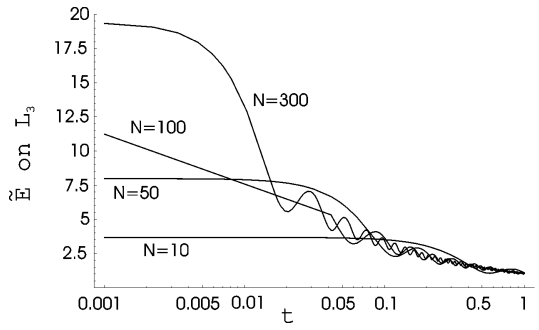

Figure 3.13: Modulus of the electric field along the line L_3 for different truncation numbers N

The most oscillating curves are found on L_3 as can be seen in Fig. 3.13. Here one can observe also that the oscillations become more frequent and smaller for greater N.

The same study can be done also numerically, by using the numerical solution obtained with FEMLAB. The different behaviour around the singularity is given in this case by the way of the mesh refinement around the singular point. For each truncation number one can find a corresponding mesh in the numerical program. The advantage of the numerical approach is that the oscillations illustrated in Fig. (3.13) are avoided and the solution has a more appropriate form to be implemented in the mechanical problem.

3.8 Conclusions

In this Chapter we have found analytical solutions for the electric potential for different mixed boundary value problems by use of the Wiener-Hopf method. These problems arise from our study of the electrorheological fluids in the channel flow under the influence of a non-uniform electric field. Because the dielectric permittivity of the ERF is very high, a considerable jump in the x_2-derivatives has to be taken into account. The solution is given in terms of infinite series involving Gamma functions. The results can be used to describe the electric field generated between two infinite grounded electrodes by either one long electrode or two long electrodes charged in an anti-symmetric or a non-symmetric way. The electric field in the vicinity of the electrode edges is asymptotically evaluated. Some parametric studies are made with respect to the ratio between the permittivity of the electrorheological fluid and the permittivity of the isolating material outside the channel. We compare the analytical with numerical solutions and find good agreement. This result is interpreted as a validation of the numerical method which will be used further for more complex electrode configurations.

Chapter 4

The mechanical problem

4.1 Constitutive laws for the Cauchy stress tensor proposed in the literature

A key step in electrorheology is to relate the theory with practical applications namely with the results from measurements and computations. Usually, the approaches within the theory are too abstract, general and difficult to use in concrete situations whereas the empirical approaches are applicable but often too particular. In the electrorheological field noticeable efforts are made from both sides to describe in a better and more accurate way the electrorheological fluids. We will review briefly the most important theoretical models for the expression of the Cauchy stress tensor according to $(2.52)_1$ proposed in the literature up to now. While these proposals are three-dimensional expressions for the Cauchy stress, in most applications one-dimensional models are used. Since we need two-dimensional models in our numerical computations, we can either generalize the one-dimensional models or choose particular forms of the general models taking into account also the experimental characterization of the ERF.

The most general form of the constitutive function for the Cauchy stress tensor that depends on the objective independent variables ρ, θ, D and E (see (2.52)) is given by (see [78])

$$\begin{aligned}\sigma_{ij} = -p\delta_{ij} + \sigma^e_{ij} = (-p+\alpha_1)\delta_{ij} + \alpha_2 E_i E_j + \alpha_3 D_{ij} + \alpha_4 D_{ik}D_{kj} \\ +\alpha_5(E_i D_{jk} E_k + D_{ik}E_k E_j) + \alpha_6(E_i D_{jk} D_{kl} E_l + D_{ik}D_{kl}E_l E_j)\,,\end{aligned} \tag{4.1}$$

where we have dropped the upper index "me" and α_i, $i = 1, ..., 6$ are functions of the invariants

$$\rho\,,\ \theta\,,\ E_k E_k\,,\ D_{kk}\,,\ D_{jk}D_{kj}\,,\ D_{jk}D_{kl}D_{lj}\,,\ E_j D_{jk} E_k\,,\ E_j D_{jk} D_{kl} E_l\,. \tag{4.2}$$

This general constitutive law was first described by Rajagopal and Wineman in [64]. However, they treated the electric field as a constant when calculating the velocity field for the flow problems formulated in the paper.

In [66] two special cases of (4.1) are discussed. In the first one it is assumed that the stress is linear in D and quadratic in E and hence the material parameters have the form

$$\alpha_1 = \alpha_{11} + \alpha_{12} D_{kk} + \alpha_{13} E_k E_k + \alpha_{14} E_k E_k D_{jj} + \alpha_{15} E_j D_{jk} E_k \,, \tag{4.3}$$
$$\alpha_2 = \alpha_{21} + \alpha_{22} D_{kk} \,, \tag{4.4}$$
$$\alpha_3 = \alpha_{31} + \alpha_{32} E_k E_k \,, \tag{4.5}$$
$$\alpha_4 = 0 \,, \tag{4.6}$$
$$\alpha_5 = \alpha_{51} \,, \tag{4.7}$$
$$\alpha_6 = 0 \,. \tag{4.8}$$

where α_{ij} are functions of ρ and θ only. The subcases of (i) a compressible, (ii) a mechanically incompressible but electrically compressible and (iii) an incompressible fluid are considered and for each of them the restrictions imposed on σ_{ij}^{me} by the Clausius-Duhem inequality are given. The second case pertains to the non-linear model of incompressible ERFs with shear dependent viscosities. First it is assumed that

$$\alpha_4 = \alpha_6 = 0 \,. \tag{4.9}$$

The choice for the material parameters α_2, α_3 and α_5 reflects a combination of a Newtonian and power-law like behaviour where the power* can be a function of $E_k E_k$. Concretely, it is assumed that

$$\begin{aligned} \alpha_2 &= \alpha_{20} + \alpha_{21} (D_{lm} D_{ml})^{n-1} \,, \\ \alpha_3 &= \alpha_{30} + \alpha_{31} (D_{lm} D_{ml})^{n-2} + \alpha_{32} E_k E_k + \alpha_{33} E_k E_k (D_{lm} D_{ml})^{n-2} \,, \\ \alpha_5 &= \alpha_{50} + \alpha_{51} (D_{lm} D_{ml})^{n-2} \,, \end{aligned} \tag{4.10}$$

where α_{ij} are functions of θ. The material function n depends on $E_k E_k$ and satisfies

$$1 < n_\infty \leq n(E_k E_k) \leq n_0 < \infty \,, \tag{4.11}$$

where

$$n_0 = \lim_{E_k E_k \to 0} n(E_k E_k) \,, \quad n_\infty = \lim_{E_k E_k \to \infty} n(E_k E_k) \,. \tag{4.12}$$

An alternative model of (4.10) is then given in which $(D_{lm} D_{ml})^\beta$ is replaced by

$$(1 + D_{lm} D_{ml})^{\beta/2} \quad \text{or} \quad (1 + (D_{lm} D_{ml})^{1/2})^\beta \,, \tag{4.13}$$

where $\beta = n - 1$ or $n - 2$. In this second model, the presence of 1 † under the power prevents the model from developing infinite zero shear viscosity for $n \in (1, 2)$ and a

*We adopted a different notation than in [66] (n instead of p) in order to avoid a confusion with the pressure p

†Here this 1 is intended to be seen not as a constant but as a dimensional quantity having the dimension $1/s^2$ in $(4.13)_1$ and $1/s$ in $(4.13)_2$ which, for the sake of simplicity in the mathematical treatment, is taken to be equal to 1

yield like behaviour as in the first model (4.10). Simplified models of (4.10) and (4.13) corresponding to specific electrorheological fluids ($n \equiv 2$ or $n \not\equiv 2$) are considered and restrictions for the corresponding coefficients α_{ij} are obtained. Finally, a model which includes all the discussed approximating models except that-one with $n \in (1,2)$ and $\alpha_{30} = \alpha_{32} = \alpha_{50} = 0$ is proposed

$$\begin{aligned}\sigma_{ij} = &-p\delta_{ij} + \alpha_{21}((1 + D_{lm}D_{ml})^{(n-1)/2} - 1)E_kE_k \\ &+(\alpha_{31} + \alpha_{33}E_kE_k)(1 + D_{lm}D_{ml})^{(n-2)/2}D_{ij} \\ &+\alpha_{51}(1 + D_{lm}D_{ml})^{(n-2)/2}(E_iD_{jk}E_k + D_{ik}E_kE_j)\,, \end{aligned} \tag{4.14}$$

where n satisfies (4.11). All the cases formulated and discussed in [66] are amenable to mathematical analysis. In [70], Růžička studied in detail mathematical issues such as existence, uniqueness and stability of the weak and strong solutions for the steady flow of incompressible shear dependent electrorheological fluids with the stress given by (4.14). Due to the dependence of the material function n on the magnitude of the electric field, this problem is described by an elliptic or parabolic system of partial differential equations (PDE) with the so-called non-standard growth conditions, i.e. the elliptic operator $\sigma^e_{ij} = \sigma_{ij} + p\delta_{ij}$ satisfies

$$\sigma^e_{ij}(D,E)D_{ij} \geq c_0(1 + E_kE_k)(1 + D_{lm}D_{ml})^{\frac{n_\infty - 2}{2}}D_{lm}D_{ml}\,, \tag{4.15}$$

$$\sigma^e_{ij}(D,E)\,\sigma^e_{ij}(D,E) \leq c_1(1 + D_{lm}D_{ml})^{\frac{n_0 - 1}{2}}E_kE_k\,. \tag{4.16}$$

In [70] the case of unsteady flows of shear dependent ERF is also treated for the constitutive function

$$\sigma_{ij} = -p\delta_{ij} + \alpha_{31}(1 + E_kE_k)(1 + D_{lm}D_{ml})^{(n-2)/2}D_{ij}\,, \tag{4.17}$$

where $\alpha_{31} > 0$ and $n = n(E_kE_k)$ satisfies (4.11) with $n_\infty \geq 2$. The existence of global in time weak and strong solutions for large data under certain restrictions on n_∞ and n_0 and the uniqueness of the strong solution are proved.

The model proposed in [28] consists of an extension of the model (4.10) modified as in $(4.13)_1$

$$\begin{aligned}\sigma_{ij} = &-p\delta_{ij} + [\alpha_{20} + \alpha_{21}Z^{-a+1/2} + \alpha_{22}Z^{-b+1/2}]E_iE_j \\ &+[\alpha_{30} + \alpha_{31}Z^{-a} + \alpha_{32}Z^{-b}]D_{ij} \\ &+[\alpha_{40} + \alpha_{41}Z^{-a-1/2} + \alpha_{42}Z^{-b-1/2}]D_{ik}D_{kj} \\ &+[\alpha_{50} + \alpha_{51}Z^{-a} + \alpha_{52}Z^{-b}](E_iD_{jk}E_k + D_{ik}E_kE_j) \\ &+[\alpha_{60} + \alpha_{61}Z^{-a-1/2} + \alpha_{62}Z^{-b-1/2}](E_iD_{jk}D_{kl}E_l + D_{ik}D_{kl}E_lE_j)\,. \end{aligned} \tag{4.18}$$

Here α_{ij} as well as the exponents a and b are material parameters that can depend only on ρ, θ and E_kE_k. $Z := D_0^2 + D_{mn}D_{nm}$ and D_0 denotes a constant reference shear rate.

The reasons for this choice of the constitutive function are explained in detail in [28]. We mention only some selected arguments. First, this model can include now the Casson model (4.45)–(4.46) which was used quite successfully (in the one-dimensional form) to fit some measured data for one of the ERFs tested in [4]. Second, by introducing two exponents a and b, it is possible to describe the measurements with constant exponents (having only one exponent that does not depend on the electric field, it is in general not possible to fit the data). This is advantageous in the case of inhomogeneous electric fields (when E_k depends on x_j) since we then avoid the exponents to be dependent on the coordinate x_j.

The quantity D_0^2, which in [66] fulfills $D_0^2 = 1$, has an important meaning. A non-vanishing D_0 plays the same role as the 1 in (4.13) namely, it prevents the model in case of certain choices of the exponents a and b, from developing the infinite viscosity limit. For numerical calculations one has to use $D_0 \neq 0$ for otherwise singularities may appear which can cause serious problems in the computations. For some particular cases of (4.18), in a viscometric flow (see (4.23)–(4.26), (4.29)–(4.32)), the choice $D_0 = 0$ allows calculation of the analytical solutions for the velocity. However, when we consider the case of an inhomogeneous electric field, the flow is no longer viscometric and the numerical solutions must be sought by choosing certain positive values for D_0.

The phenomenological approach was continued in [28] with the investigation of model (4.18) in a viscometric flow with a constant electric field perpendicular to the flow direction (e.g. a shear flow in a plane channel under an electric field produced by two infinite electrodes placed along the channel walls – see Section 2.2.1)

$$E_1 = E_3 = 0\,, \quad E_2 = -\frac{V}{h}\,, \tag{4.19}$$

$$D_{12} = D_{21} = \tfrac{1}{2}\,v_{1,2} =: \tfrac{1}{2}\,\dot\gamma\,, \quad D_{ij} = 0_{ij} \quad \text{otherwise}\,. \tag{4.20}$$

Then, it follows that

$$Z = D_0^2 + \tfrac{1}{2}\dot\gamma^2\,, \tag{4.21}$$

$$\tau := \sigma_{12}^{me} = \sigma_{21}^{me} = (\bar\beta_0 + \bar\beta_1 Z_{vf}^{-a} + \bar\beta_2 Z_{vf}^{-b})\dot\gamma\,, \tag{4.22}$$

where $\bar\beta_i := \frac{1}{2}\,(\,\alpha_{3i} + \alpha_{5i}\,V^2/h^2)$, $i = 0, 1, 2$, $Z_{vf} = D_0^2 + \frac{1}{2}\dot\gamma^2$. For certain choices of D_0, a, b and $\bar\beta_i$, one can deduce from (4.22) the model (4.13) for the viscometric flow in question. Model (4.22) with $D_0 = 0$ includes also the most representative models[‡] used in a one-dimensional form in electrorheology: the Bingham model, the Casson model and the power-law model [4, 59, 87, 92, 93]. Let us employ the upper indices B, C and P to denote the quantities corresponding to each of them. By choosing $\bar\beta_0 = \eta^B$, $a = \frac{1}{2}$,

[‡]For models with yield stress one can deduce only the equations describing the liquid like behaviour.

$\bar{\beta}_1 = \frac{1}{\sqrt{2}}\tau_y^B$ and $\bar{\beta}_2 = 0$ the linear Bingham model[§] is found

$$\tau^B = \tau_y^B + \eta^B\dot{\gamma}\,, \quad \tau^B > \tau_y^B\,,\ \dot{\gamma} > 0\,, \tag{4.23}$$

$$\tau^B = -\tau_y^B + \eta^B\dot{\gamma}\,, \quad \tau^B < -\tau_y^B\,,\ \dot{\gamma} < 0\,, \tag{4.24}$$

where $\tau_y^B \geq 0$ is the yield stress and $\eta^B > 0$ is the viscosity.

The non-linear Casson-model possesses also two material parameters: the yield stress $\tau_y^C \geq 0$ and the viscosity $\eta^C > 0$. Its equation reads

$$\tau^C = \tau_y^C + 2\,(\tau_y^C\eta^C\dot{\gamma})^{1/2} + \eta^C\dot{\gamma}\,, \quad \tau^C > \tau_y^C\,,\ \dot{\gamma} > 0\,, \tag{4.25}$$

$$\tau^C = -\tau_y^C - 2\,(\tau_y^C\eta^C(-\dot{\gamma}))^{1/2} + \eta^C\dot{\gamma}\,, \quad \tau^C < -\tau_y^C\,,\ \dot{\gamma} < 0\,, \tag{4.26}$$

and it is obtained by choosing the parameters in (4.22) as follows

$$\bar{\beta}_0 = \eta^C\,,\ a = \tfrac{1}{2}\,,\ \bar{\beta}_1 = \tfrac{1}{\sqrt{2}}\tau_y^C\,,\ b = \tfrac{1}{4}\,,\ \bar{\beta}_2 = 2^{3/4}(\eta^C\tau_y^C)\,. \tag{4.27}$$

The power-law model is also non-linear and it does not determine a yield region. To derive it one must choose

$$\bar{\beta}_0 = 0\,,\ a = \tfrac{1}{2}(1-n)\,,\ \bar{\beta}_1 = 2^{-(1-n)/2}m\,,\ \bar{\beta}_2 = 0\,, \tag{4.28}$$

where $m > 0$ and $n > 0$ are the two model parameters and (4.22) becomes

$$\tau^P = m\dot{\gamma}^n\,,\ \dot{\gamma} > 0\,, \tag{4.29}$$

$$\tau^P = -m(-\dot{\gamma})^n\,,\ \dot{\gamma} < 0\,. \tag{4.30}$$

Then, analysing the experimental data measured for the electrorheological fluid Rheobay TP AI 3565, the Casson-like model introduced by choosing $D_0 = 0$, $a = \frac{1}{2}$ and $b = \frac{1}{4}$ is found as a very suitable model (at least for the fluid Rheobay)

$$\tau^{CL} = (\eta_0 + \beta_0)\dot{\gamma} + 2^{1/2}\beta_1 + 2^{1/4}\beta_2\dot{\gamma}^{1/2}\,,\ \tau^{CL} > 2^{1/2}\beta_1 \geq 0\,,\ \dot{\gamma} > 0\,, \tag{4.31}$$

$$\tau^{CL} = (\eta_0 + \beta_0)\dot{\gamma} - 2^{1/2}\beta_1 - 2^{1/4}\beta_2(-\dot{\gamma})^{1/2}\,,\ \tau^{CL} < -2^{1/2}\beta_1 \leq 0\,,\ \dot{\gamma} < 0\,. \tag{4.32}$$

Here $\beta_1 = \bar{\beta}_1$, $\beta_2 = \bar{\beta}_2$ and $\beta_0 = \bar{\beta}_0 - \eta_0$ fulfill

$$\beta_i(V = 0) = 0\,, \quad i = 0, 1, 2\,, \tag{4.33}$$

where η_0 is the dynamic viscosity without electric field. By imposing (4.33) it is demanded that the fluid has Newtonian behaviour at vanishing electric field. Whereas in the Casson model, the coefficient of $\dot{\gamma}^{1/2}$ is connected to the other material coefficients, in the

[§]In [28], the equations (4.23), (4.25), (4.29) and (4.31) are said to be valid also for $\dot{\gamma} = 0$. We agree with this only in the sense of a subsequent extension by continuation and not as a deduction from the model (4.22) since when $a > 0$, Z_{vf} is not defined for $\dot{\gamma} = 0$ (except the case $n > 1$ for the power law model which is valid for $\dot{\gamma} = 0$). The equations (4.24), (4.26) and (4.30) are not given in [28]; these can also be deduced from (4.22) and we give them here for completeness.

model (4.31)-(4.32) it is independent of these. Consequently the Casson-like model can be particularized to the Bingham model.

The values of η_0 and β_1, β_2 may differ for different electric fields. A table with values found by fitting the data from the measurements obtained in a rotational viscometer for the ER-fluid Rheobay at different electric fields is given.

Finally, taking into account the experimental results, some new assumptions are made in the general model (4.18) in order to obtain a constitutive function which is able both to describe the measurements and to make the analytical solutions possible. First the parameters responsible for the normal stress effects are neglected,

$$\alpha_{40} = \alpha_{41} = \alpha_{42} = \alpha_{60} = \alpha_{61} = \alpha_{62} = 0\,, \tag{4.34}$$

and then the values $a = \frac{1}{2}$ and $b = \frac{1}{4}$ are established. This leads to

$$\begin{aligned}\sigma_{ij} &= -p\delta_{ij} + [\alpha_{20} + \alpha_{21} + \alpha_{22}(D_0^2 + D_{mn}D_{nm})^{1/4}]E_iE_j + 2\eta_0 D_{ij} \\ &+[\alpha_{30} + \alpha_{31}(D_0^2 + D_{mn}D_{nm})^{-1/2} + \alpha_{32}(D_0^2 + D_{mn}D_{nm})^{-1/4}]D_{ij} \\ &+[\alpha_{50} + \alpha_{51}(D_0^2 + D_{mn}D_{nm})^{-1/2} + \alpha_{52}(D_0^2 + D_{mn}D_{nm})^{-1/4}][E_iD_{jk}E_k + D_{ik}E_kE_j]\,,\end{aligned} \tag{4.35}$$

which is called in [28] the extended Casson model. When the electric field vanishes, the factors α_{30}, α_{31} and α_{32} must be null in order to have Newtonian behaviour without electric field. The entropy inequality imposes some restrictions on the material parameters. The necessary condition (2.66) requests that

$$\alpha_{20} + \alpha_{21} + \alpha_{22}D_0^{1/2} = 0\,, \tag{4.36}$$

while from the sufficient condition (2.67) the following relations can be deduced:

$$\eta_0 \geq 0\,, \tag{4.37}$$

$$2\eta_0 + [\alpha_{30} + \alpha_{31}D_0^{-1} + \alpha_{32}D_0^{-1/2}] + 2[\alpha_{50} + \alpha_{51}D_0^{-1} + \alpha_{52}D_0^{-1/2}]E_1^2 \geq 0\,, \tag{4.38}$$

$$\begin{aligned}&2\eta_0 + [\alpha_{30} + \alpha_{31}D_0^{-1} + \alpha_{32}D_0^{-1/2}] \\ &+[\alpha_{50} + \alpha_{51}D_0^{-1} + \alpha_{52}D_0^{-1/2}](E_1^2 + E_2^2) \geq 0\,.\end{aligned} \tag{4.39}$$

The paper contains a Section where the problem formulated in our work in Section 2.2.1 is solved analytically for a Casson-like constitutive model. The plug zone is characterized and the velocity field is given. Moreover the volumetric flow rate (D.1) (the width of the channel is taken into account) is calculated as a function of k, the pressure drop in the x_1-direction. Since the Casson-like model includes the Newtonian ($\beta_0 = \beta_1 = \beta_2 = 0$), Bingham ($\beta_2 = 0$) and Casson ($\beta_2 = 2\sqrt{(\eta_0 + \beta_0)\beta_1}$) behaviours, the given solution may be particularized for all these types of fluids.

The two approaches presented in [28] and [66] are the most important and relevant ones for our treatment. Nevertheless, in order to give a larger view of the attempts to describe ER-fluids, we consider it worthwhile to mention also some other constitutive

models introduced in the specific literature. We continue by mentioning two studies which are interesting, to a greater extent, from the mathematical point of view. Both of them treat extensions of the Bingham model.

In [31] the authors propose a so-called extension of the Bingham model determined in terms of the minimization of the global dissipation energy. The Cauchy stress is given (in a tensorial form) by

$$\sigma = -pI + \gamma \frac{|E|}{|DE|}(DE \otimes E + E \otimes DE) + \eta D \,, \tag{4.40}$$

and it is not well defined when $DE = 0$ which characterizes the "rigid zones". It can be proved that the shear stress has to exceed the threshold $\gamma|E|^2$ outside the rigid zones so this quantity may be viewed as an equivalent of the yield limit of the standard Bingham model. However, the stress tensor is not used directly to formulate the boundary value problem to be solved. The velocity field is computed as the solution of a non-smooth minimization problem for the global energy dissipation. This one is solved numerically by the method of augmented Lagrangians combined with an operator-splitting technique. Numerical results are given that illustrate the ER-effect for a pure shear mode (Couette flow) and for a more complicated flow structure in case of an electrorheological clutch.

Another mathematical study of the flow of electrorheological fluids and of their constitutive description is done in [17]. First, a boundary value problem for the unsteady flow of an electrorheological fluid is formulated. Starting from the most general constitutive function for the stress (4.1) the authors assume that σ^{me} is quadratic in E and affine in D and $D/|D|$ and neglect the term containing $E \otimes E$. The resulting constitutive law has the form

$$\begin{aligned} \sigma_{ij} = -p\delta_{ij} + \left(\alpha_{30} + \alpha_{31}\frac{1}{|D|} + \alpha_{32}E_kE_k + \alpha_{33}E_kE_k\frac{1}{|D|}\right) D_{ij} \\ +\alpha_{50}(E_iD_{jk}E_k + D_{ik}E_kE_j) \,, \end{aligned} \tag{4.41}$$

where the coefficients α_{ij} are constants that have to fulfill

$$\begin{aligned} &\alpha_{30} \geq 0 \,,\ \alpha_{31} \geq 0 \,,\ \alpha_{32} \geq 0 \,,\ \alpha_{33} \geq 0 \,, \\ &\alpha_{32} + \tfrac{4}{3}\alpha_{50} \geq 0 \,. \end{aligned} \tag{4.42}$$

The restrictions (4.42) are deduced from the Clausius-Duhem inequality and they are essential in the further proofs of existence and uniqueness. The model (4.41) is viewed as a combination of Newtonian and Bingham behaviour. As in [31], (4.41) does not make sense if $|D| = 0$ so it cannot be used in the boundary value problem. Instead of this, a variational inequality is formulated for the stress which makes sense. So, the problem is formulated in a variational form. Existence and uniqueness are proved for the solution in the two-dimensional case for any initial data, while in the three-dimensional case global existence of a weak solution is proved for small initial data only. In the end of the paper an interesting result is given concerning the estimation of the time when the fluid stops.

4.2 Constitutive laws used in our numerical approach

In the majority of the experimental evaluations, the constitutive assumptions for the ERF used in the literature are confined to one-dimensional modeling. This corresponds to (steady) plane shear flows for which the constitutive equations take the form of a stress-shear relation [4, 59, 68, 82, 92, 93]). Most popular in the literature are the Bingham, Casson and power law models, depending on the electrorheological material at hand. As mentioned previously, the Casson-like model was introduced in [28]. It generalizes the usual Casson model and includes the Bingham model as a particular case. However, when the more realistic case of finite electrodes is considered, the flow is two-dimensional and bidirectional. So we have to deal with two-dimensional constitutive equations. Let us recall here the two-dimensional form of the aforementioned constitutive equations (the indices take the values 1 and 2). The Bingham model is described by

$$\sigma^e_{ij} = 2\eta_0 D_{ij} + 2^{1/2}\tau_y \frac{D_{ij}}{|D|}\,, \qquad |\sigma^e| > 2^{1/2}\tau_y\,, \tag{4.43}$$

$$|D| = 0\,, \qquad |\sigma^e| \le 2^{1/2}\tau_y\,, \tag{4.44}$$

where $|D| := \sqrt{D_{mn}D_{nm}}$ denotes the second invariant of D. The classical Casson model is given by

$$\sigma^e_{ij} = 2\eta_0 D_{ij} + 2^{1/2}\tau_y \frac{D_{ij}}{|D|} + 2^{7/4}(\eta_0\tau_y)^{1/2}\frac{D_{ij}}{|D|^{1/2}}\,, \qquad |\sigma^e| > 2^{1/2}\tau_y\,, \tag{4.45}$$

$$|D| = 0\,, \qquad |\sigma^e| \le 2^{1/2}\tau_y\,. \tag{4.46}$$

When these equations are used to describe the ERF behaviour, one has to take into account the dependence of the yield stress and, possibly of the viscosity, on the magnitude of the electric field.

For the power-law model we have (see [79])

$$\sigma^e_{ij} = m\dot\gamma^{n-1}2D_{ij}\,, \tag{4.47}$$

when $n > 1$ (shear-thickening behaviour). Here $\dot\gamma = 2^{1/2}|D|$ denotes a generalized shear rate. When $n < 1$ (shear-thinning or pseudoplastic behaviour) we can no longer use (4.47) since for $\dot\gamma \to 0$ the generalized viscosity $m\dot\gamma^{n-1} \to \infty$. The difficulty is overcome by modifying the model (4.47) through the introduction of a new free parameter $\dot\gamma_0$

$$\sigma^e_{ij} = \begin{cases} m\dot\gamma_0^{n-1}2D_{ij} & , \quad \dot\gamma \le \dot\gamma_0\,, \\ m\dot\gamma^{n-1}2D_{ij} & , \quad \dot\gamma > \dot\gamma_0\,. \end{cases} \tag{4.48}$$

$\dot\gamma_0$ is a constant value of the generalized shear rate below which Newtonian behaviour with the viscosity $\eta_0 = m\dot\gamma_0{}^{n-1}$ is found. For electrorheological fluids the parameters m, n and $\dot\gamma_0$ may depend on the electric field.

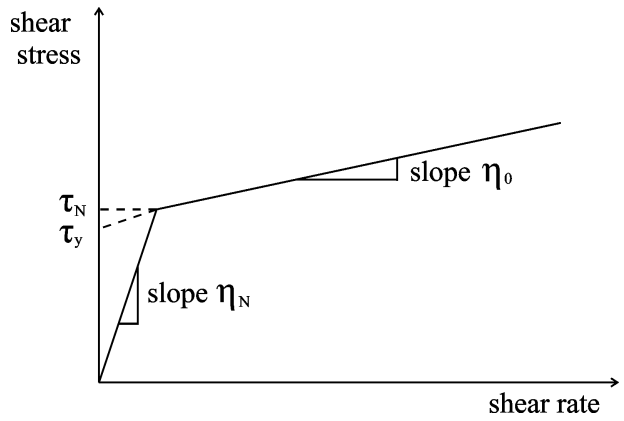

Figure 4.1: One-dimensional form of the bi-viscosity model (4.51)–(4.52) (only for positive shear rates)

Now we will generalize (4.31)-(4.32) and we introduce the two-dimensional form of the Casson-like constitutive function as

$$\sigma^e_{ij} = 2\eta_0 D_{ij} + \beta_1 \frac{2D_{ij}}{|D|} + \beta_2 \frac{2D_{ij}}{|D|^{1/2}}\,, \qquad |\sigma^e| > 2|\beta_1|\,, \tag{4.49}$$

$$|D| = 0\,, \qquad |\sigma^e| \le 2|\beta_1|\,, \tag{4.50}$$

where the parameters η_0, β_1 and β_2 are positive and may depend on the magnitude of the electric field. The Bingham model and the classical Casson model are obtained from (4.49), (4.50) for $\beta_1 = 2^{-1/2}\tau_y$, $\beta_2 = 0$ and $\beta_1 = 2^{-1/2}\tau_y$, $\beta_2 = 2^{3/4}(\eta_0\tau_y)^{1/2}$, respectively.

All these models may cause serious mathematical difficulties since they are expressed by two-branched functions which are not smooth and differentiable. The presence of the $|D|$ denominator is an obstacle against numerical modeling of flow in complex geometries because it is difficult to determine a priori where it vanishes. For instance, for models with yield behaviour such as the Bingham, Casson and Casson-like models, it is not possible to determine a priori the yield surfaces (the interfaces which separate a non-deforming solid from a liquid state region) since they have to be determined as part of the solution. Similarly, it is not possible to determine explicitly in what regions of the problem domain $\dot\gamma = \dot\gamma_0$ for the model (4.48). We wish to mention here some attempts done in order to overcome this difficulty. Most of them concern the Bingham model. In 1999 Barnes published a review [12] on models with yield stress. In a special section of the article,"Problems with yield stress and mathematics", the author mentions important approaches for several complex flow problems dealing with yield stress. These are mainly based on the modification of the Bingham model in such a way that the mathematical problem concerning the yield stress is avoided. The most important approximations of the Bingham model mentioned by Barnes are the 'bi-viscosity' model and the Papanastasiou model. In the bi-viscosity model, the rigid body character (4.44) is replaced by a Newtonian flow behaviour with very high viscosity ($\eta_N \gg \eta_0$). Then, instead of (4.43)–(4.44)

we have the law

$$\sigma_{ij}^e = 2\eta_0 D_{ij} + 2^{1/2}\tau_y \frac{D_{ij}}{|D|}\,, \qquad |\sigma^e| > 2^{1/2}\tau_N\,, \tag{4.51}$$

$$\sigma_{ij}^e = 2\eta_N D_{ij}\,, \qquad |\sigma^e| < 2^{1/2}\tau_N\,, \tag{4.52}$$

where the constant τ_N is related with τ_y by

$$\tau_y = \tau_N(1 - \eta_0/\eta N)\,. \tag{4.53}$$

The law (4.51)–(4.52) for $\eta_N \to \infty$ becomes (4.43)–(4.44). In Figure 4.1 one can see how the shear stress depends on the shear rate (one-dimensional case) within the bi-viscosity assumption. This model was used in the treatment of squeeze-flow of an electrorheological fluid (see [82]).

Papanastasiou introduced in [58] a modified constitutive equation that smoothes the yield criterion, permitting the numerical treatment of the flow problems based on this model. We give here his law by using our notation (for a better comparison)

$$\sigma_{ij}^e = \left(2\eta_0 + 2^{1/2}\tau_y \frac{1 - \exp\left[-n2^{1/2}|D|\right]}{|D|}\right) D_{ij}\,, \tag{4.54}$$

where the exponent n is a material parameter, relatively big, that can be determined from experiments. The Bingham law in the unyielded region is recovered from equation (4.54) for $n \to \infty$. In comparison with (4.43), equation (4.54) is not singular since

$$\lim_{|D|\to 0} \sigma_{ij}^e = 2(\eta_0 + n\tau_y)D_{ij}\,, \tag{4.55}$$

and, consequently, it is valid for both the yielded and unyielded regions.

We should also mention here the so-called alternative Bingham model introduced by Mellgren in [52]

$$\sigma_{ij}^e = \left(2\eta_0 + 2^{1/2}\tau_y \frac{1}{(\varepsilon/2 + |D|^2)^{1/2}}\right) D_{ij}\,, \tag{4.56}$$

where ε is a positive material parameter. For $\varepsilon \to 0$ (4.56) reduces to (4.43) but since ε is required to be positive, (4.56) is defined for all possible values of D_{ij}. As in (4.54) the material takes on only a liquid state and therefore does not cause any mathematical difficulties.

In Figure 4.2 one can see how the models (4.54) and (4.56) approximate the Bingham model in the one-dimensional case. τ_y is only a material parameter without the significance of a yield stress. (4.54) and (4.56) may be seen not only as mathematical approximations of the Bingham model. In [11] a revolutionary but also controversial idea in rheology was introduced according to which the concept of yield stress should be seen only as an idealization and "given accurate measurements, no yield stress exists" So, the viscosity is always finite. This point of view was supported by some experiments done with rheometers

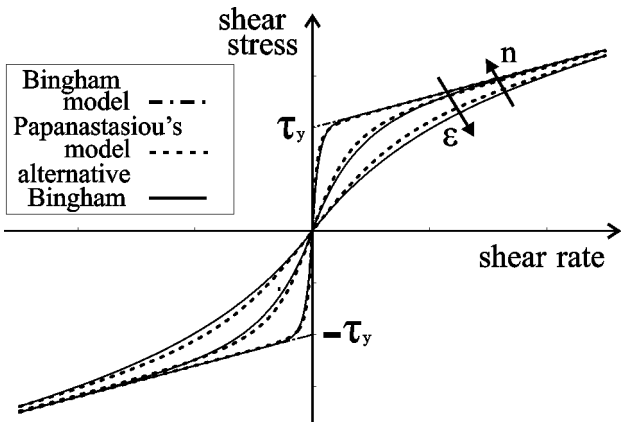

Figure 4.2: Comparison (one-dimensional form) between the Bingham constitutive function (4.23), (4.24) and the modified Bingham models (Papanastasiou's model, alternative Bingham model) for different values of the parameters (n and ϵ, respectively)

which allow stress measurements for lower shear rates. As the experiment was performed for lower shear rates (for the same material), the value of the yield stress was smaller. Consequently, from this point of view, the models (4.54) and (4.56) are closer to reality.

Let us denote by f and g the functions shear stress vs. shear rate appearing in the one-dimensional versions of (4.54) and (4.56),viz.,

$$f(x) = (\eta_0 + \tau_y \frac{1 - \exp(-n|x|)}{|x|})x \,, \tag{4.57}$$

$$g(x) = (\eta_0 + \tau_y \frac{1}{(\varepsilon + x^2)^{1/2}})x \,. \tag{4.58}$$

If we seek n and ε such that the slopes of the curves are equal in $x = 0$ i.e. $f'(0) = g'(0)$ (where $f'(0) := f'(0^+) = f'(0^-)$) then we obtain $n = 1/(\delta)^{1/2}$. For n and ε in this relation the curves for f and g are very closed (see Figure 4.2) showing very similar behavior.

One can apply the ingenious ideas from the models (4.54) and (4.56) to the Casson and Casson-like models, too and even to the power-law model. However, when we use these functions to describe the electrorheological fluids the material parameters (η_0, τ_y and n, ε, respectively) may depend on the electric field. For a space-dependent electric field the constitutive equations modified as in (4.54) become too complicated due to the presence of the exponential. Due to its simplicity, (4.56) is easier to handle than (4.54). Let us show how this trick can be applied to the power-law model: for instance, in the one-dimensional case of (4.48), one may consider instead of the two-branched function (we used the notation from (4.22))

$$\tau = \begin{cases} m|\dot\gamma|^{n-1}\dot\gamma \,, & |\dot\gamma| > \dot\gamma_0 \,, \\ m\dot\gamma_0^{n-1}\dot\gamma \,, & |\dot\gamma| \le \dot\gamma_0 \,, \end{cases} \tag{4.59}$$

the form

$$\tau = m(\varepsilon + \dot\gamma^2)^{(n-1)/2}\dot\gamma \,, \tag{4.60}$$

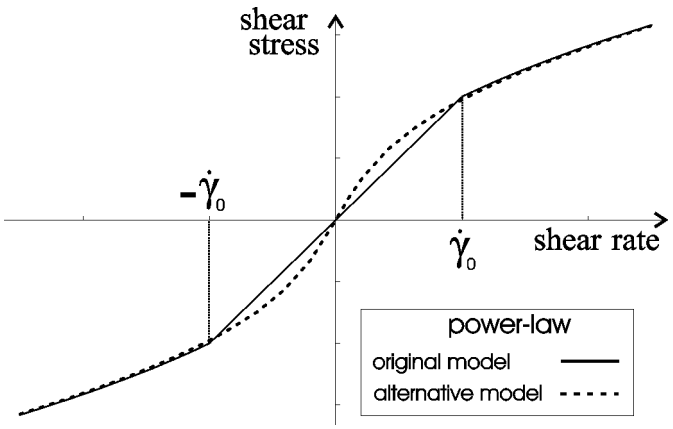

Figure 4.3: Comparison between the models (4.59) and (4.60)

which eliminates the branching (for illustration and comparison with the original model (4.59) see Figure 4.3). This law was used by Hutter (see [39], [40], [41]) to derive the generalized Glen law in glaciology. At $\dot{\gamma} \to 0$ it exhibits Newtonian behaviour. We found this approach more appropriate for our study.

Even though the boundary value problem is quite different than ours it is worth mentioning the recent work of P. Hild et al. [36] who applied the Bingham model to landslides modeling. In their model the viscosity coefficient and the yield stress depend on density which in turn is time- and space-dependent. This makes this approach interesting also in our case. By using variational methods the authors studied the blocking property of the flow and described the rigid zones and the stagnant regions (which are stuck on the boundaries) for certain boundary value problems. However, they could find explicitly the yield surfaces only for one-dimensional cases.

Now synthesizing all the previous issues we will introduce two constitutive models for electrorheological fluids which will be used further in the numerical approach: the alternative Casson-like model (which contains also the alternative forms of the Bingham and Casson models),

$$\sigma_{ij}^e = 2\eta_0 D_{ij} + \beta_1(E)\frac{2D_{ij}}{(\delta + |D|^2)^{1/2}} + \beta_2(E)\frac{2D_{ij}}{(\delta + |D|^2)^{1/4}}\,, \tag{4.61}$$

and the alternative power-law model

$$\sigma_{ij}^e = m(E)(\delta + 2|D|^2)^{(n(E)-1)/2} 2D_{ij}\,, \tag{4.62}$$

where $E = (E_1^2 + E_2^2)^{1/2}$ is the electric field modulus and δ is a small positive material parameter. With these two models it is possible to cover a large area of electrorheological materials. They are suitable to numerical simulations and are consistent with the phenomenological approaches presented in the previous Section. Namely, the alternative

Casson-like model may be seen as a particularization of (4.35) if we take

$$\alpha_{20} = \alpha_{21} = \alpha_{22} = \alpha_{30} = \alpha_{50} = \alpha_{51} = \alpha_{52} = 0 \,, \tag{4.63}$$

$$\alpha_{31} = \beta_1 \,, \quad \alpha_{32} = \beta_2 \,, \tag{4.64}$$

$$D_0^2 = \delta \,. \tag{4.65}$$

while the alternative power-law model is included in (4.18) as a particular case and it is similar with a particularization of $(4.14)_1$ (for $\alpha_1 = \alpha_2 = \alpha_5 = 0$) with a few small deviations:

- the term δ from (4.62) takes the value 1 in $(4.14)_1$; the advantage of taking a variable quantity δ is twofold: on the one hand one can consider δ as a constitutive parameter and obtain its value with respect to each investigated material from fitting the experimental data; on the other hand one can consider δ as an arbitrary small parameter; then studying the influence of δ on the solution may permit to consider the model (4.62) as an approximation of the classical power-law model (where $\delta = 0$) (see Subsection 5.2.3 for such an approach).

- the function m from (4.62) depends only on the magnitude of the electric field and its expression has to be determined for each ER-material; the dependence on the magnitude of the electric field of α_3 (with the coefficients $\alpha_{31} = \alpha_{33} = 0$), the correspondent of m in $(4.14)_1$, takes the particular form $\alpha_{30} + \alpha_{33}E^2$.

For both models the dependence of the coefficients (β_1, β_2 for the Casson-like model and m, n for the power-law model) on the electric field are established for a certain ERF from the experimental data. The measurements are usually performed with rotational viscometers based on the Couette system (made by two concentric cylinders or plate-plate geometry). These devices provide curves shear stress vs. shear rate for different values of the electric fields. The material parameters are obtained from the measured data by fitting techniques, and they are given in tables for different values of the electric field [4, 28, 92]. By interpolation we can obtain the desired functions.

4.3 The dimensionless problem

Let us return to the problem formulated in Section 2.2. It consist of the electrical problem which may be solved independently and the mechanical problem, equations which contain terms based on the electric field components, namely on the solution of the electrical problem. We recall below the equations of the mechanical problem

$$-p_{,i} + \sigma^e_{ij,j} + \frac{1}{2}\varepsilon_2 (E_j E_j)_{,i} = \rho v_j v_{i,j} \,, \tag{4.66}$$

$$v_{i,i} = 0 \,, \tag{4.67}$$

with the boundary conditions

$$v_{1,1}(-L, x_2) = 0,\ v_2(-L, x_2) = 0\,, \quad |x_2| \le h\,, \tag{4.68}$$
$$p(L, x_2) = 0\,, \quad |x_2| \le h\,, \tag{4.69}$$
$$v_i(x_1, \pm h) = 0\,, \quad |x_1| \le L\,. \tag{4.70}$$

The x_1-coordinates $-L$ and L mark the entrance and the exit of the fluid in the channel, respectively. We assume that L is sufficiently large, namely the inlet boundary is far enough from the electrode edge so that the electric field is constant at the entrance; moreover, we may say that it is negligible. Consequently, one may impose there the velocity as in a one-directional channel flow (described in Section 2.2.1). At the channel exit we assume vanishing pressure. For the extra stress σ^e_{ij} we will use the models (4.61) and (4.62). We may define a generalized viscosity η_{gen} so that $\sigma^e_{ij} = 2\eta_{gen} D_{ij}$. We have

$$\eta_{gen} = \eta_0 + \frac{\beta_1(E)}{(\delta + |D|^2)^{1/2}} + \frac{\beta_2(E)}{(\delta + |D|^2)^{1/4}}\,, \tag{4.71}$$

for the alternative Casson-like model and

$$\eta_{gen} = m(E)(\delta + 2|D|^2)^{(n(E)-1)/2}\,, \tag{4.72}$$

for the alternative power-law model.

4.3.1 The Casson-like model

We introduce the non-dimensional quantities $\tilde{x_i}$, $\tilde{v_i}$, $\tilde{E_i}$ and $\tilde{p}$ according to

$$x_i = h\tilde{x_i}\,,\ \ v_i = v_0\tilde{v_i}\,,\ \ E_i = E_0\tilde{E_i}\,,\ \ p = p_0\tilde{p}, \tag{4.73}$$

where h, v_0, E_0 and p_0 are characteristic quantities of the problem: h is one half of the channel height, v_0 is the maximum inlet velocity, E_0 is a typical value for the electric field and $p_0 = \eta_0 v_0/h$. Application of these transformations upon (4.66), multiplying it with h/p_0 and dropping the "tilde" yield

$$-p_{,i} + 2\,(\eta_{gen}\, D_{ij})_{,j} + \frac{1}{2Ma}(E_j E_j)_{,i} = Re\, v_j v_{i,j}\,, \tag{4.74}$$

where

$$\eta_{gen} = 1 + \frac{h\,\beta_1(E_0 E)}{v_0\eta_0}\,\frac{1}{(n_\delta + |D|^2)^{1/2}} + \frac{\sqrt{h}\,\beta_2(E_0 E)}{\sqrt{v_0}\eta_0}\,\frac{1}{(n_\delta + |D|^2)^{1/4}}\,, \tag{4.75}$$

is the dimensionless generalized viscosity,

$$Re = \rho h v_0/\eta_0\,, \tag{4.76}$$

is the Reynolds number,

$$Ma = \eta_0 v_0/(h\varepsilon_2 E_0^2)\,, \tag{4.77}$$

is the Mason number and $n_\delta = \delta h^2/v_0^2$. The Reynolds number is usually interpreted as the ratio of the inertial force to the viscous force while the Mason number can be interpreted as the ratio of the viscous force to the electrostatic force. We have chosen a non-dimensionalization appropriate to creeping flows since the Reynolds number in our case takes low values. The dimensionless form of the equation (4.67), after dropping "tilde", remains unchanged.

Usually β_1, β_2 vanish when the electric field is zero so that the fluid is Newtonian. Consequently, at the channel exit, where the electric field is zero, we have before non-dimensionalization

$$v_1(-L, x_2) = v_0(1 - (x_2/h)^2)\,. \tag{4.78}$$

The non-dimensionalized boundary conditions (4.68)–(4.70) and (4.78) become

$$v_1(-L/h, x_2) = 1 - x_2^2\,,\quad v_2(-L/h, x_2) = 0\,, \qquad |x_2| \le 1\,, \tag{4.79}$$

$$p(L/h, x_2) = 0\,, \qquad |x_2| \le 1\,, \tag{4.80}$$

$$v_i(x_1, \pm 1) = 0\,, \qquad |x_1| \le L/h\,. \tag{4.81}$$

The problem is formulated now by equations (4.67), (4.74), (4.75) together with the boundary conditions (4.79)–(4.81), where E_j is the non-dimensionalised solution of (2.69)–(2.76). It will be solved numerically for the domain $|x_1| \le L/h$, $|x_2| \le 1$ using the commercial software FEMLAB [21] (see 5.1). This is a powerful tool for solving partial differential equations by applying the finite element method.

4.3.2 The power-law model

We apply the same procedure as in the previous case, namely we introduce the non-dimensional quantities as in (4.73) but now consider $p_0 = m_0(v_0/h)^{n_0}$, where $m_0 = m(0)$, $n_0 = n(0)$ (which are usually non zero). The non-dimensional momentum balance for a power-law fluid has the same form as (4.74) with the Mason number, the Reynolds number and the non-dimensional generalized viscosity given by

$$Ma = \frac{m_0(v_0/h)^{n_0}}{\varepsilon_2 E_0^2}\,, \quad Re = \frac{\rho v_0^2}{m_0(v_0/h)^{n_0}}\,, \tag{4.82}$$

$$\eta_{gen} = \frac{m(E_0E)(v_0/h)^{n(E_0E)}}{m_0(v_0/h)^{n_0}}\,(n_\delta + 2|D|^2)^{(n(E_0E)-1)/2}\,. \tag{4.83}$$

We remark that, since the dimension of m is Pas^n and since n, which is dimensionless, is space dependent, the quantity m has variable dimension in space. Even though we can fit the values of m (from the experimental data) and we may obtain the function

$m(E_0E)$, this quantity is meaningless from the physical point of view. In order to avoid this problem, we will fit directly the dimensionless function (see (4.83))

$$f(E_0E, v_0/h) = m(E_0E)(v_0/h)^{n(E_0E)} . \tag{4.84}$$

An example for this operation will be presented in Chapter 5.

In order to establish the non-dimensional form of the boundary conditions we must calculate first the dimensional velocity at the entrance of the channel; i.e., we must find the velocity in a one-directional channel flow for a power-law fluid. This is given by

$$v_1(-L, x_2) = v_0 \left(1 - \left(\frac{|x_2|}{h} \right)^{(n_0+1)/n_0} \right) . \tag{4.85}$$

Consequently, the non-dimensional inlet boundary condition has the form

$$v_1(-L/h, x_2) = 1 - |x_2|^{(n_0+1)/n_0} , \;\; v_2(-L/h, x_2) = 0. \tag{4.86}$$

The non-dimensional boundary conditions at the channel exit and on the channel walls are identical with their correspondents from the Casson-like case: (4.80) and (4.81). The problem formulated by equations (4.67), (4.74), (4.83) together with the boundary conditions (4.86), (4.80) and (4.81), where E_j is the non-dimensionalised solution of (2.69)–(2.76) will be solved numerically for the domain $|x_1| \leq L/h$, $|x_2| \leq 1$ in Section 5.2 using the commercial software FEMLAB.

Chapter 5

Numerical results

5.1 The Casson-like model

5.1.1 Material and configuration properties used for the simulations

An ER-fluid chosen for simulations is Rheobay TP AI 3565 which is produced by the Bayer Company (Germany). It is water-free and consists of polyurethan particles in silicone oil, some additional additives and an emulsifier [4, 93, 13]. In [28], the Casson-like model (4.31)-(4.32) is recommended for this fluid since this model reproduces well the data measured in a rotational viscometer. The fluid shows Newtonian behaviour in the absence of an electric field i.e. $\beta_1 = 0$ and $\beta_2 = 0$ for $E_0E = 0$, ($E = (E_1^2 + E_2^2)^{1/2}$ is the modulus of the dimensionless electric field). The value $\eta_0 = 0.037$ Pa·s for the viscosity and the values of the parameters β_1 and β_2 given in Table 5.1 were obtained in [29] using the experimental plots stress vs. shear rate. Fitting these data we obtained the dependence of the parameters on the dimensional electric field E_0E:

$$\beta_1(E_0E) = \alpha_{11}(E_0E) + \alpha_{12}(E_0E)^2\,, \tag{5.1}$$

$$\beta_2(E_0E) = \alpha_{21}(E_0E) + \alpha_{22}(E_0E)^2 + \alpha_{23}(E_0E)^3\,, \tag{5.2}$$

Table 5.1: Values of the parameters β_1 and β_2 of (4.31) for different electric field strengths

$E_0E\,[\frac{\text{kV}}{\text{mm}}]$	0.5	1	2	3
β_1 [Pa]	19.3	100.32	312.94	582.81
β_2 [Pa·s$^{1/2}$]	0.44	5.84	9.7	32.21

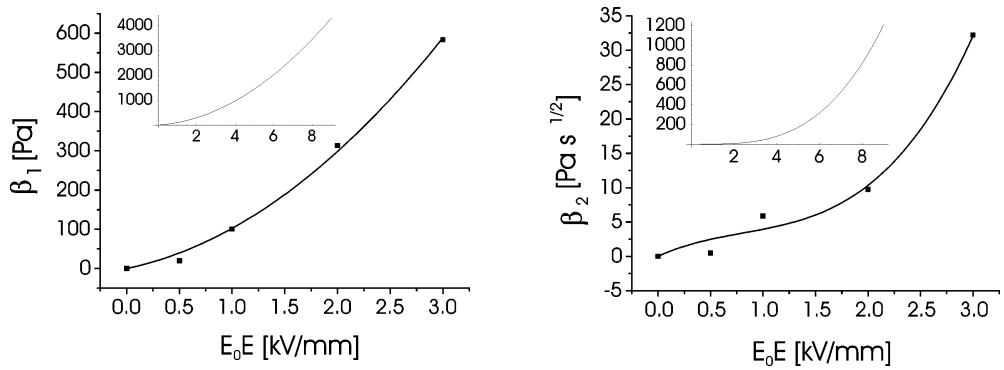

Figure 5.1: Fitting curves for the dependence of the coefficients β_1 and β_2 on the electric field. The insets show how the fit is extrapolated

where $\alpha_{11} = 55.322\,\mathrm{Pa{\cdot}mm/kV}$, $\alpha_{12} = 46.946\,\mathrm{Pa{\cdot}mm^2/kV^2}$, $\alpha_{21} = 7.009\,\mathrm{Pa{\cdot}s^{1/2}{\cdot}mm/kV}$, $\alpha_{22} = -5.22\,\mathrm{Pa\cdot s^{1/2}\cdot mm^2/kV^2}$ and $\alpha_{23} = 2.149\,\mathrm{Pa\cdot s^{1/2}\cdot mm^3/kV^3}$. The functions β_1 and β_2 are written as series expansions by retaining only the terms up to the second and the third order, respectively. The experimental data are provided for a limited range of the electric field and do not cover the range of the electric field used in the simulations. We use the formulas (5.1) and (5.2) also to extrapolate the given data for β_1 and β_2 for larger values of E. Figure 5.1 illustrates how the fitting curves approximate the data and how they are extrapolated. We shall use the alternative bidimensional Casson-like model (4.61) in the further approach. Consequently, the generalized viscosity is expressed by a low degree polynomial function in E. Substituting (5.1) and (5.2) in (4.75) yields

$$\eta_{gen} = 1 + n_{11}\frac{E}{d} + n_{12}\frac{E^2}{d} + n_{21}\frac{E}{d^{1/2}} + n_{22}\frac{E^2}{d^{1/2}} + n_{23}\frac{E^3}{d^{1/2}}\,, \tag{5.3}$$

where we used the short-hand notation

$$d = (n_\delta + D_{mn}D_{mn})^{1/2}\,. \tag{5.4}$$

The non-dimensional coefficients n_{ij}, $i = 1, 2$, $j = 1, 2, 3$ are defined as

$$n_{11} = \frac{h\alpha_{11}E_0}{v_0\eta_0}\,, \quad n_{12} = \frac{h\alpha_{12}E_0^2}{v_0\eta_0}\,, \tag{5.5}$$

$$n_{21} = \frac{\sqrt{h}\alpha_{21}E_0}{\sqrt{v_0}\eta_0}\,, \quad n_{22} = \frac{\sqrt{h}\alpha_{22}E_0^2}{\sqrt{v_0}\eta_0}\,, \quad n_{23} = \frac{\sqrt{h}\alpha_{23}E_0^3}{\sqrt{v_0}\eta_0}\,. \tag{5.6}$$

For all graphs that subsequently will be shown we used a geometry characterized by the value $H/h = 10$. The value of L/h is always chosen so that the inlet boundary is sufficiently far from the electrode edge in order to insure a negligible electric field at the entrance of the channel. The electric permittivity of Rheobay is $\varepsilon_2 = 1.4\cdot 10^{-9}$ A·s/(V·m) and we choose $\varepsilon_1 = 0.02\,\varepsilon_2$. The density of Rheobay is $\rho = 1041$ kg/m^3. All simulations except those done to make the comparison with the experimental data from Fig. 5.24

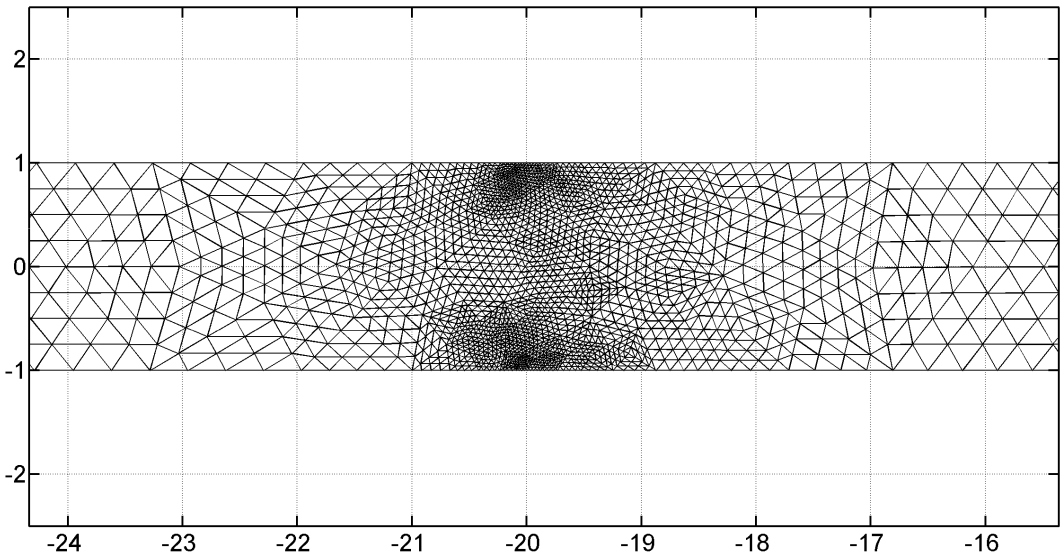

Figure 5.2: The mesh arround the electrodes edges

are performed for $h = 1$ mm, $E_0 = 1$ kV/mm and $v_0 = 0.3$ m/s. So, $Re = 7.849$, , $Ma = 0.007$, $n_{11} = 5.417$, $n_{12} = 4.597$, $n_{21} = 11.433$, $n_{22} = -8.515$ and $n_{23} = 3.506$. We considered here $n_\delta = 0.002$. In Subsection 5.1.4 we study the influence of this parameter on the solution.

For the configurations with two long electrodes, analysed in Chapter 3, one can use the analytical solution of the electric field when implementing the problem in the program. Concretely, we can formulate Dirichlet conditions for the electric problem on the part of the channel boundaries outside the electrodes so that the domain of the electric problem is also reduced to the channel only as for the mechanical problem. These conditions are obtained by interpolating truncations of the analytical solution of the electric potential on the lines $|x_1| \geq l$, $x_2 = \pm h$. The non-dimensionalisation of the conditions is obtained by dividing the dimensional potential by $V_0 = E_0 h$. In this way space memory and computing time can be saved. We call this approach **numerical analytic**. When we treat configurations with two short electrodes or with more than two electrodes then the electric field will be calculated numerically. This is the so-called **completely numerical** approach.

5.1.2 The flow near the electrode ends (long electrodes)

Let us first illustrate the effect of the electric field inhomogeneity produced by the electrode edges on the flow. To do this we solved the problem (4.67), (4.74), (5.3) together with the boundary conditions (4.79)–(4.81), where E_j is the non-dimensionalised solution of (2.69)–(2.76) with two long electrodes charged anti-symmetrically, using the numerical analytic approach (as defined in the previous Subsection). We took $V = 2$ kV.

A triangular mesh consisting of approximately 10000 elements (9984) was used. The

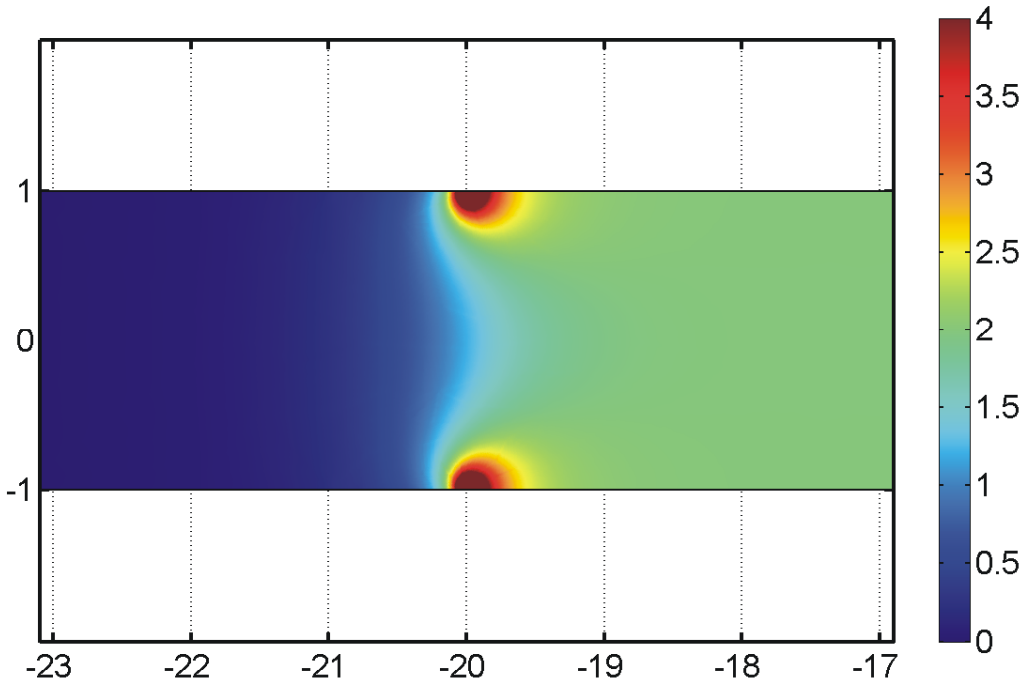

Figure 5.3: Surface plot of the dimensionless electric field modulus

default mesh is twice refined (with a regular refinement) so that the obtained mesh is characterized by 8 elements between the channel walls in the regions far from the electrode ends. The maximum element size near the vertices given by the electrode ends is taken to be 0.1. A detail of the mesh in the region close to the electrode edges is plotted in Fig. 5.2.

We chose the linear Lagrange elements for the electric problem and p2p1 Lagrange elements for the fluid problem. We present and describe here the most relevant fields in an area close to the electrode ends chosen in order to set in evidence the effects ahead, near and after the electrode ends. This is a crossing zone in which the quantities of the studied problem are passing from the regime without electric field to a regime with uniform electric field through a transition zone with strong inhomogeneities. The ranges for the color bars corresponding to Figures 5.3, 5.11 and 5.12 were chosen so that the transition zone is illustrated in an especially relevant fashion. Consequently, the values from the zones with the darkest red could be greater than the maximum values indicated on the scale. We mention that the maximum values in a given area surrounding the electrode edges are much larger than the maximum value within a similar area with uniform electric field (inside the electrodes, far from the edges). The closest area to the edges is difficult to be described exactly for three reasons. First, the electric field is singular there (see Section 3.6). Second, the material properties (β_1 and β_2) are not provided for high values of the electric field (see Table 5.1). Third, in practice, the electrodes can not be infinitely thin as approximated here, so E is not singular at the edges but has a large value.

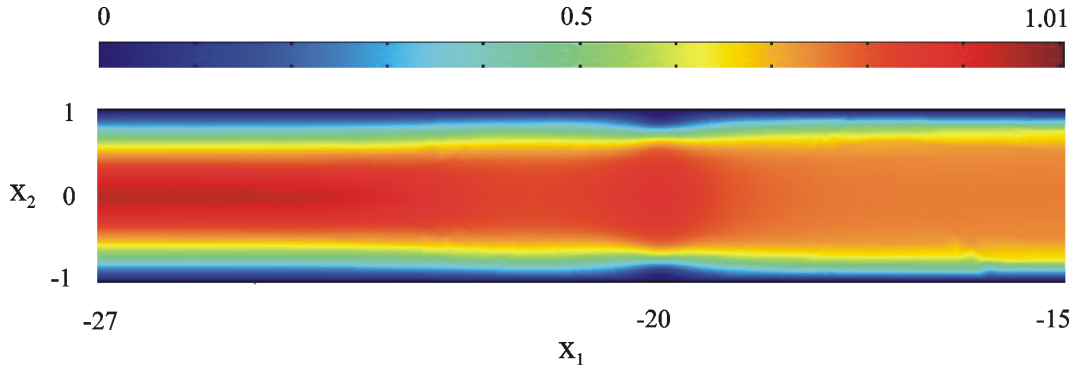

Figure 5.4: Surface plot of the non-dimensional velocity modulus in the vicinity of the electrodes edges ($x_1 = -20$)

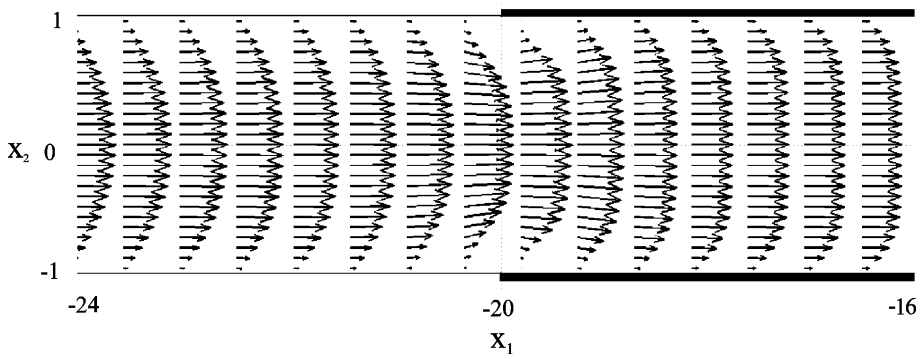

Figure 5.5: Vector plot of the non-dimensional velocity

Let us show first in Fig. 5.3 the electric field produced by this configuration. The inhomogeneities of the electric field extend over a length of order h. In the vicinity of an order smaller than $h/10$ around the electrode ends, the electric field is very large, its value exceeding the ranges for which experimental data are provided. In this vicinity, due to the singularity of the electric field, the numerical simulation of the electric field is not stable (since mesh dependence was observed). However, this vicinity is small in comparison with the characteristic length of the experimental configuration.

In Fig. 5.4 we plotted the non-dimensional velocity modulus

$$v(x_1, x_2) = \sqrt{v_1^2(x_1, x_2) + v_2^2(x_1, x_2)} \tag{5.7}$$

in the vicinity of the electrode edges ($x_1 = -20$). We remark the two small domains formed around the electrode ends where the fluid is almost solidified and the difference outside and between the electrodes. To have a better view over the flow in the inhomogeneous area, we made in Fig. 5.5 an arrow plot of the velocity in the same area. Immediately before and immediately after the electrode ends, v_2 is not negligible and influences the profile of

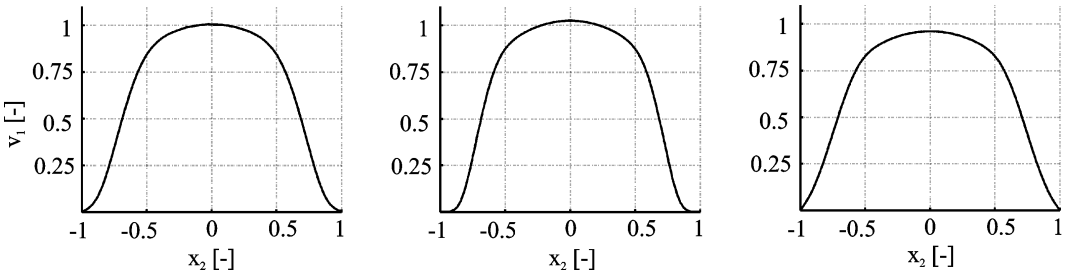

Figure 5.6: Profiles of v_1 at $x_1 = -20.2, -20, -19.5$, respectively

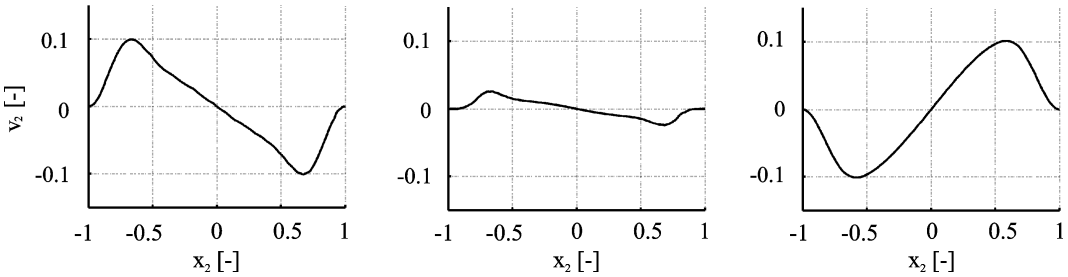

Figure 5.7: Profiles of v_2 at $x_1 = -20.2, -20, -19.5$, respectively

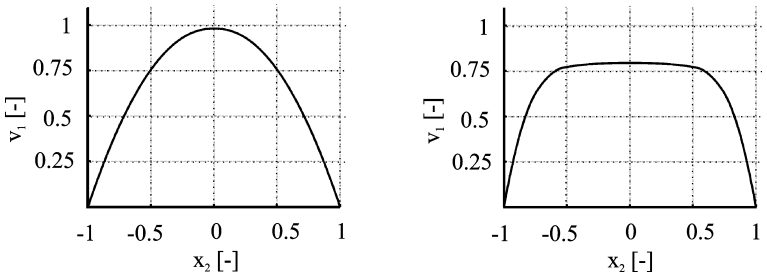

Figure 5.8: Profiles of v_1 at $x_1 = -23.5, -16.5$, respectively

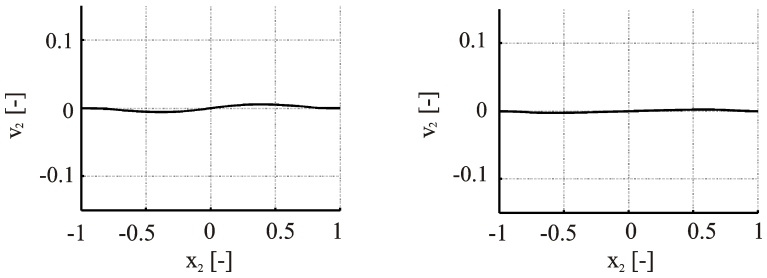

Figure 5.9: Profiles of v_2 at $x_1 = -23.5, -16.5$, respectively

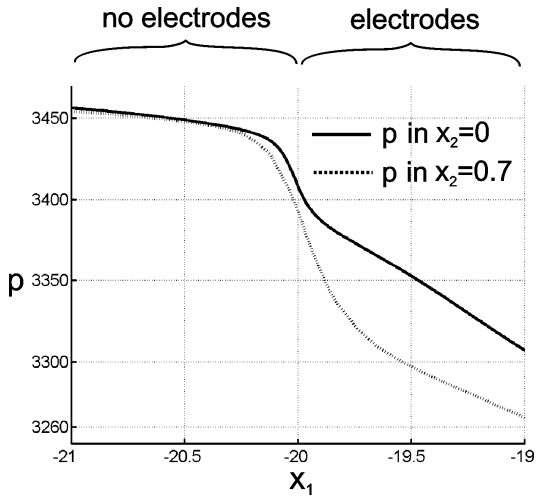

Figure 5.10: Dimensionless pressure in the transition zone ($x_1 = -20$ marks the electrode ends)

the x_1-component as one can see in Figures 5.6 and 5.7. It is worth mentioning that the two extreme values of v_2 at $x_1 = -20.2$ (first positive and then negative) and $x_{-19.5}$ (first negative and then positive) indicate that the fluid goes around the electrode tips. For x_1 outside, far ahead of the electrode ends where the profile of the v_1 is Newtonian the x_2-component of the velocity almost vanishes (see Figs. 5.8 (left) and 5.9). Between the electrodes, far downstream from the electrode edges the fluid velocity assumes the known one-dimensional Casson-like profile (see Figs. 5.8 (right) and 5.9).

In Fig. 5.10 we plotted the pressure along a part of the channel including the transition area. The distinguished three regions are characterized by different pressure gradients. First one can see a region with a very small gradient corresponding to the Newtonian fluid; then a steep region with high gradient corresponding to the entrance between the electrodes is followed by the third region with the gradient corresponding to the Casson-like fluid. For $x_1 < -20.3$ and for $x_1 > -19.5$ the gradients may be calculated analytically from the formulas corresponding to the Newtonian fluid and the Casson-like fluid, respectively (see Appendix D). The increase in pressure drop produced by the second region (the so-called transition zone) is important and shows that the inhomogeneity produced by the end effects may be used to obtain an enhancement of the ER-effect.

In Figure 5.11 the second invariant of the strain rate tensor $D_{ij} = \frac{1}{2}(v_{i,j} + v_{j,i})$ is plotted. As expected, the domains with higher values of $|D|^2$ are near the walls (since the velocity is zero on the walls), except for the vicinity of the electrode ends. One can see there zones with reduced shear rate which suggest the presence of near solid zones. This behaviour can be attributed to the high electric field generated by the electrode edge. In the middle of the channel, $|D|^2$ keeps a small value.

In Fig. 5.12 we display the generalized viscosity. As one can see from (4.75) and from

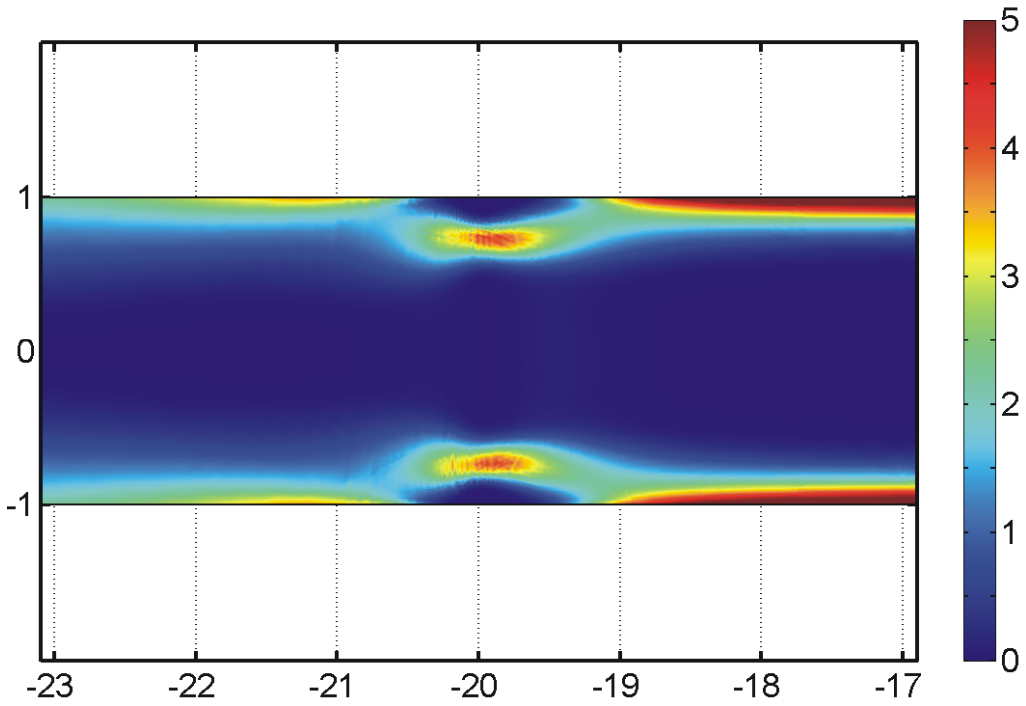

Figure 5.11: Surface plot of dimensionless $|D|^2$

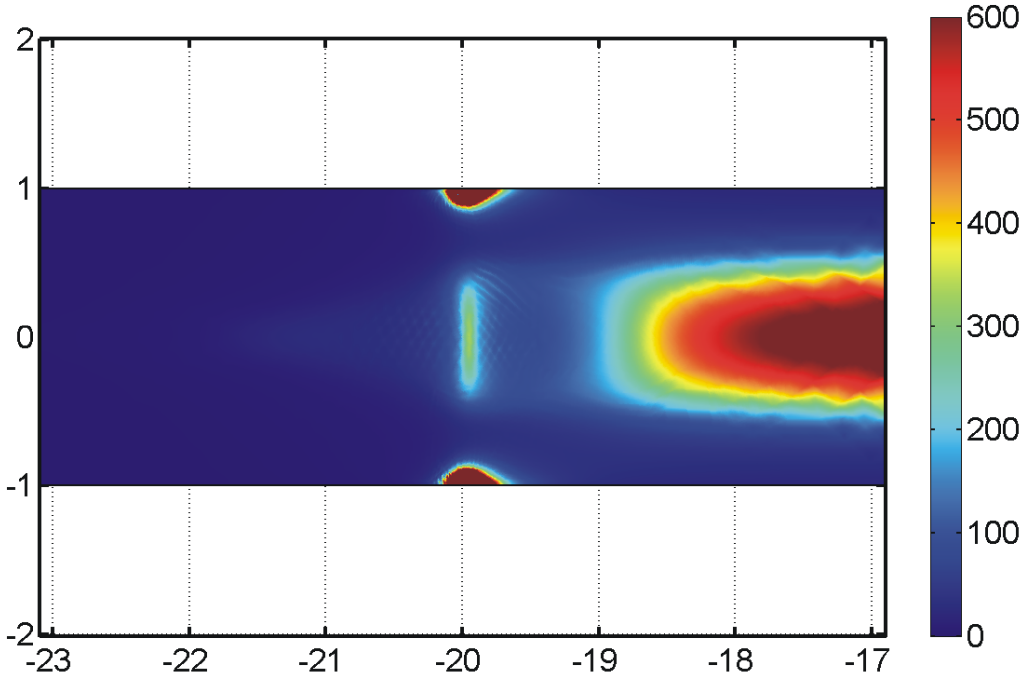

Figure 5.12: Surface plot of the generalized dimensionless viscosity

Fig. 5.1, η_{gen} is decreasing when $|D|$ is increasing, and it is increasing when E is increasing (since β_1 and β_2 are increasing with E). The electrode edges can be again identified; close to them, both E and $|D|$ give increasing contributions. An interesting shape of the viscosity η_{gen} ought to be noticed: right between the electrode ends a high viscosity "island" is formed after which it quickly decreases; then it increases again, assuming the known shape of the Casson-like fluid far downstream (with the unyielded region in the middle).

5.1.3 Inhomogeneity vs. strength of the electric field

The appearance of this island shape in the viscosity plot may be due in principle to two reasons: either an inhomogeneity in the electric field or an inhomogeneity in the flow. Since these effects are coupled we attempt to separate them by considering two special configurations, each of them containing only one type of inhomogeneity. First, in order to isolate the effect of the influence of the electric field inhomogeneity on the viscosity we considered an inhomogeneous electric field modulus in the x_2-direction in the channel according to

$$E(x_2) = \frac{2}{\pi}\arctan(x_2) + 1\,. \tag{5.8}$$

Using the electric field (5.8) we solve the problem (4.67), (4.74), (5.3) together with the boundary conditions (4.79)–(4.81). Figure 5.13 shows that an uniform increase in the electric field in the x_2-direction does not produce special effects on the viscosity and the transition is smooth. We conclude that the electrode edges are essential for the presence of these kind of inhomogeneities in the viscosity.

Further, we considered a configuration with uniform electric field where the electrode edges are replaced by notches as in the Fig. 5.14. The equations to be solved are also (4.67), (4.74), (5.3) together with the boundary conditions (4.79)–(4.81). The deduced viscosity has a similar island type shape as in Fig. 5.12. The reason why we introduced notches is that in our initial problem (treated in the previous Sections) solid-like regions with small velocity relative to the channel walls are formed at the tips of the electrodes (see Figs. 5.5, 5.12), which can be approximated by irregularities of the same shape in the channel walls. The other solid-like region (the usual plug zone specific to the Casson-like model) is moving with a velocity close to the maximum velocity relative to the channel walls.

One may conclude that the modification of the flow via the geometry may determine similar irregularities in the viscosity as those-ones produced via the inhomogeneous electric field.

5.1.4 Influence of the parameters c and δ

Figure 5.15 shows the behaviour of the electric field outside the electrodes for different values of the electric permittivity ratio (c). As it was shown in Section 3.7, the electric field is stronger in the area without electrodes when the permittivity of the material outside

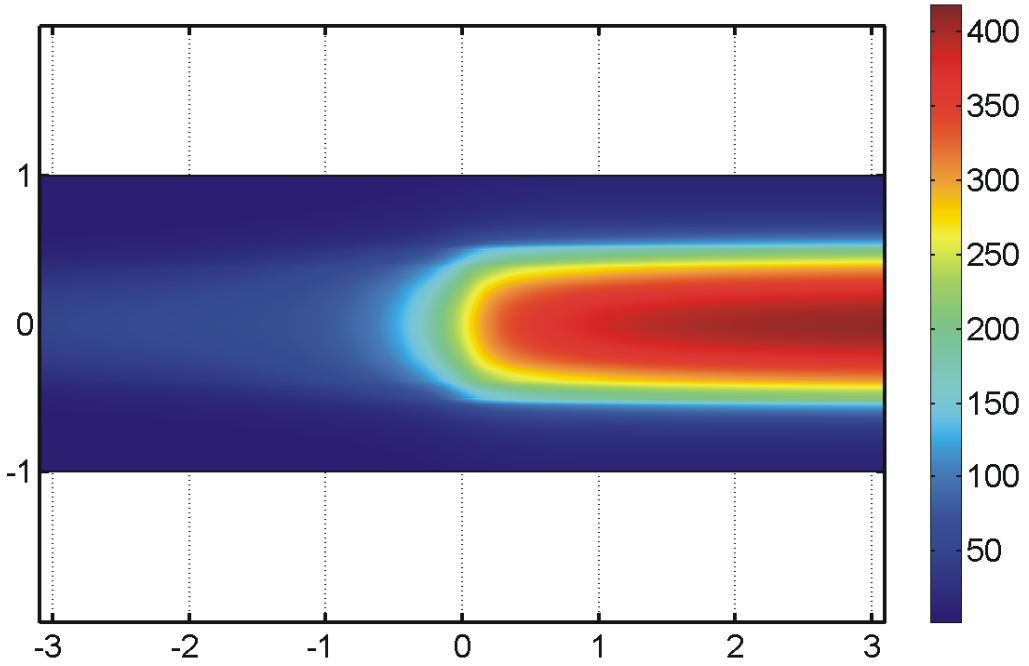

Figure 5.13: Surface plot of the generalized viscosity in an electric field of the form (5.8)

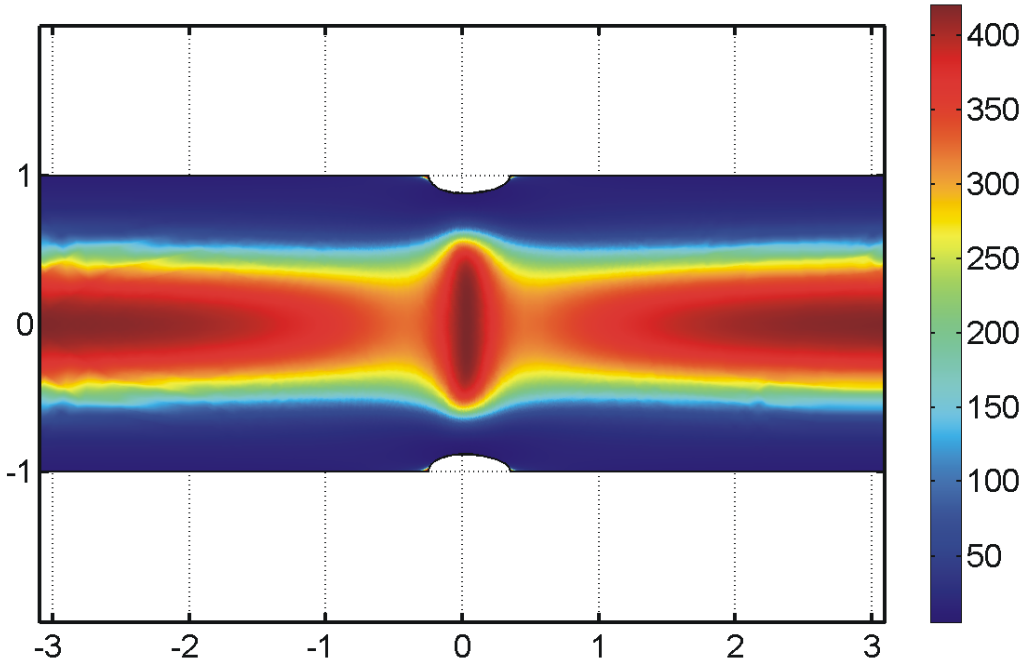

Figure 5.14: Surface plot of the viscosity in a notched configuration but in uniform electric field

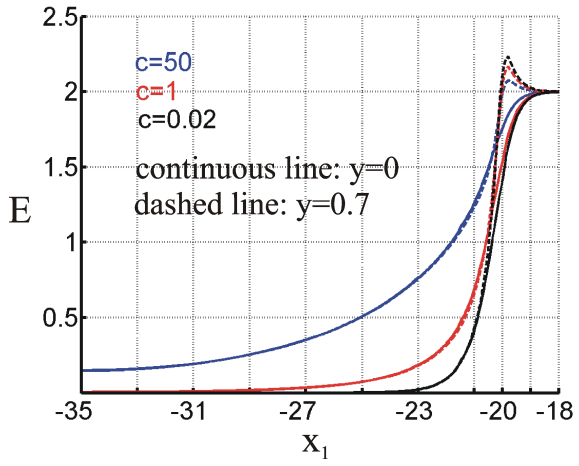

Figure 5.15: Line plots of $E(x, 0)$ (continuous line) and $E(x, 0.7)$ (dashed line) for different values of c (electrodes end in $x_1 = -20$)

the electrodes is larger than the permittivity of the ER-fluid. The plot also shows that in the small area close to the electrode edges this effect is reversed. As a consequence, we expect a contribution to the pressure drop from the region outside the electrodes when c is bigger than 1. We plot in Fig. 5.16 the pressure in the region where the ERF exits the electrodes in order to include in the plot the reference value $p = 0$. Indeed one can see that the pressure drop immediately at the electrode ends is slightly decreasing with the value of c. This effect may be important in configurations with short electrodes. For long electrodes the difference is not relevant because the main contribution to the pressure drop comes from the E =cst. region between the electrodes, see Fig. 5.10.

In Fig. 5.17 we plotted the pressure drops between $x_1 = 19$ or $x_1 = 21$ and the end of the channel, $x_1 = 35$ (where the outlet boundary condition imposes $p = 0$), denoted by p_{19} and p_{21}, respectively, versus the electric permittivity ratio (c). The pressures were calculated in the middle of the channel height $x_2 = 0$ and at $x_2 = 0.7$. One can see from the figure that the pressure in the region outside the electrodes does not depend on x_2 while a small dependence of the pressure drop on x_2 can be observed across the electrode edges. We remark that for c larger than 50 the change in pressure drop is negligible. Since the permittivity of the ER-fluid is quite small, in practice $c \ll 1$. To see the effects for smaller ratios c we repeated the same plot in Fig. 5.18 on a logarithmic scale.

Another key parameter of the model is δ. This can be viewed as a parameter which has to be chosen as small as possible in order to recover from equation (4.61) the Casson-like model, (equation (4.49)). On the other hand, δ can be viewed as a constitutive parameter which can be obtained from the experimental data fitted with equation (4.61).

Further on we study the influence of $n_\delta = \delta h^2/v_0^2$ (the dimensionless form of δ) on the solution. In Figs. 5.19 and 5.20 we plotted $\eta_{gen}(|D|^2, E = 2)$ for different values of n_δ according to formula (4.71). The two figures differ in the range of the argument $|D|^2$.

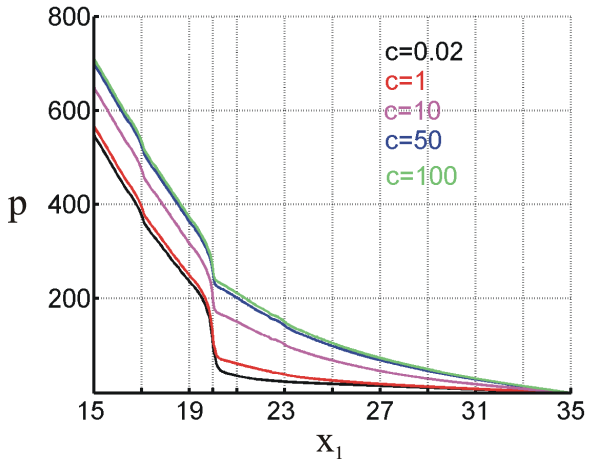

Figure 5.16: Pressure (at $x_2 = 0$) over the electrode ends for different c

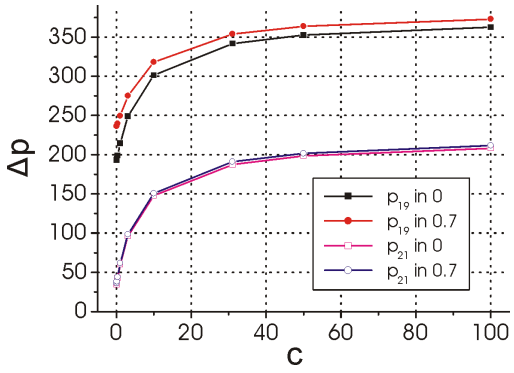

Figure 5.17: Pressure drop vs. ratio of the permittivities c - linear scale

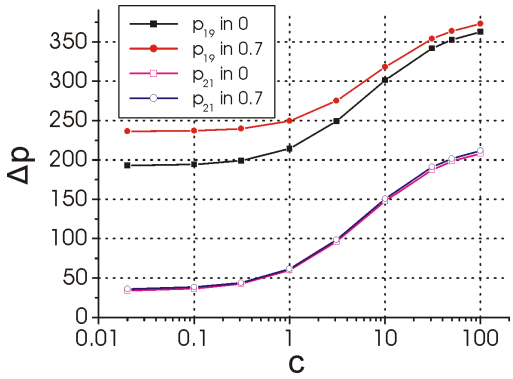

Figure 5.18: Pressure drop vs. ratio of the permittivities c - logarithmic scale

One can see from Fig. 5.19 that our choice of n_δ ($n_\delta = 0.002$) implies that the generalized viscosity differs from the classical generalized Casson-like viscosity (for $n_\delta = 0$) only for $|D|^2 < 0.01$. Fig. 5.20 shows that the parameter δ can still have a strong influence on the generalized viscosity for $|D|^2 < 0.1$.

For determining the yielded/unyielded regions we can introduce a criterion using the quantity $|\sigma^e| = \eta_{gen}|D|$ (we say the material is yielded where $\eta_{gen}|D| > 2|\beta_1(E)|$). As a consequence the yielded regions are influenced by the choice of δ if $|D|^2 < 0.1$; for $|D|^2 > 0.1$, δ does not change significantly the shape of the yielded regions.

In Fig. 5.21 we plot the computed pressure evolution in the channel for different values of n_δ. In the region with constant electric field (between the electrodes far from the electrode edge) the pressure drop is not influenced by n_δ while in the transition region n_δ produces some differences. For values smaller that n_δ used in the simulations (0.002) the differences are unnoticeable. In order to see the influence of δ on the flow field we

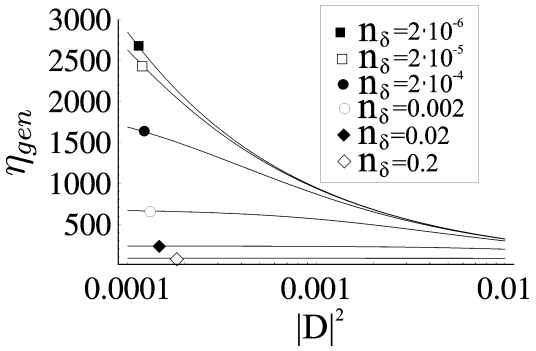

Figure 5.19: $\eta_{gen}(E = 2, |D|^2)$ for different n_δ in the range $0.0001 < |D|^2 < 0.01$ (Casson-like model)

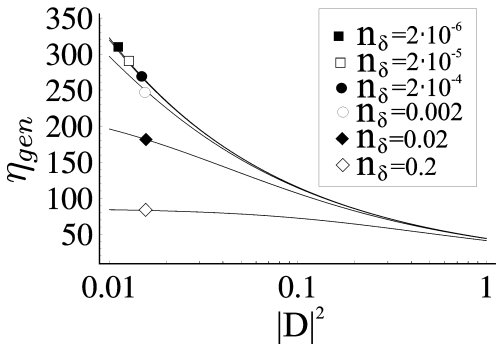

Figure 5.20: $\eta_{gen}(E = 2, |D|^2)$ for different n_δ in the range $0.01 < |D|^2 < 1$ (Casson-like model)

plotted the velocities in the transition area (see Fig. 5.22) and in the middle of the electrodes (see Fig. 5.23) for different values of n_δ. Again we see that for small values of n_δ ($n_\delta < 0.002$), the profiles are almost congruent. Figures 5.22 and 5.23 permit to identify those fluids which are described by our model containing a larger n_δ value. For increasing n_δ, the plateau is curving, indicating a reduced yielded region.

5.1.5 Comparison with the experiment

In order to compare the numerical modeling with the experimental results reported in [29] we considered in the numerical program a configuration as in Figure 3.1 consisting of two electrodes, charged non-symmetrically, of length $2l = 40$ mm, with a channel height of $2h = 2$ mm and a length of the channel of $2L = 70$ mm which corresponds to the geometry used in the experiments [29, 92]. Experiments are performed in a channel of width $b = 20$ mm. For computations the input value is the volumetric flow rate in the channel $Q = 4/3\, hbv_0$ and the output is the dimensional pressure drop calculated from $x_1 = -30$ mm on a length of 60 mm. In Fig. 5.24 we compare the obtained results for different values of $E_u = V/h$. The quantity E_u represents the value of the uniform electric field established in the middle of the channel, far from the electrode edges, and it is in fact the value of the magnitude of the electric field if the electrodes were infinitely long (see Section 2.2.1). While good agreement is obtained, the remaining inaccuracy of the calculations is given by the uncertainty in fitting of β_1 and β_2 (see (5.1) and (5.2)).

We considered this result as a validation of our computing model and we used it to simulate further configurations in our search for a possible enhancement of the electrorheological effect (see Section 5.4).

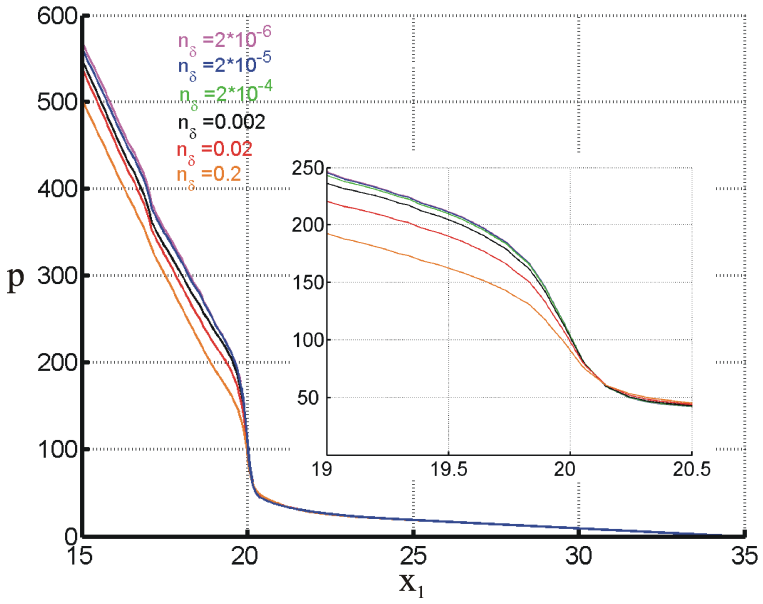

Figure 5.21: Pressure (at $x_2 = 0$) over the electrode ends for different values of n_δ; insets show a detail of the pressure near $x_1 = 20$

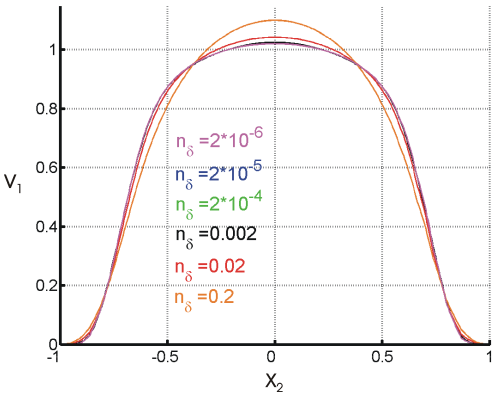

Figure 5.22: Profiles of v_1 in $x_1 = -20$ (electrode ends) for different values of n_δ

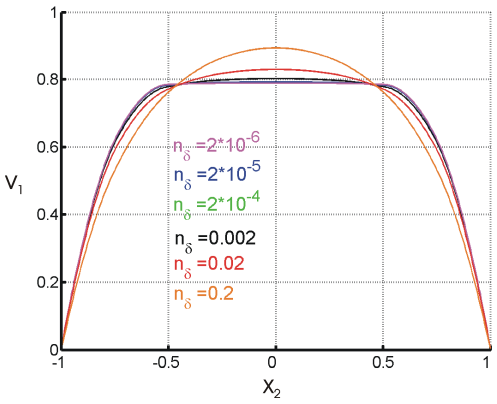

Figure 5.23: Profiles of v_1 in $x_1 = -16$ (between the electrodes) for different values of n_δ

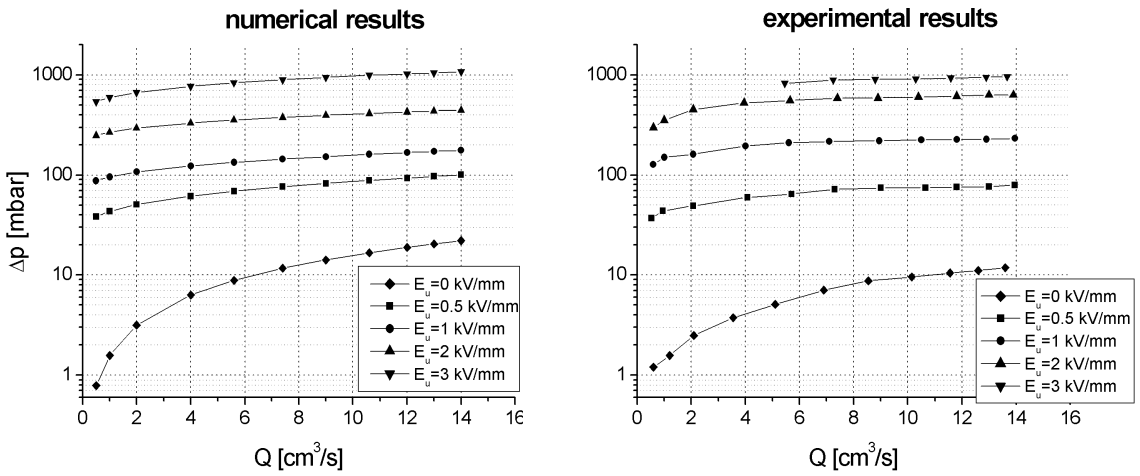

Figure 5.24: Comparison of the numerical and experimental results (dimensional pressure-drop vs. volumetric flow rate

5.2 The power-law model

5.2.1 Material and configuration properties used for the simulations

To illustrate the power-law constitutive equation we chose the ER-fluid EPS 3301 because, as shown in [92] it is described well by this model. EPS 3301 is produced by the company CONDEA Chemie AG (Germany). It is a particle-free fluid and consists of an acid metal soap which is dissolved homogeneously in a conventional hydraulic basis liquid. It contains also some additional hydraulic oil additives [22, 62, 92]. The fluid was studied experimentally by Wunderlich [92]. In order to better characterize the fluid, it was found (see [8]) that a dilution with 40% (weight percent) white oil (Weissöl) is appropriate.

Unlike the ER-fluid Rheobay 3565, the ER-fluid EPS 3301 shows pseudoplastic behaviour (the shear viscosity decreases with increasing shear rate) in the absence of the electric field. Under the application of the electric field also pseudoplastic behaviour is observed. In [92] the power law model (4.29) was found the most appropriate model to describe the data. Fitting the experimental curves "stress vs. shear rate" (obtained with the rotational viscometer), the values of m and n were calculated (see Table 5.2).

We used these values in our bidimensional model (4.83). First, by fitting the values of $f = m(v_0/h)^n$ (see Subsection 4.3.2) and n we have to obtain their dependence on the dimensional electric field E_0E:

$$f(E_0E) = f_1 + f_2(E_0E) + f_3(E_0E)^2\,, \tag{5.9}$$

$$n(E_0E) = n_1((E_0E)^2 + n_2)^{n_3}\,. \tag{5.10}$$

The coefficients f_1, f_2 and f_3 depend on the values of v_0 and h. For $v_0 = 0.1647$ m/s and $h = 0.001$ m we obtained $f_1 = 41.431$, $f_2 = 33.284$ mm/kV, $f_3 = 2.958$ mm^2/kV^2. For the

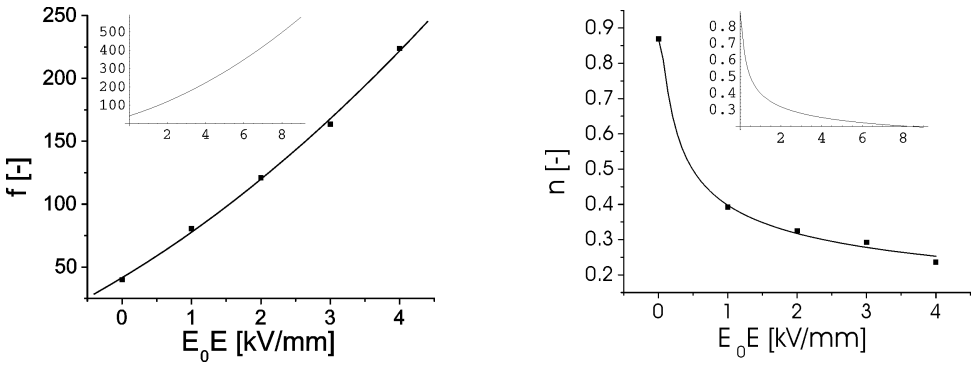

Figure 5.25: Fitting curves for the dependence of the coefficients f and n on the electric field. The insets show how the fit is extrapolated

function n we found $n_1 = 0.398$ (mm/kV)$^{2-n_3}$, $n_2 = 0.008$ kV^2/mm^2 and $n_3 = -0.163$. The function f is written as a series expansion by retaining only the terms up to the second order while n is described by a power function. The experimental data (see Table 5.25) are provided for a limited range of the electric field and does not cover the range of the electric field employed in the simulations. We use the formulas (5.9) and (5.10) also to extrapolate the given data for f and n for larger values of E. Figure 5.25 illustrates how the fitted curves approximate the data and the extrapolations, for $v_0/h = 164.7$ s^{-1}.

The geometry used for the simulation of EPS 3301 is the same as that used for Rheobay. The electric permittivity of EPS is $\varepsilon_2 = 1.4 \cdot 10^{-10}$ A·s/(V·m) and we chose $\varepsilon_1 = 0.02\,\varepsilon_2$. The density of EPS 3301 is 850 kg/m^3. All simulations except those done in order to make the comparison with the experimental data from Fig. 5.39 are performed for $h = 1$ mm, $E_0 = 1$ kV/mm, $V = 2$ kV and $v_0 = 0.1647$ m/s. So, $Re = 0.578$ and $Ma = 0.284$. We considered here also $n_\delta = 0.002$. In Subsection 5.2.3 we show the influence of this parameter on the solution.

Table 5.2: Values of the parameters m and n of (4.29) for different electric field strengths

$E_0E\,[\frac{\text{kV}}{\text{mm}}]$	0	1	2	3	4
m [Pas^n]	0.4702	10.8695	23.0439	36.8244	67.0970
n [−]	0.8697	0.3923	0.3249	0.2921	0.2361

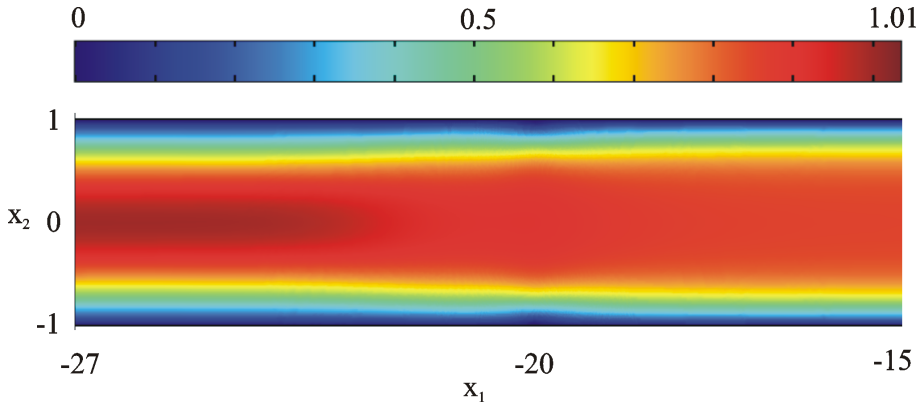

Figure 5.26: Surface plot of the non-dimensional velocity modulus in the vicinity of the electrodes edges ($x_1 = -20$)

5.2.2 The flow near the electrode ends (long electrodes)

In this Section a similar analysis as in Section 5.1.2 is carried out. In order to study the influence of the electrode edges on the flow we chose the same configuration of the electrodes and boundary conditions for the electrical problem as for the ER-material Rheobay, in Section 5.1.2. Consequently, the different rheological behaviour comes from the material properties.

One can distinguish three regions: one with small electric field, upstream the entrance between the electrodes; the transition zone with strongly inhomogeneous electric field right between the edges and the uniform electric field zone, between the electrodes, far downstream the edges.

In Fig. 5.26 the velocity modulus is plotted. In the areas ahead and after the electrode edges, the x_2-component of the velocity is very small and does not practically influence the x_1-component of the velocity. The end effect is reduced and the velocity develops smoothly from the region with reduced electric field to the region with constant electric field. Cross sectional cuts of the surface plot in these regions are presented in Figures 5.27 and 5.28. The scale of the plot from Fig. 5.28 indicates also the negligible character of v_2 (1/1000 from v_1). The profile of v_1 from the first zone is close to a Newtonian profile (reduced pseudoplastic behaviour as it was observed in the experiments for small electric fields in [92]). It presents the character of the unyielded region in the middle of the channel, as expected in general for an ER-fluid. To characterize the transition region we chose three points near the electrode ends: $x_1 = -20.2$, $x_1 = -20$ and $x_1 = -19.5$. Notice the plateau parts in the plots of v_1. The curvature change for v_1 in $x_1 = -20$ is very close to the electrode edge and slightly visible compared with the corresponding plot of the Casson-like model (middle plot of Fig. 5.6). The x_2 component of the velocity is smaller with 5% relative to the maximum inlet velocity. As for the Casson-like model, the two extreme values of v_2 in $x_1 = -20.2$ (first positive and then negative) and $x_1 = -19.5$

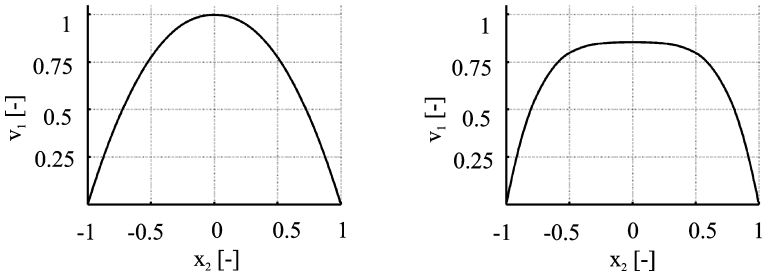

Figure 5.27: Profiles of v_1 at $x_1 = -23.5, -16.5$, respectively

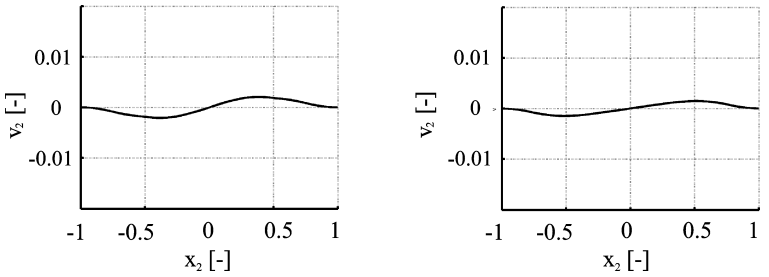

Figure 5.28: Profiles of v_2 at $x_1 = -23.5, -16.5$, respectively

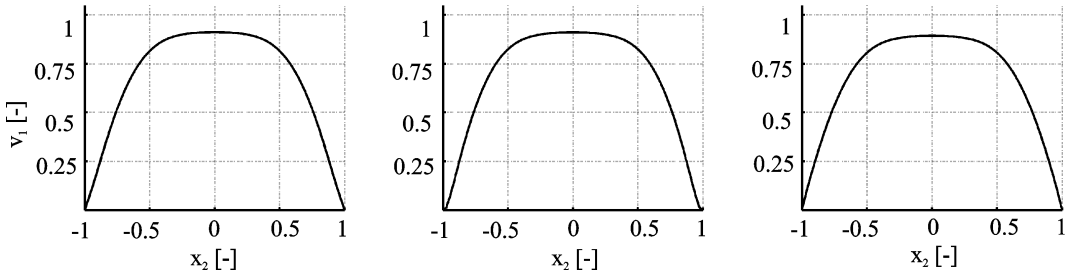

Figure 5.29: Profiles of v_1 at $x_1 = -20.2, -20, -19.5$, respectively

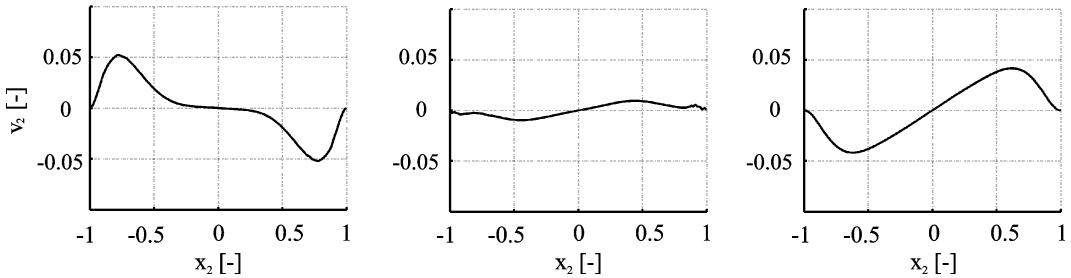

Figure 5.30: Profiles of v_2 at $x_1 = -20.2, -20, -19.5$, respectively

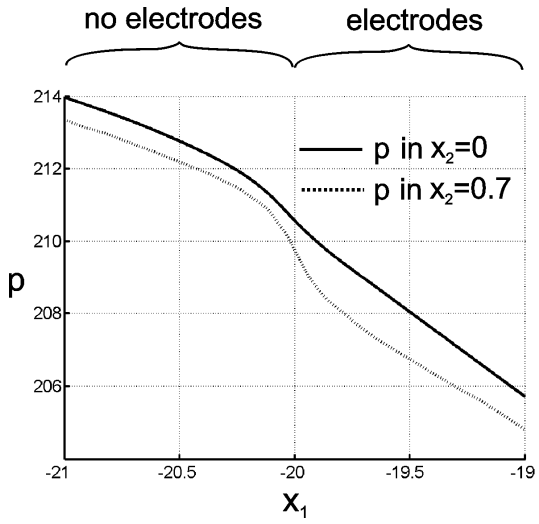

Figure 5.31: Pressure in the transition zone ($x_1 = -20$ marks the electrode ends)

(first negative and then positive) indicate that the fluid goes around the electrode tips.

In order to study the influence of the electric field on the pressure we plot in Fig. 5.31 the pressure along the channel, over the electrode ends. The transition area is characterized by a higher pressure gradient compared with the pressure gradient in the region with small electric field (outside the electrodes) and with the region with constant electric field (between the electrodes, far from the edges). The difference between these two regions is not significant. The presence of a higher gradient in the transition zone led us to the study from Section 5.4 where, on the basis of this observation, we investigated the possibilities to obtain a better ER-efect.

We continue our study of the transition region near the electrode ends with the plots of the second invariant of the stretching tensor $|D|^2$ in Fig. 5.32 and of the generalized viscosity η_{gen} (4.83) in Fig. 5.33.

Regarding the plot of $|D|^2$ against x_1, x_2 one can see that the regions with smaller values of $|D|^2$ around the electrode edges are reduced in comparison with the Casson-like model (Fig. 5.32). This can be explained by the fact that the ER-fluid EPS is a material with a reduced ER-effect. However, the plot is qualitatively similar with the corresponding plot for Rheobay (Fig. 5.11).

In Fig. 5.33 as in Fig. 5.12 one can observe a transition "solid" island between the electrode ends.

5.2.3 Influence of the parameter δ

As for the Casson-like model, δ can be viewed as a parameter which has to be chosen as small as possible in order to recover the power-law model (equations (4.47) and (4.48)) from equation (4.62). On the other hand, δ can be viewed as a constitutive parameter

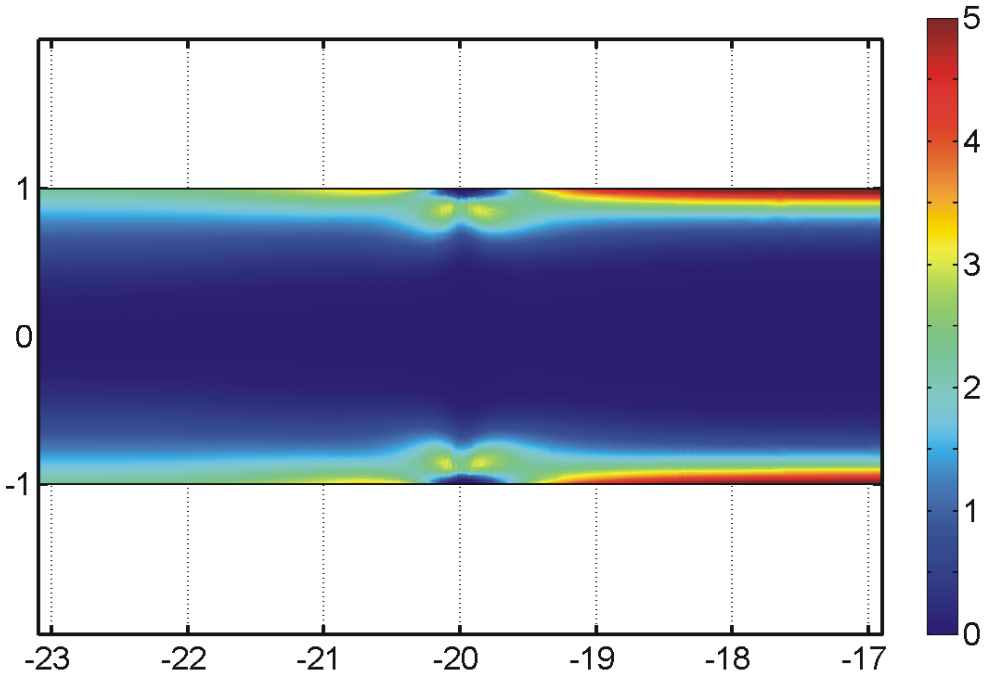

Figure 5.32: Surface plot of dimensionless $|D|^2$

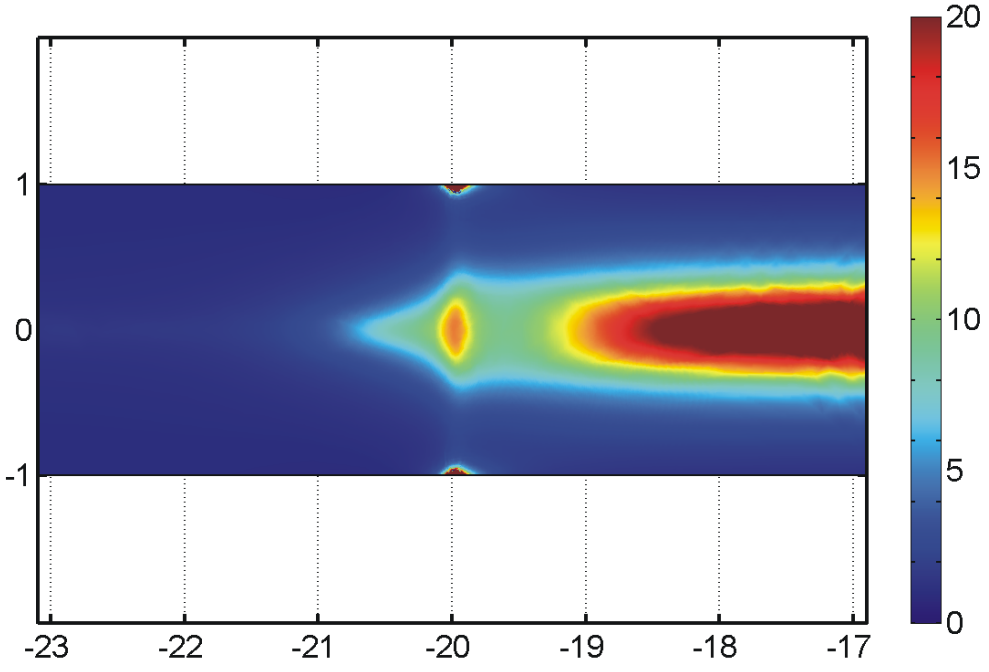

Figure 5.33: Surface plot of the generalized dimensionless viscosity

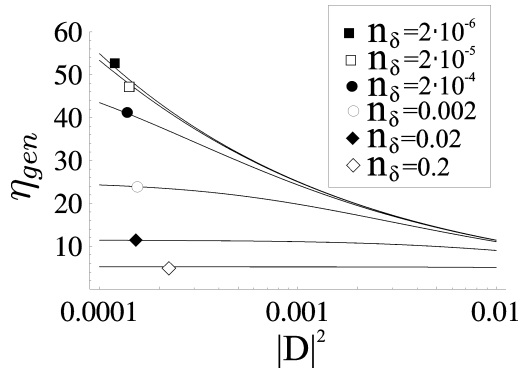

Figure 5.34: $\eta_{gen}(E = 2, |D|^2)$ for different values of n_δ in the range $10^{-4} < |D|^2 < 0.01$ (power-law model)

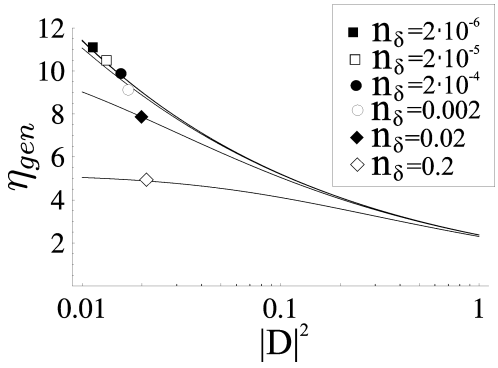

Figure 5.35: $\eta_{gen}(E = 2, |D|^2)$ for different values of n_δ in the range $0.01 < |D|^2 < 1$ (power-law model)

which can be obtained from the experimental data fitted with equation (4.62). Here we treat it as a small parameter. The number $n_\delta = \delta h^2/v_0^2$ is the dimensionless form of δ. Figures 5.34 and 5.35 show the influence of n_δ on the dimensionless viscosity $\eta_{gen}(E = 2, |D|^2)$ (according to the formula (4.83)) for different ranges of the argument $|D|^2$. One can see that its influence becomes more drastic for small values of $|D|^2$. In order to study the influence of n_δ on the solution we plotted in Fig. 5.36 the pressure along the channel axis containing also the electrode ends for different values of this parameter. The differences are slightly visible for $n_\delta > 0.002$ while for smaller values of n_δ the curves are practically congruent. Similarly, the plots of the velocity profiles in the uniform electric field and right between the electrode tips are shown in Figs. 5.37 and 5.38, respectively; they indicate a negligible influence of this parameter on the flow.

5.2.4 Comparison with the experiment

The experiments given in [92] have been performed in configurations consisting of two parallel electrodes charged non-symmetrically with three different lengths: $2l = 6$ mm, $2l = 20$ mm, and $2l = 40$ mm. The channel height is $2h = 2$ mm, the channel length is $2L = 70$ mm and the channel width is $b = 20$ mm. The potential imposed on the upper electrode is $V = 2$ kV. The input value for computations is the volumetric flow rate in the channel $Q = \frac{2(n+1)}{2n+1} v_0 hb$. The output is the ER-effect which is the dimensionless quantity

$$F_{\Delta p}(Q) = \frac{\Delta p_E(Q)}{\Delta p_{E=0}(Q)} - 1\,, \tag{5.11}$$

where Δp is the dimensional pressure drop calculated from $x_1 = -30$ mm on a length of 60 mm. In Fig. 5.39 the experimental results are compared with the numerical results for the three lengths of the electrodes. We found qualitative agreement: the ER-effect is decreasing with increasing volumetric flow rate. As expected, the ER-effect is larger for

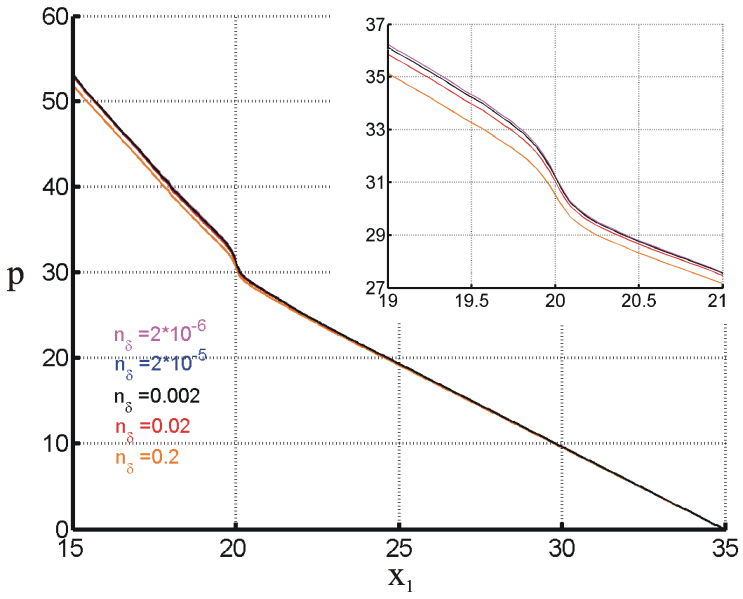

Figure 5.36: Pressure (at $x_2 = 0$) across the electrode end for different values of n_δ; insets show a detail of the pressure near $x_1 = 20$

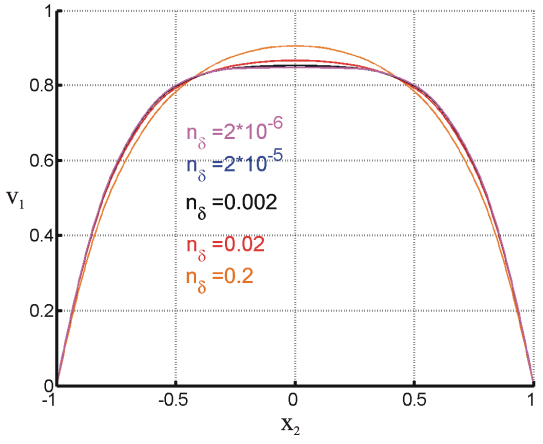

Figure 5.37: Profiles of v_1 in $x_1 = -16$ (between the electrodes) for different values of n_δ

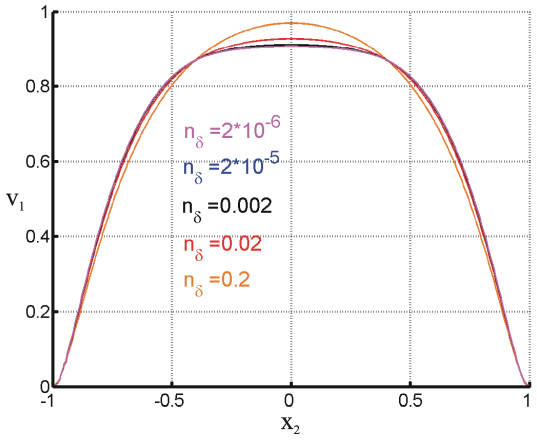

Figure 5.38: Profiles of v_1 in $x_1 = -20$ (electrode ends) for different values of n_δ

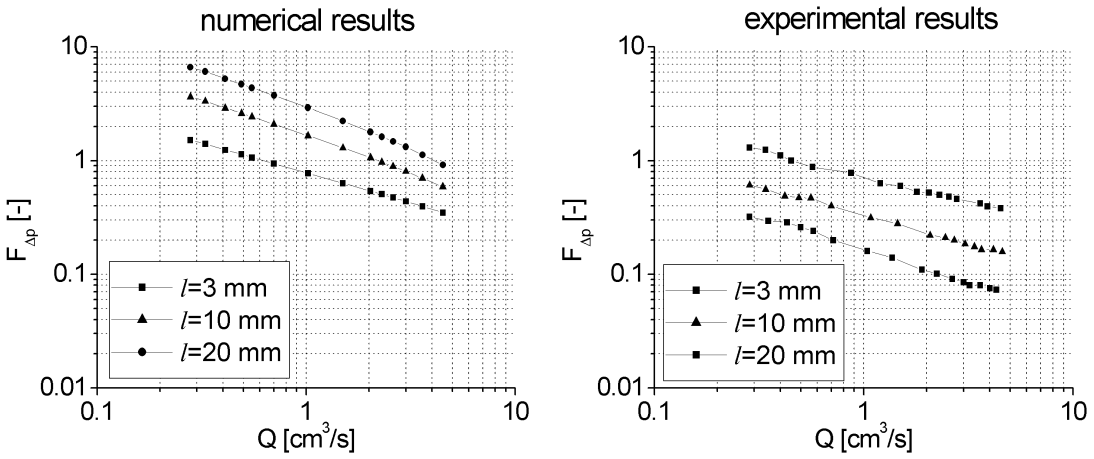

Figure 5.39: Comparison of the numerical and experimental results (electrorheological effect vs. volumetric flow rate)

larger l. The FEMLAB results are close to the approximate analytic computations (see Appendix D.2); the end effect is reduced as expected for a big length of the electrode.

5.3 Casson-like vs. power-law for the ER-material Rheobay

In this Section we perform a parallel analysis of the two models by applying them to the same material. We investigate the numerical solution dependence on the model. At the same time we examine the differences between different fittings, especially in the domains for which no experimental data are provided. We choose for this the ER-fluid Rheobay and we describe it with the power-law model (4.72) through a refitting process, using the data of Table 5.1. Let us consider the functions $\eta^i_{CL}(|D|) = \eta_{gen}(|D|, E_i)$, $i = 1, 2, 3, 4, 5$, where $E_1 = 0$ kV/mm, $E_2 = 0.5$ kV/mm, $E_3 = 1$ kV/mm, $E_4 = 2$ kV/mm, $E_5 = 3$ kV/mm, η_{gen} is according to the Casson-like model (4.71) applied to the data of Rheobay (see Table 5.1 and the paragraph before the Table) and with $\delta = 150$ ($n_\delta = 0.002$). By refitting each of these functions we obtain $\eta^i_{PL}(|D|) = \eta_{gen}(|D|, E_i)$ where η_{gen} corresponds to the power-law model (4.72). In Table 5.3 the values of the identified parameters m and n are given. We mention that we denoted exceptionally, only in this paragraph, by $|D|$ and η_{gen} the second invariant of the dimensional strain rate and the dimensional generalized viscosity, respectively. We did this in order to be consistent with the notation from the dimensional formulas given in Section 4.3 which are referred here. From now on $|D|$ and η_{gen} will denote again the corresponding dimensionless quantities.

Table 5.3: The values of the parameters m and n obtained for the electric field strengths E_i
in the case of the Rheobay ER-fluid

$E_0E\ [\frac{\text{kV}}{\text{mm}}]$	0	0.5	1	2	3
$m\ [\text{Pas}^n]$	0.0368	11.7015	68.4871	227.91	410.684
$n\ [-]$	1	0.2547	0.2498	0.1943	0.2344

By fitting the values of $f = m(v_0/h)^n$ (see Subsection 4.3.2) and n we obtained their dependence on the dimensional electric field E_0E:

$$f(E_0E) = f_1 + f_2(E_0E) + f_3(E_0E)^2\,, \tag{5.12}$$

$$n(E_0E) = n_1 + 1/((E_0E)n_2 + n_3)\,. \tag{5.13}$$

The coefficients f_1, f_2 and f_3 depend on the values of v_0 and h. For $v_0 = 0.3$ m/s and $h = 0.001$ m we obtained $f_1 = 11.04$, $f_2 = 60.1436$ mm/kV, $f_3 = 150.972$ mm^2/kV^2. For the function n we found $n_1 = 0.2096$, $n_2 = 38.7459$ mm/kV and $n_3 = 1.2653$. The function f is written as a series expansion by retaining only the terms up to second order,

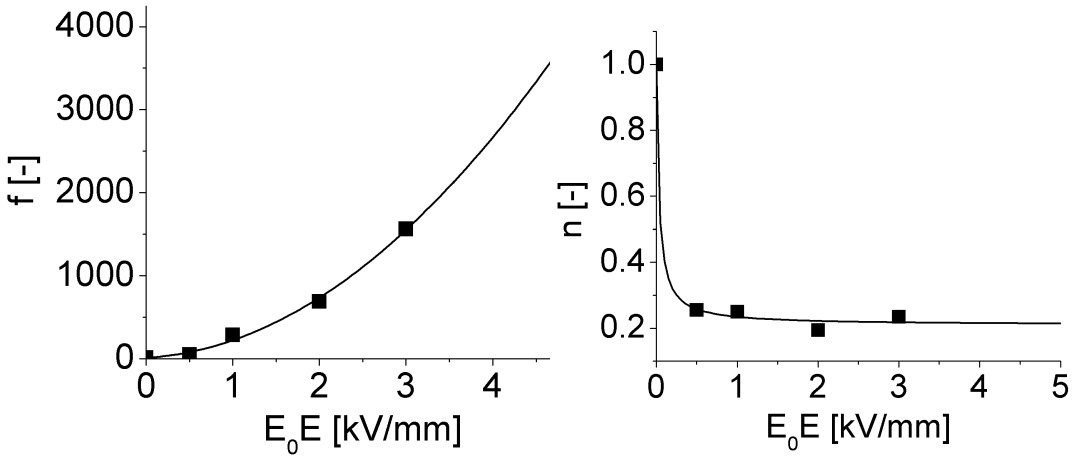

Figure 5.40: Fitting curves for the dependence of the coefficients f and n on the electric field (for the ER-fluid Rheobay)

while n is described by a rational polynomial function. Figure 5.40 illustrates how the fitting curves approximate the data. We observe that for $E < 0.5$ there is a big variation in the value of n while for $E > 0.5$, n stays almost constant. The extrapolated part of the functions f and n ($E > 3$) reflects the choice of the fitting functions and may be different according to the type of the used function.

Now substituting f and n as functions of E in formula (4.83) we obtain the dimensionless power-law viscosity for the Rheobay material.

In Fig. 5.41 we plotted the relative variation of the dimensionless viscosity of the Rheobay fluid described with the power-law model relative to the Casson-like dimensionless viscosity (obtained in Subsection 5.1.1), $(\eta_{gen}^{CL} - \eta_{gen}^{PL})/\eta_{gen}^{CL}$. The domains of $|D|$ and E are chosen to cover all the values obtained in a typical numerical simulation. The obtained relative variation has a range from -20% to 80% which is relatively small if we take into account that the extrapolation of f and n contains a high degree of freedom.

In Fig. 5.42 we plotted the same quantity in gray levels. Therefore, we can see that in the region for which experimental data are given, the relative difference is in the range of $\pm 20\%$. In the region with high values of the electric field, the discrepancy between the two viscosities increases to 80%. However the regions of intense electric field (in which the two viscosities differs by more than 20%) from the cases which we simulated are reduced to small domains (of order $0.1\,h$, h being half of the channel height) around the electrodes edges.

Subsequently we simulate the Rheobay fluid with the power-law model, for the same conditions as in Section 5.2.1, except the inlet velocity which is taken as $v_0 = 0.3$ m/s. By doing this, we try to trace the finger prints of the Casson-like and power-law models. We plotted the velocity profiles right at the electrodes tips and the pressure drop across the transition zone. In Fig. 5.43 the difference is hardly visible (the velocity profiles are overlapping) while in Fig. 5.44 we realize a small difference in the pressure fields near the

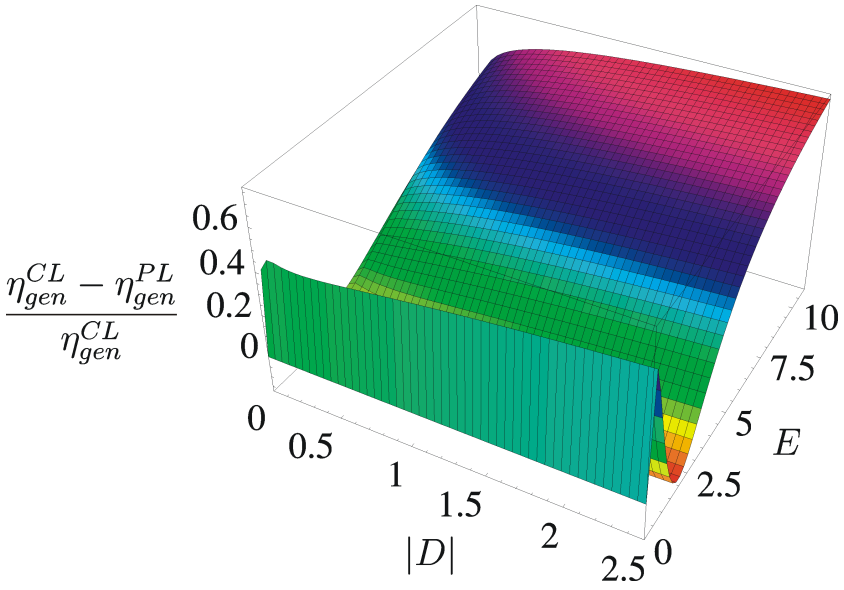

Figure 5.41: The relative difference of the viscosities of the two models for the same material (all variables are dimensionless); the plot is colored according to the height of the surface for a better understanding of the surface form

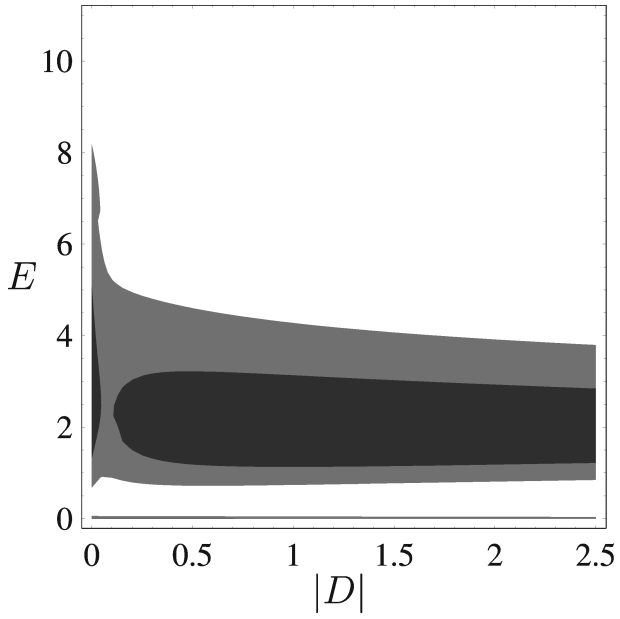

Figure 5.42: Contours for the relative difference of the viscosities of the two models for the same material (black accounts for values between -0.2 and 0, grey accounts for values between 0 and 0.2 and white accounts for value larger than 0.2)

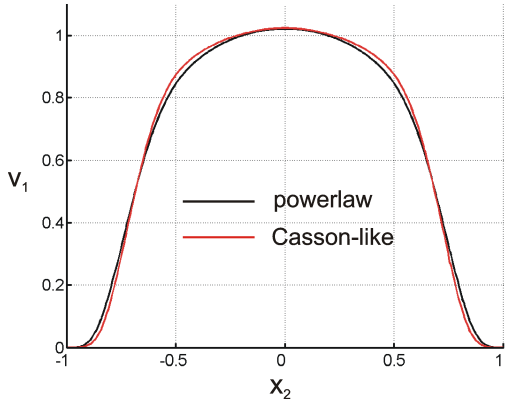

Figure 5.43: Transition profile of v_1 ($x_1 = 0$) for the two models

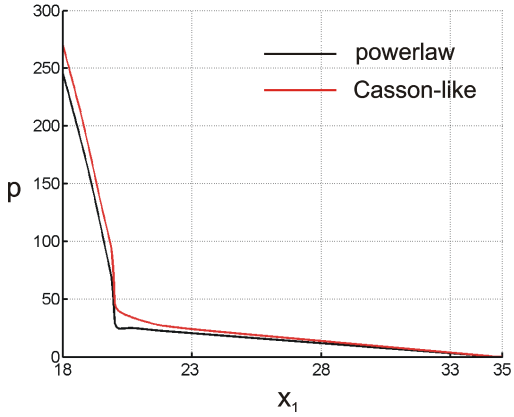

Figure 5.44: Pressure across the transition zone in $x_2 = 0$ for the two models

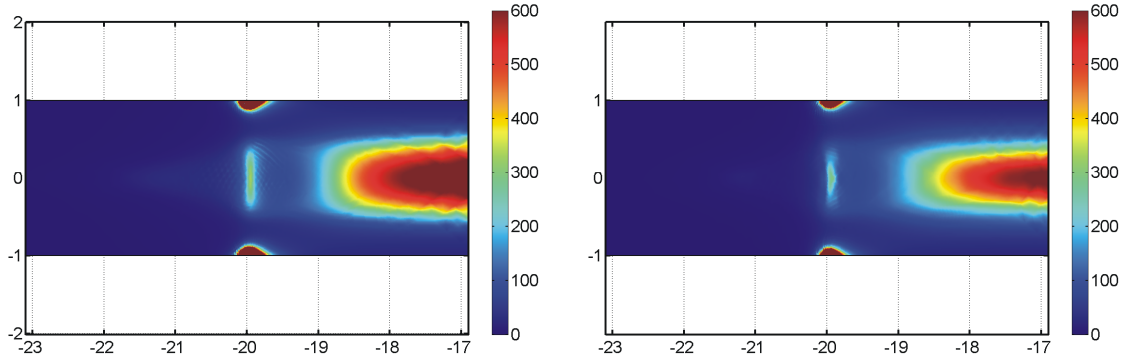

Figure 5.45: Generalized viscosities for the Rheobay fluid as obtained with Casson-like (left) and power-law models (right)

exit from the channel part between the electrodes. Nevertheless, along the whole channel, the pressure drop is only 3% larger when simulating with the Casson-like model than with the power-law model.

We also analysed the viscosities in Fig. 5.45. The observed differences are in agreement with the error range shown by Fig. 5.41. We may conclude that both models may be considered valid ones with a good approximation, and no distinct model characteristics are observed.

5.4 Enhancing the ER-effect

In technical applications there is a strong interest in obtaining an enhanced ER-effect (5.11). Many experimental works (see e.g. [4, 92]) have been performed in this direction. Most attempts are based on the modification of the geometry in such a way that inhomogeneities in the electric field are introduced. These investigations show that changes in the geometrical configurations may lead to a reduction or an enhancement of the ER-effect. However, it is difficult to distinguish by what measure this enhancement is produced, i.e. by the electric field inhomogeneities or by the inhomogeneities in the flow which are due to the modification of the geometry (which appear also when the electric field is switched off).

The configurations studied in this Section are based on inhomogeneities caused by the end effects of the electrodes. This means that instead of modifying the geometry, the electric field inhomogeneities are introduced here by changing the boundary conditions in the electrical problem. Since by each such change, the formulation of the problem for vanishing electric field remains unchanged, the increase/decrease in $F_{\Delta p}$ (see (5.11)) is equivalent to an increase/decrease in Δp. Consequently, our study will focus on the examination of the possibilities to obtain larger values of the pressure drop at the same value of the volumetric flow rate by using the inhomogeneities produced by the electrode ends.

As Fig. 5.10 and Fig. 5.31 show, the pressure decreases more rapidly around the electrode edges. In order to analyse how one can use this effect in an optimal way the simplest elements are investigated: short electrodes (which imply also an interaction between the left and right electrode edges), an electrode interrupted by a hole and a short electrode between two holes. The study is performed for both ER-materials Rheobay and EPS (which are modeled with the Casson-like and power-law equations, respectively, as described in the previous Sections). Since we treat here (almost) only cases with short electrodes, all the calculations are done using a completely numerical approach (as defined in Subsection 5.1.1). The data introduced in FEMLAB are those given in Subsections 5.1.1 and 5.2.1 (all the lengths in this Section are given relative to the channel height).

Let us investigate first the influence of the electrode length. To obtain the plots of Fig. 5.46 different lengths $2l$ of the electrodes were considered, and the pressure drop $\Delta p = p_{x_1=-30} - p_{x_1=0}$ vs. l was computed. For $l < 1.5$ for the Casson-like fluid and for $l < 2$ for the power-law fluid the curves (square points interpolation with continuous lines) deviate from the linear behaviour (continuous straight lines) which is a consequence of the electrode ends coupling in the electrical problem. For very short electrodes (stronger inhomogeneities) the pressure drop is significantly decreasing. For the Casson-like fluid, a better electrorheological effect is obtained when the electrode edges do not interact while for the power-law fluid the largest value of the ER-effect is obtained for short electrodes of length around 0.5 where the electrode ends are strongly interacting. Note that 2 is the dimensionless height of the channel. The dotted lines of the same figures represent the pressure drop calculated analytically by neglecting the end effects, namely by applying

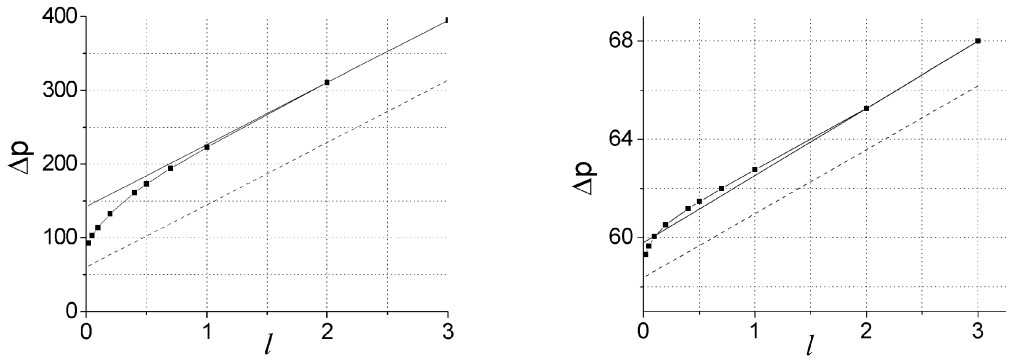

Figure 5.46: Pressure drop from $x_1 = -30$ to $x_1 = 0$ vs. the half length of the electrodes (Casson-like fluid (left) and power-law fluid (right)): dotted line – analytical evaluation with 1D model; square points interpolated with continuous line – numerical evaluation with 2D model; continuous straight line – fit for the behaviour of the pressure drop for long electrodes

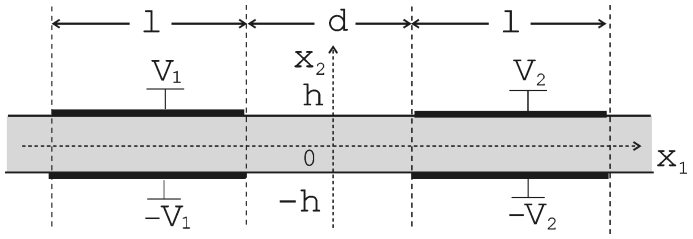

Figure 5.47: Configuration with electrodes interrupted by one "hole"

the formulas of Appendix D. The difference between this curve and the curves obtained numerically shows the values of additive pressure drops due to the end effects.

In order to see how the value of the pressure drop can be increased, we will investigate further what happens when the electrodes are interrupted by "holes" of length d (see Fig. 5.47). We study the effect in two cases of charging the 4 electrodes: for $V_1 = V_2 = V$ and for $V_1 = -V_2 = V$. We call these situations normal and inverse polarity of the electrodes, respectively. For inverse polarity, when the hole is sufficiently short, there will appear a stronger electric field that influences the flow more significantly. To illustrate this effect we plot in Fig. 5.48 the velocity surface in the channel for the Casson-like fluid. The behaviour for the power-law model is similar. The inhomogeneities in the flow are stronger near the electrode edges bounding the hole than around the exterior edges. Of course, one should avoid too short holes which can lead to short circuits.

We computed the average pressure gradient $k_1 = (p(x_1 = -\frac{l+d}{2}) - p(x_1 = \frac{l+d}{2}))/(l+d)$ for $l = 10$ and for variable d. Since the electrodes are sufficiently long, the electric field

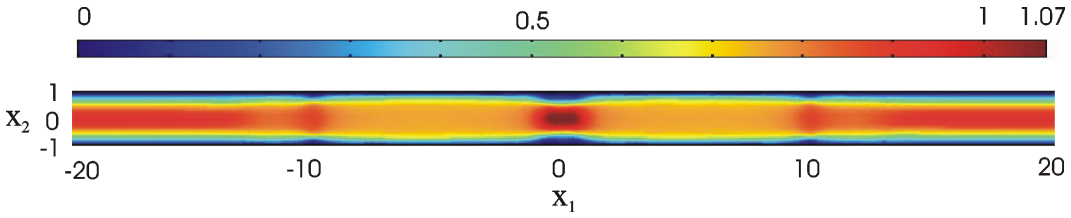

Figure 5.48: Surface plot of the velocity modulus – long electrodes ($2l + d = 20$) with holes (of length $d = 1$) in the middle (inverse polarity) (Casson-like fluid)

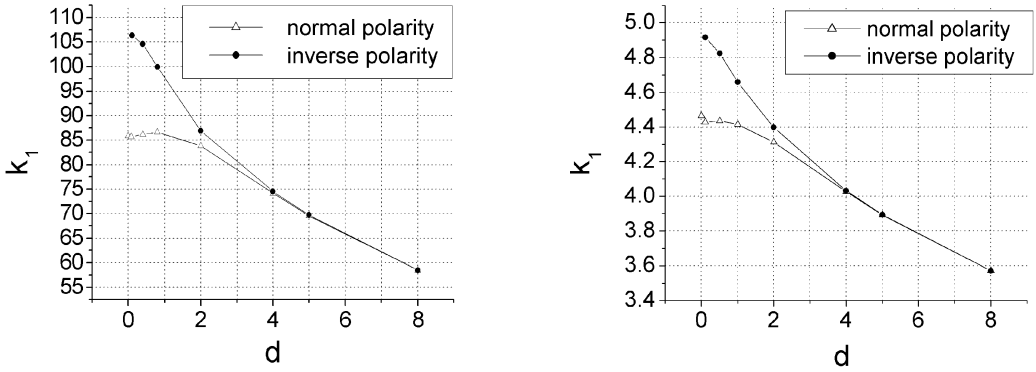

Figure 5.49: Average pressure gradient vs. hole length: normal and inverse polarity (Casson-like fluid (left) and power-law fluid (right))

becomes homogeneous and the flow will be of Poiseuille type around $x_1 = \pm\frac{l+d}{2}$, the middles of the electrodes. By plotting k_1 for different lengths of the hole one can compare the hole effect on the pressure drop. From Fig. 5.49 one can infer pretty similar qualitative behaviours for both fluids. For $d > 1$ and normal polarity and for $d > 2$ and inverse polarity, the pressure gradient is smaller than that calculated for electrodes without any hole, $k_1 = 85.84$ (for the Rheobay) and $k_1 = 4.464$ (for the EPS) (corresponding to the case $d = 0$ for normal polarity). The behaviour for short holes is different for the two polarity cases due to the different interaction of the electrode edges in the hole: smaller values of the pressure gradient for normal polarity due to a reduced electric field in the hole and higher pressure gradient for inverse polarity since a stronger electric field occurs in this case in the hole. The optimal length of the hole is the shortest possible without electric short circuit.

If we introduce more holes, the next step is to study, for inverse polarity, how close the holes should be placed. To answer this question we study the case of one variable electrode of length l_1 placed between 2 holes of constant length d (see Fig. 5.50).

The electrodes on the left and right sides have length l_2. In Fig. 5.51 we plotted the average pressure gradient $k_2 = (p(x_1 = -\frac{l_1+l_2+2d}{2}) - p(x_1 = \frac{l_1+l_2+2d}{2})/(l_1 + l_2 + 2d)$ vs. l_1

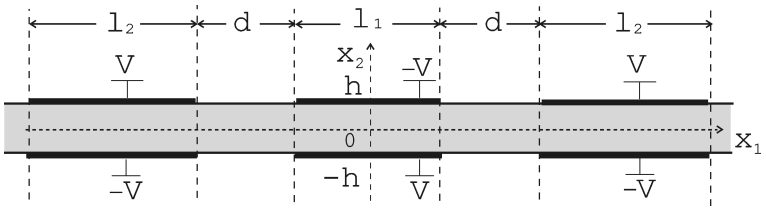

Figure 5.50: Configuration with electrodes between holes (inverse polarity)

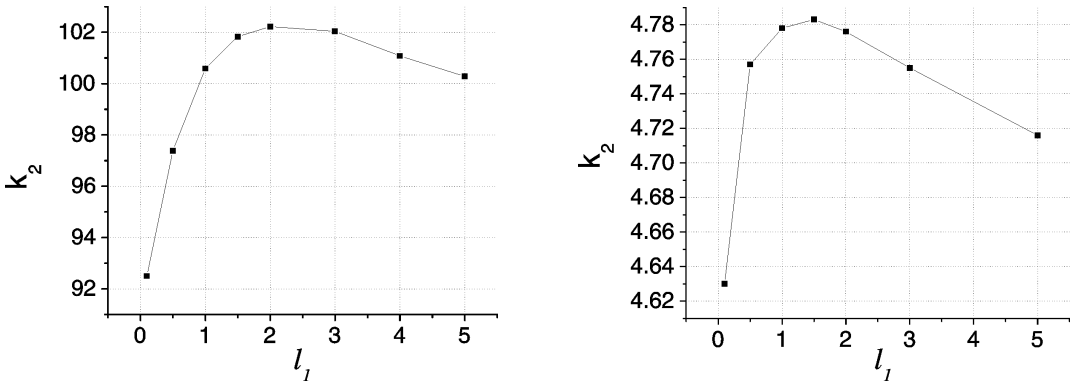

Figure 5.51: Average pressure gradient vs. length of the middle electrode (one electrode placed between two holes, alternating polarity) (Casson-like fluid (left) and power-law fluid (right))

for $l_2 = 10$ and $d = 1$. The optimal length of an electrode between holes of length $d = 1$ is around $l_1 = 2$ in the Casson-like case while in the power-law case it is around $l_1 = 1.5$.

Having the optimal parameters, one can now design optimal series of electrodes. As an example we consider a series of five electrode pairs and we compare the pressure over an interrupted electrode pair with the pressure over an uninterrupted electrode pair (see Fig. 5.52). One can see that it can be obtained up to 30% enhancement of the pressure drop when combined optimized series of holes and electrodes are used. To get a better insight we display in Fig. 5.53 the generalized viscosity. In the case of the Rheobay fluid we remark two regions with increased viscosity: one along the walls and another one in the middle of the channel. The first one is due to the high electric field around the edges of the electrodes. If we had not interrupted electrodes, we would have a continuous yielded region characterized by a high viscosity in the middle of the channel. But in the case presented here this region is splitted in islands of high viscosity. One observes a similar behaviour in the case of the EPS fluid but in a lower extent.

5.4.1 Conclusions

In this Section we focused on the pressure drop simulation due to its importance for application. The effects of the holes and of the length of the electrodes have been computed that provide direct insight to the building blocks of typical experimental set-ups. The analysis has been carried out by taking into account the polarity of the electrodes which critically influence the distribution of the electric field in the channel. A better effect is obtained by introducing holes in the electrodes and by alternating the polarity of the electrode cuts as depicted in Fig. 5.50 than taking continuous electrodes. We found optimal lengths for the electrodes and holes relative to the height of the channel.

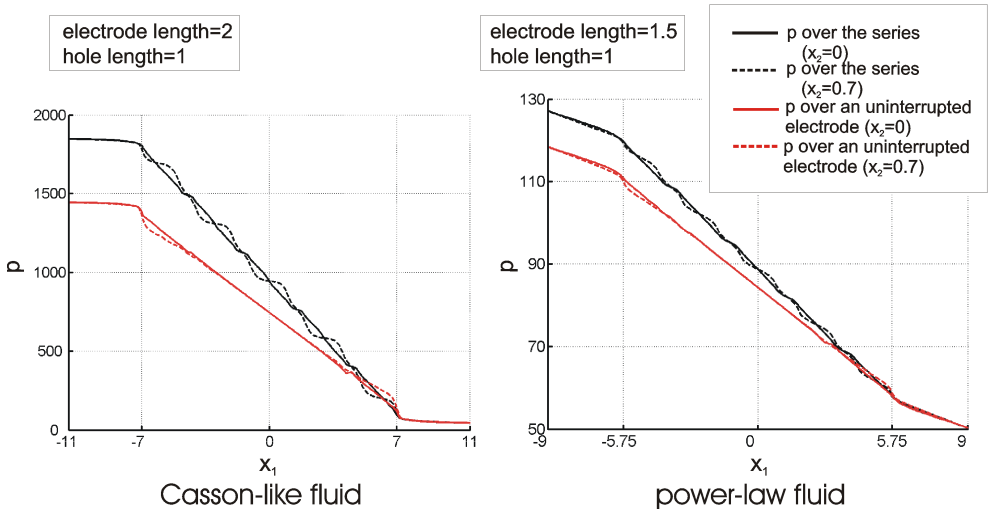

Figure 5.52: Comparison between the pressure over an uninterrupted electrode pair and the pressure over an optimized series of five electrode pairs (inverse polarity)

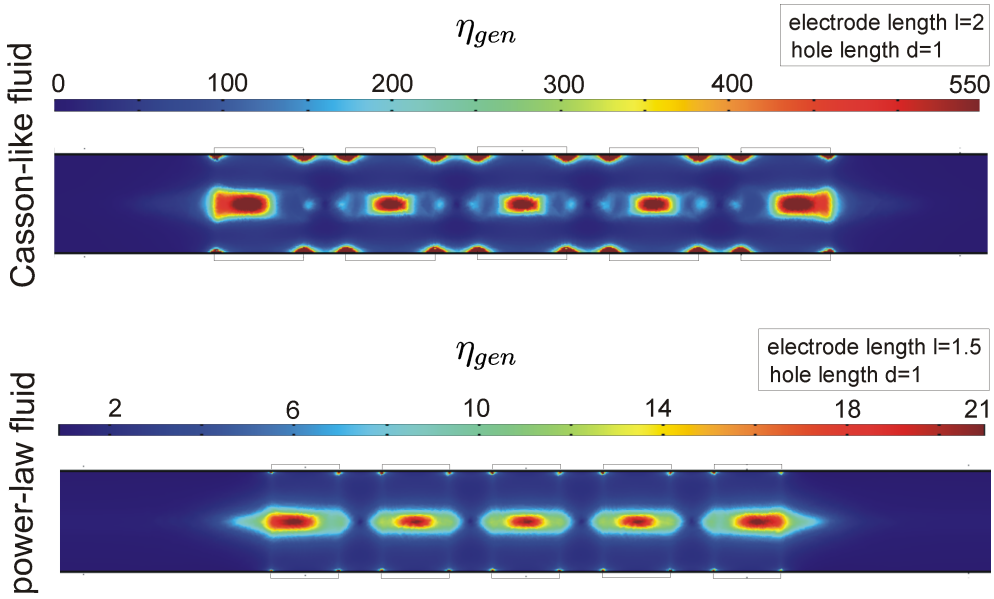

Figure 5.53: Surface plot of the generalized viscosity for an optimized series of five electrode pairs (inverse polarity)

Chapter 6

Summary and concluding remarks

Using the governing equations of electrorheology we formulated a boundary value problem for the steady pressure driven channel flow of electrorheological fluids under inhomogeneous electric fields and we analysed this electrorheological problem by means of applied mathematics. To our knowledge, this is the first time when an ER-problem involving an inhomogeneous electric field (the electric field is not a constant parameter but a variable to be determined from the problem) is solved mathematically.

The electro-mechanical problem is decoupled in a pure electrical problem and a mechanical problem which is influenced by the electric field.

The **electrical problem** consists in the Laplace equation while the boundary conditions are formulated by taking into account the end effects of the electrodes and the influence of the material outside the channel. First the problem is solved in the case of semi-infinite electrodes by using the Wiener-Hopf method which is appropriate to this elliptic BVP with mixed boundary conditions. The solution has a high degree of generality. First it can be applied to several configurations of electrodes: with non-symmetric boundary conditions, with symmetric and anti-symmetric boundary conditions or to a configuration with one electrode inside the fluid. Second, each of this configurations can be extended to the case of finite electrodes provided that the far edges of the electrodes do not interact. Third the solution depends on parameters like the height of the domain, the height of the channel and the ratio of the permittivities, each of them having a certain influence on the profile of the electric field. Let us mention briefly the advantages of this analytical solution for the electric field:

- it gives us the possibility to determine explicitly the singularity at the electrode tips; we obtained square root singularities there.
- comparing with the numerical solution, the analytical one is determined for an infinite domain in the x_1-direction.
- it was used to test, validate and benchmark the corresponding numerical solution.
- when simulating the ERF flow, we used it in the fluid problem to reduce computing time and usage memory in this way.

The inconvenience is the form of the solution but this is overcome by using truncation of the infinite sums in the numerical approach.

Concerning the **mechanical problem** one remarks that due to the end effects the flow is no longer viscometric but bidirectional.

In order to decide the constitutive function for the Cauchy stress tensor we took into account both the experimental evaluations of several ER-fluids and the theoretical approaches in the literature. We chose two models which can be viewed either as generalization of the one-dimensional Casson-like (which in its turn includes the Bingham and Casson models as particular models) and power-law models or as the particularization of certain three-dimensional models existing in the literature. We have used a trick to eliminate the two branched form of these functions and to avoid vanishing denominator by including a small parameter δ in the denominator in such a way that the original models are recovered when $\delta \to 0$. We denoted these adapted functions for the numerical approach as "alternative". The constitutive parameters depend on the electric field and since this is inhomogeneous, they are space dependent. The dependence on the electric field is obtained for each ER-material by fitting data measured in viscometric flows.

One cannot find analytical solutions for this non-linear problem except for the particular case of constant electric field which is solved analytically for both constitutive models. By using the Femlab software, a program based on the finite element method, we simulated the channel flow of two commercially available electrorheological fluids: Rheobay TP AI 3565 and EPS 3301. We have used the alternative Casson-like model to describe the Rheobay ER-fluid and the alternative power-law model to describe the EPS ER-fluid.

As the validation of our computing model we found good agreement between our results and experiments.

The simulations proved that the inhomogeneities in the electric field may lead to an enhancing of the ER-effect but may also reduce the ER-effect.

First, simulating the pressure along the part of the channel containing the electrode ends we shown that due to the inhomogeneities present there the pressure decreases more rapidly around the electrode edges. This was more clearly seen in the case of the Rheobay fluid but in a lower extent was also observed for the EPS fluid. We further analysed how can one use this effect in an optimal way. We investigated the simplest elements: short electrodes (which imply also the interaction between the left and the right edges of the electrode) and electrodes interrupted by a hole. Here there were defined two special cases of charging the electrodes denoted by normal and inverse polarity. Eventually the last one proved to be the most efficient one. We observed stronger inhomogeneities in the flow near the electrode edges bounding the hole than around the exterior edges. The third building block consists in the configuration with a short electrode between two holes (inverse polarity). We found optimal length of an electrode, of a hole and of the distance between two holes. Having the optimal parameters we could design optimal series of electrodes. At last we mention that beside the optimization studies, our computing model can be applied also to examine the behaviour of several fields such as velocity, second invariant of the strain rate tensor and generalized viscosity for both constitutive

models in inhomogeneous electric fields.

Appendix A

Selected results from Complex Analysis

For more details we refer the reader to [71, 89] for the subject treated in A.1, to [1, 54] for A.2 and to [54, 89] for A.3.

A.1 The Fourier transform with complex argument

Let us recall first the definition of the Fourier integral

$$F(\omega) = \frac{1}{\sqrt{2\pi}} \int_{-\infty}^{\infty} f(t) e^{i\omega t} dt \tag{A.1}$$

of an absolutely integrable function $f(t)$ of the real variable t. The right-hand side of (A.1) is the ordinary Fourier transform of f denoted by $\mathcal{F}[f(t)]$. Now let s be a real number such that $e^{-st} f(t)$ is absolutely integrable. Then

$$\mathcal{F}[e^{-st} f(t)] = \frac{1}{\sqrt{2\pi}} \int_{-\infty}^{\infty} f(t) e^{(i\omega - s)t} dt \,. \tag{A.2}$$

We can define now the Fourier transform with the complex argument $\zeta = \omega + is$ of the function f

$$F(\zeta) = \frac{1}{\sqrt{2\pi}} \int_{-\infty}^{\infty} f(t) e^{i\zeta t} dt \,. \tag{A.3}$$

If there are two real numbers $s_1 < s_2$ such that both $e^{-s_1 t} f(t)$ and $e^{-s_2 t} f(t)$ are absolutely integrable then $F(\zeta)$ is defined for all ζ in the strip $-\infty < \omega < \infty$ and $s_1 < s < s_2$ and it is an analytic function of ζ in this strip.

It is easy to verify that all the operational rules valid for the ordinary Fourier transform hold also for complex values of ζ. We mention here that if $e^{-st}f(t)$ is absolutely integrable and continuous and $e^{-st}f'(t)$ is absolutely integrable then

$$\mathcal{F}[f'](\zeta) = -i\zeta\mathcal{F}[f]\,. \tag{A.4}$$

Similarly we have

$$\frac{d}{ds}\mathcal{F}[f] = \mathcal{F}[itf(t)](\zeta)\,, \tag{A.5}$$

provided that $tf(t)e^{i\zeta t}$ is absolutely integrable.

Concerning the inversion of the complex Fourier transform we should mention that when prescribing an analytic function $F(\zeta)$ it is necessary to specify for what values of $Im\,\zeta$ it is to be a Fourier transform. Different ranges of $Im\,\zeta$ may give different inverse transforms.

A.1.1 The unilateral Fourier transforms

In the Wiener-Hopf procedure not only the bilateral Fourier transform (A.3) is used but also the unilateral Fourier integrals

$$F_+(\zeta) = \frac{1}{\sqrt{2\pi}}\int_0^\infty f(t)e^{i\zeta t}dt\,, \tag{A.6}$$

$$F_-(\zeta) = \frac{1}{\sqrt{2\pi}}\int_{-\infty}^0 f(t)e^{i\zeta t}dt\,. \tag{A.7}$$

We recall here an important property of these functions [71]:

If the function $f(t)e^{-at}$ is absolutely integrable over the positive real axis, then it can be easily shown that the infinite Fourier integral (A.6) is absolutely and uniformly convergent for all values of ζ in the half plane $Im\,\zeta \geq a$. Similar conclusions can be drawn if we assume that the function $f(t)$ is absolutely integrable over any finite subinterval of the positive real axis and is of exponential growth at infinity,

$$f(t) = O(e^{at})\,, \quad t \to \infty\,. \tag{A.8}$$

In this case it can be shown that the unilateral Fourier integral is absolutely and uniformly convergent for all values of ζ in the upper half plane $Im\,\zeta > a$.

In the same manner one can show that the unilateral Fourier integral (A.7) is absolutely integrable and uniformly convergent for all values of ζ in the lower half plane $Im\,\zeta \leq b$ provided that the function $f(t)e^{-bt}$ is absolutely integrable over the negative real axis. Similarly, the supposition that the function $f(t)$ is absolutely integrable over any finite subinterval of the negative real axis and is of exponential type on the negative real axis, then

$$f(t) = O(e^{bt})\,, \quad t \to -\infty\,. \tag{A.9}$$

is sufficient to ensure the absolute and uniform integrability of the function $f(t)e^{i\zeta t}$ over the negative real axis for all values of ζ in the lower half plane $Im\,\zeta < b$.

A.2 Formulas related with the Gamma function

The Gamma function has the well-known representation and property

$$\Gamma(\alpha) = \int_0^\infty f(t)e^{-t}t^{\alpha-1}dt\,, \tag{A.10}$$

$$\Gamma(\alpha+1) = \alpha\Gamma(\alpha)\,. \tag{A.11}$$

$\Gamma(\alpha)$ is an analytic function, regular except when $\alpha = 0, -1, -2, ...$ At these points there are simple poles, the residue at $\alpha = -n$ being $(-1)^n/(n!)$. The following formula can be deduced

$$\mathrm{Res}\,(\,\Gamma(z_1\alpha+z_2)\,,\,\frac{-n-z_2}{z_1}) = (-1)^n/n!\,\frac{1}{z_1}\,. \tag{A.12}$$

We have also

$$\pi\alpha/\sinh\pi\alpha = \Gamma(1-i\alpha)\;\Gamma(1+i\alpha)\,, \tag{A.13}$$

$$\pi/\cosh\pi\alpha = \Gamma(\frac{1}{2}+i\alpha)\;\Gamma(\frac{1}{2}-i\alpha)\,, \tag{A.14}$$

$$\{\Gamma(\alpha)\}^{-1} = \alpha e^{C\alpha}\prod_{n=1}^{\infty}\{1+(\alpha/n)\}e^{-\alpha/n}\,, \tag{A.15}$$

$$\prod_{n=1}^{\infty}\left\{1+\frac{\alpha}{an+b}\right\}e^{-\alpha/an} = e^{C\alpha/a}\Gamma\left(\frac{b}{a}+1\right)/\Gamma\left(\frac{\alpha}{a}+\frac{b}{a}+1\right), \tag{A.16}$$

where $C = 0.5772...$, is the Euler constant.

$$\begin{aligned}\Gamma(\alpha)/\Gamma(2\alpha) &= 2e^{C\alpha}\prod_{n=1}^{\infty}\left\{1+\frac{\alpha}{n-1/2}\right\}e^{-\alpha/(n-1/2)}\\ &= \Gamma\left(\frac{1}{2}\right)e^{\ln 2(1-2\alpha)}/\Gamma(\alpha+1/2)\,.\end{aligned} \tag{A.17}$$

Stirling's formula states that

$$\Gamma(\alpha) \sim e^{-\alpha}\,\alpha^{\alpha-1/2}\,(2\pi)^{1/2}\,\{1+(12\alpha)^{-1}+...\}\;\;\text{as}\;\;\alpha\to\infty\,,\;\;|\arg\alpha|<\pi\,. \tag{A.18}$$

A.3 Specific theorems which we use in the Wiener-Hopf approach

Liouville's theorem. *If $f(\zeta)$ is an integral function (an analytic function which is regular in every finite region of the ζ-plane) such that $|f(\zeta)| \leq M$ for all $\zeta \in \mathcal{C}$, M being a constant, then $f(\zeta)$ is a constant.*

Extended Liouville's theorem. *If $f(\zeta)$ is an integral function such that $|f(\zeta)| \leq M|\zeta|^p$ as $|\zeta| \to \infty$ where M, p are constants, then $f(\zeta)$ is a polynomial of degree less than or equal to $[p]$ where $[p]$ is the integral part of p.*

The infinite product theorem. *If $f(\alpha)$ is an integral function of α with simple zeros at α_1, α_2,..., then we have the following infinite product representation of $f(\alpha)$*

$$f(\alpha) = f(0)e^{\{\alpha\, f'(0)/f(0)\}} \prod_{n=1}^{\infty} \left(1 - \frac{\alpha}{\alpha_n}\right) e^{\alpha/\alpha_n} \,. \tag{A.19}$$

In this form the exponential factors are necessary to ensure convergence, since we can have e.g. $\alpha_n \sim an + b$ as $n \to \infty$ in applications. If $f(\alpha)$ is an even function of α, the roots occur in pairs, $\pm\alpha_n$, and $f'(0) = 0$, so that we can write

$$f(\alpha) = f(0) \prod_{-\infty}^{\infty} \left(1 - \frac{\alpha}{\alpha_n}\right) e^{\alpha/\alpha_n} = f(0)(\prod_{n=1}^{\infty}{}')\left\{1 - \left(\frac{\alpha}{\alpha_n}\right)^2\right\} \,, \tag{A.20}$$

where $\alpha_{-n} = -\alpha_n$ and the dash denotes that the term $n = 0$ is omitted.

As examples of this type we have

$$(\alpha a)^{-1} \sin\, \alpha a \,, \;\; \alpha_n a = n\pi \,, \tag{A.21}$$

$$\cos\, \alpha a \,, \;\; \alpha_n a = (n - 1/2)\pi \,. \tag{A.22}$$

Next consider the decomposition of a function $K(\alpha)$ in the form of a product, $K(\alpha) = K_+(\alpha)K_-(\alpha)$, where K_+ and K_- are regular and non-zero in upper and lower half-planes $\tau > \tau_-$, $\tau < \tau_+$ respectively, where $\tau_- < \tau_+$. Sometimes this decomposition can be guessed. Obviously any decomposition of this type is not unique since we can multiply K_+ by any integral non-zero function providing that we divide K_- by the same factor.

If $K(\alpha)$ is an integral function which can be expressed as an infinite product then the decomposition is immediate. The important case from our point of view occurs when $K(\alpha)$ is an even function of α. Then the roots occur in pairs, say $\alpha = \pm\alpha_n$, and $K'(0) = 0$. From (A.20) we can write

$$K(\alpha) = K(0) \prod_{n=1}^{\infty} \{1 - (\alpha/\alpha_n)^2\} \,. \tag{A.23}$$

This can be decomposed in the form

$$K_{\pm}(\alpha) = K(0)^{1/2} e^{\mp\chi(\alpha)} \prod_{n=1}^{\infty} \{1 \pm (\alpha/\alpha_n)\} e^{\mp(\alpha/\beta_n)} \,, \tag{A.24}$$

where upper and lower signs go together and the terms have been arranged so that all the zeros of $K_+(\alpha)$ ($K_-(\alpha)$) lie in the lower (upper) half-plane. Hence $K_+(\alpha)$ is regular and non-zero in the upper half-plane $(Im\,\alpha) > -(Im\,\alpha_1)$. The function $\chi(\alpha)$ is arbitrary and can be chosen to ensure that K_+, K_- have suitable behaviour as $\alpha \to \infty$ in appropriate half-planes. The infinite product has in general exponential behaviour as $\alpha \to \infty$ whereas the functions which need be decomposed have algebraic behaviour at infinity due to additional terms multiplying the infinite product. These facilitate usually the choice of $\chi(\alpha)$. The correct choice of $\chi(\alpha)$ is crucial for the successful application of the Wiener-Hopf technique.

When the function has a branch point, the infinite product method will break down.

Asymptotic relations between functions and their Fourier transform (Abelian theorem). *If, for* $-1 < \eta \leq 0$

$$f(x) \sim A\,x^{\eta} \,, \quad \textit{when} \quad \left.\begin{array}{c} x \to \pm 0 \\ x \to \infty \end{array}\right\} \,, \tag{A.25}$$

then

$$F_{\pm}(\alpha) \sim A(2\pi)^{-1/2}\Gamma(\eta+1) e^{\frac{1}{2}\pi i(\eta+1)} \alpha^{-\eta-1} \,, \quad \textit{when} \quad \left.\begin{array}{c} \alpha \to \infty \\ \alpha \to \pm 0 \end{array}\right\} \,, \tag{A.26}$$

respectively, where α *tends to zero or infinity along paths in the upper half-plane ,* $(Im\,\alpha) > 0$ *in the case of upper-sign (+) and in the lower half-plane,* $(Im\,\alpha) < 0$ *in the case of lower-sign (−).* F_+ *and* F_- *are the unilateral Fourier transforms of* $f(z)$ *defined in (A.6) and (A.7), respectively.*

Jordan's Lemma. *If* $f(z)$ *is analytic for* $Im\,z \geq 0$ *except at points* $z_1, z_2, ..., z_n$ *with positive imaginary parts, if*

$$\lim_{R\to\infty} \left[\max_{\substack{|z|=R \\ Im\,z \geq 0}} |f(z)| \right] = 0 \,, \tag{A.27}$$

and if $\omega > 0$*, then*

$$\lim_{R\to\infty} \int_{-R}^{R} f(x) e^{i\omega x} dx = 2\pi i \sum_{l=1}^{n} Res(f(z)e^{i\omega z}, z_l) \,. \tag{A.28}$$

Similarly we have for the lower half plane: if $f(z)$ is analytic for $Im\, z \leq 0$ except at points $z'_1, z'_2, ..., z'_n$ with negative imaginary parts, if

$$\lim_{R\to\infty} \left[\max_{\substack{|z|=R \\ Im\, z\leq 0}} |f(z)| \right] = 0 \,, \tag{A.29}$$

and if $\omega < 0$, then

$$\lim_{R\to\infty} \int_{-R}^{R} f(x) e^{i\omega x} dx = -2\pi i \sum_{l=1}^{n} Res(f(z)e^{i\omega z}, z'_l) \,. \tag{A.30}$$

Appendix B

Why to consider a bounded domain in the x_2-direction?

Here we give an explanation by presenting the difficulties encountered when we tried to solve analytically the problem treated in Chapter 3 but with an infinite domain in the x_2-direction. Let us consider the anti-symmetric problem in the upper-half plane unbounded in x_2-direction. Instead of (3.18)-(3.23) we have

$$\nabla^2\varphi^a = 0 \quad \text{in} \quad -\infty < x_1 < \infty, \quad 0 \le x_2 \le \infty\,, \tag{B.1}$$

with the boundary conditions

$$\varphi^a\,(x_1, h) = V, \quad x_1 \ge 0\,, \tag{B.2}$$
$$\varphi^a\,(x_1, 0) = 0, \quad -\infty < x_1 < \infty\,, \tag{B.3}$$
$$\varphi^a_{,1}\,(x_1,\, h^+) = \varphi^a_{,1}\,(x_1,\, h^-), \quad x_1 \le 0\,, \tag{B.4}$$
$$\varphi^a_{,2}\,(x_1,\, h^-) = c\,\varphi^a_{,2}\,(x_1,\, h^+), \quad x_1 \le 0\,, \tag{B.5}$$
$$\lim_{x_2\to\infty} \varphi^a(x_1, x_2) = 0, \quad -\infty < x_1 < \infty\,. \tag{B.6}$$

We mention that the approach we employ below does not depend on the type of configuration (our explanation is valid also for the symmetric and the non-symmetric cases). We drop in what follows the upper index "a". If we apply the Fourier transform (3.49) in x_1 to equation (B.1) we find an ordinary differential equation

$$d^2\Phi(\alpha, x_2)/dx_2^2 - \alpha^2\Phi(\alpha, x_2) = 0 \quad \text{in} \quad -\infty < \alpha < \infty, \quad 0 \le x_2 < \infty\,. \tag{B.7}$$

which has the solution

$$\Phi(\alpha, x_2) = \begin{cases} A_1(\alpha)\, e^{-\gamma x_2} + B_1(\alpha)\, e^{\gamma x_2}\,, & 0 \le x_2 \le h\,, \\ A_2(\alpha)\, e^{-\gamma x_2} + B_2(\alpha)\, e^{\gamma x_2}\,, & h \le x_2 < \infty\,. \end{cases} \tag{B.8}$$

where $\gamma = \sqrt{\alpha^2}$. A difficulty arises since γ is a multi-valued function of α. Which branch of the function $\sqrt{\alpha^2}$ should be chosen so that (B.8) represents a solution of (B.7) which

can be inverted to give $\varphi(x_1, x_2)$? In order to apply the Wiener-Hopf method we should implicitly assume that for any x_2, Φ exists in a strip $\tau_- < \tau < \tau_+$, $-\infty < \sigma < \infty$ of the α-plane ($\alpha = \sigma + i\tau$) and that $\Phi(\alpha, x_2)$ is bounded as $x_2 \to \infty$ for all α in this strip. Related to this, the sign of $Re\gamma$ is a critical quantity. For instance, if we choose $\sqrt{\alpha^2} = \alpha$ or $\sqrt{\alpha^2} = -\alpha$, then the boundedness restriction of Φ as $x_2 \to \infty$ applied to (B.8) yields $A_2 = B_2 = 0$.

It seems that this problem is difficult in this point just because we deal with the Laplace equation. Usually the Wiener-Hopf technique is applied to solve problems connected with the steady-state wave equation

$$\frac{\partial^2 \varphi}{\partial x_1^2} + \frac{\partial^2 \varphi}{\partial x_2^2} + k^2 \varphi = 0\,, \tag{B.9}$$

where k^2 has a positive imaginary part, when damping is present. The solution of this equation after the Fourier transformation looks exactly as (B.8), the only difference being the form of the function $\gamma = \sqrt{\alpha^2 + k^2}$. Now, $\gamma(\alpha)$ can be interpreted in such a way that it has a domain of analyticity for $-Im\,k < \tau < Im\,k$, in which, $Re\,\gamma > 0$. Then it is easy to see from (B.8) that the boundedness of Φ when $y \to \infty$ yields $B_2(\alpha) = 0$ (see [54]). However, $k = 0$ cannot be considered as a particular case of this problem because then, the domain of analyticity collapses to zero. That is why one way to solve the Laplace equation is to consider it as a limiting case of the Helmholtz equation (B.9), for which we apply the Wiener-Hopf technique and then let $k \to 0$ in the final solution but we found this way too difficult for our problem.

There is another possibility (for which we made our choice) suggested by Carrier [19]. First it should be realized from (B.8) that only one branch of the multi-valued function $\sqrt{\alpha^2}$ can be chosen which can lead to a solution of the problem (in order to avoid the trivial coefficient pair $A_2 = B_2 = 0$)

$$\sqrt{\alpha^2} = \begin{cases} \alpha\,, & Re\,\alpha > 0\,, \\ -\alpha\,, & Re\,\alpha < 0\,. \end{cases} \tag{B.10}$$

Unfortunately, there is no horizontal strip (not even a horizontal line) in the α-plane on which this interpretation of the $\sqrt{\alpha^2}$ function is analytic. In order to avoid this difficulty, a parameter can be introduced. Using a similar idea as in [19, p. 380] we can write

$$\sqrt{\alpha^2} = \lim_{\delta \to 0,\, \delta > 0} \sqrt{\alpha^2 + \delta^2}\,. \tag{B.11}$$

We take $\gamma = \sqrt{\alpha^2 + \delta^2} = \sqrt{\alpha^2 - (i\delta)^2}$ and we defer the limiting process until we obtain the solution of the problem. If the branch of the function $\gamma = \sqrt{\alpha^2 + \delta^2}$ is so chosen such that $\gamma \to \sigma$ as $\alpha = \sigma \to +\infty$, where the α-plane is cut by two straight lines from $-i\delta$ to $-\infty$ in the lower half-plane and from $i\delta$ to $+\infty$ in the upper half-plane respectively, then γ is regular for $-\delta < \tau < \delta$ [54, p. 10, 29]. We have also, $\gamma = \delta$ when $\alpha = 0$ and $\gamma \to |\sigma|$ when $\alpha = \sigma \to -\infty$. From these considerations, from the assumptions before

(3.71) about the function $\varphi(x-1, x-2)$ and since the limiting process for δ will be done before the limiting process for ε (so we consider $0 < \delta < \varepsilon$), we will choose $\tau_- = -\delta$ and $\tau_+ = 0$. Taking into account that $Re\gamma > 0$ for $\tau_- < \tau < \tau_+$ [54, ex. 1.3, p. 39], solution (B.8) becomes

$$\phi(\alpha, y) = \begin{cases} A_1(\alpha)\, e^{-\gamma x_2} + B_1(\alpha)\, e^{\gamma x_2}\,, & 0 \le x_2 < h\,, \\ A_2(\alpha)\, e^{-\gamma x_2}\,, & h \le x_2 < \infty\,, \end{cases} \tag{B.12}$$

where $\gamma = \sqrt{\alpha^2 + \delta^2}$. The Fourier boundary conditions are

$$\Phi_+(\alpha, h^+) = \Phi_+(\alpha, h^-) = \Phi_0\,, \tag{B.13}$$
$$\Phi_-(\alpha, h^+) = \Phi_-(\alpha, h^-)\,, \tag{B.14}$$
$$(\Phi_-)'(\alpha, h^-) = c\,(\Phi_-)'(\alpha, h^+)\,, \tag{B.15}$$
$$\lim_{x_2 \to \infty} \Phi_-(\alpha, x_2) = \lim_{x_2 \to \infty} \Phi_+(\alpha, x_2) = 0\,, \tag{B.16}$$
$$\Phi_+(\alpha, 0) = \Phi_-(\alpha, 0) = 0\,, \tag{B.17}$$

where $\Phi_+(\alpha, x_2)$, $\Phi_-(\alpha, x_2)$ and Φ_0 are given in (3.55)-(3.57).

Writing (B.12) on the boundaries yields

$$\phi_+(\alpha, h^+) + \phi_-(\alpha, h^+) = A_2(\alpha)\, e^{-\gamma h}\,, \tag{B.18}$$
$$\phi_+(\alpha, h^-) + \phi_-(\alpha, h^-) = A_1(\alpha)\, e^{-\gamma h} + B_1(\alpha)\, e^{\gamma h}\,, \tag{B.19}$$
$$\phi_+(\alpha, 0) + \phi_-(\alpha, 0) = A_1(\alpha) + B_1(\alpha)\,, \tag{B.20}$$

$$\phi'_+(\alpha, h^+) + \phi'_-(\alpha, h^+) = -\gamma\, A_2(\alpha)\, e^{-\gamma h}\,, \tag{B.21}$$
$$\phi'_+(\alpha, h^-) + \phi'_-(\alpha, h^-) = -\gamma\, A_1(\alpha)\, e^{-\gamma h} + \gamma\, B_1(\alpha)\, e^{\gamma h}\,, \tag{B.22}$$
$$\phi'_+(\alpha, 0) + \phi'_-(\alpha, 0) = -\gamma\, A_1(\alpha) + \gamma\, B_1(\alpha)\,. \tag{B.23}$$

From now on, the α-argument of the functions will be dropped.

Substituting (B.13), (B.14) and (B.17) in (B.18)-(B.20) we obtain first

$$A_2 = A_1(1 - e^{2\gamma h}) = -B_1(1 - e^{2\gamma h})\,. \tag{B.24}$$

Consequently, (B.12) becomes

$$\phi(\alpha, x_2) = \begin{cases} -2A_1\, \sinh(\gamma x_2)\,, & 0 \le x_2 < h\,, \\ -2A_1\, \sinh(\gamma h)\, e^{\gamma(h - x_2)}\,, & h \le x_2 < \infty\,. \end{cases} \tag{B.25}$$

Using (B.24) in (B.18)-(B.23) we have also the following relations from which we intend to obtain equations of Wiener-Hopf type

$$\Phi_0 + \phi_-(h) = -2A_1\, \sinh(\gamma h)\,, \tag{B.26}$$
$$\phi'_+(h^+) + \phi'_-(h^+) = 2\gamma\, A_1\, \sinh(\gamma h)\,, \tag{B.27}$$
$$\phi'_+(h^-) + c\phi'_-(h^+) = -2\gamma\, A_1\, \cosh(\gamma h)\,, \tag{B.28}$$
$$\phi'_+(0) + \phi'_-(0) = -2\gamma\, A_1\,. \tag{B.29}$$

We multiply (B.27) by c and subtract it from (B.28). Let us denote $F_+ = c\phi'_+(h^+) - \phi'_+(h^-)$ and $F_- = \Phi_-(\alpha, h)$. If we eliminate A_1 between the original equation and (B.26) we finally obtain

$$F_+ = -\gamma\,[\,c + \coth(\gamma h)\,]\,F_- - \gamma\,\Phi_0\,[\,c + \coth(\gamma h)\,]\,, \tag{B.30}$$

where $\gamma = \sqrt{\alpha^2 + \delta^2}$. For the particular case $c = 0$, this equation becomes much simpler but $c = 0$ has no physical sense.

(B.30) can be written as a Wiener-Hopf equation

$$K(\alpha)F_+(\alpha) + F_-(\alpha) = -\Phi_0(\alpha)\,, \tag{B.31}$$

where

$$K(\alpha) = \frac{1}{\sqrt{\alpha^2+\delta^2}\;\left[\,c + \coth\left(\sqrt{\alpha^2+\delta^2}\,h\right)\,\right]}\,, \tag{B.32}$$

where $F_+(\alpha)$, $\Phi_0(\alpha)$ are regular for $\tau > \tau_-$, $F_-(\alpha)$ is regular for $\tau < \tau_+$ and $K(\alpha)$ is regular for $\tau_- < \tau < \tau_+$.

Unfortunately we didn't succeed to derive a correct factorization of $K(\alpha)$, namely to derive two functions $K_-(\alpha)$ regular for $\tau < \tau_+$ and $K_+(\alpha)$ regular for $\tau > \tau_-$ so that $K(\alpha) = K_-(\alpha)/K_+(\alpha)$. We tried to apply the following procedure: first we derived an appropriate form of $K(\alpha)$ for its factorization,

$$K(\alpha) = \frac{h}{\dfrac{\gamma h}{\sinh(\gamma h)}\;\left[\,c\,\sinh(\gamma h) + \cosh(\gamma h)\,\right]}\,. \tag{B.33}$$

For $c \neq 1$ we calculated

$$\begin{aligned}
&\frac{1}{c\,\sinh(\gamma h) + \cosh(\gamma h)} = \frac{2e^{\gamma h}}{e^{2\gamma h}(c+1) + 1 - c} \\
&= \frac{2e^{\gamma h}}{(1-c)\left[\,e^{2(\gamma h + c_1)} + 1\right]} = \frac{1}{(1-c)\,e^{c_1}\,\dfrac{e^{2(\gamma h + c_1)} + 1}{2e^{\gamma h + c_1}}} \\
&= \frac{1}{e^{c_1}(1-c)\,\cosh(\gamma h + c_1)}\,,
\end{aligned} \tag{B.34}$$

where $c_1 = \dfrac{1}{2}\,\ln\dfrac{c+1}{1-c}$ is a positive constant and we wrote $K(\alpha)$ in the form

$$K(\alpha) = \frac{h}{c_2}\,\frac{\sinh(\gamma h)\,(\gamma h)^{-1}}{\cosh(\gamma h + c_1)}\,, \tag{B.35}$$

where $c_2 = e^{c_1}(1-c)$.

To factorize the function K in the general case ($c \neq 1$) seems to be quite complicated. The function $L(\alpha) := \sinh(\gamma h)(\gamma h)^{-1}$ can be factorized using the infinite product theorem for an even function (see Appendix A.3). However this is not valid for the function $H(\alpha) := \cosh(\gamma h + c_1)$ because H is not an analytic function. To be precise, it has branch points due to the presence of γ (in some points, where the branch cuts are chosen, γ can have two values which differ from each other only by the sign). The expression γ enters also in L but L is even in γ and in those branch points of γ, L has one unique value.

When $c = 1$ the factorization can be done using some results from [54] but $\varepsilon_1 = \varepsilon_2$ is only a particular case from the physical point of view.

By taking a bounded domain in the x_2 direction we are no longer restricted by the boundedness requirement of Φ in the choice of the branch of the function γ. By choosing the branch $\gamma = \alpha$ we could solve successfully the problem formulated in Chapter 3.

Appendix C

Zeros of the denominators of the W-H kernels

C.1 Zeros of the denominators are purely imaginary

We shall prove here that if α is the solution of the equation (which is the denominator of (3.74))

$$(c+1)\cosh(\alpha H)+(c-1)\cosh(\alpha H-2\alpha h)=0\,, \tag{C.1}$$

then α is a pure imaginary number. The real counterparts of equation (C.1) are

$$\begin{cases} \cos(\tau H)\cosh(\sigma H)=c_1\,\cos(\tau G)\sinh(\sigma G)\,, \\ \\ \sin(\tau H)\sinh(\sigma H)=c_1\,\sin(\tau G)\sinh(\sigma G)\,. \end{cases} \tag{C.2}$$

where $c_1=\dfrac{1-c}{1+c}$, $|c_1|<1$, $G=H-2h<H$, $\sigma=Re\,\alpha$ and $\tau=Im\,\alpha$. It is obvious that the system (C.2) is even in σ and τ so it is sufficient to prove the result in $[0,\infty)\times[0,\infty)$.

Case 1. Let us suppose $\sigma>0$ and τ is so that neither $\cos(\tau G)$ nor $\cos(\tau H)$, $\sin(\tau G)$, $\sin(\tau H)$ vanish. Then we can write from (C.2)

$$\frac{\cosh(\sigma G)}{\cosh(\sigma H)}=\frac{1}{c_1}\,\frac{\cos(\tau H)}{\cos(\tau G)}\,,\quad \frac{\sinh(\sigma G)}{\sinh(\sigma H)}=\frac{1}{c_1}\,\frac{\sin(\tau H)}{\sin(\tau G)}\,. \tag{C.3}$$

Taking into account that the hyperbolic sine and the hyperbolic cosine functions are positive increasing functions for positive arguments, we may write

$$0<\frac{1}{c_1}\,\frac{\cos(\tau H)}{\cos(\tau G)}<1\,,\quad 0<\frac{1}{c_1}\,\frac{\sin(\tau H)}{\sin(\tau G)}<1\,. \tag{C.4}$$

Let us denote for simplicity by $a:=\cos(\tau H)$, $b:=\cos(\tau G)$. If we square now the previous inequations system, we obtain

$$0<\frac{1}{c_1^2}\,\frac{a^2}{b^2}<1\,,\quad 0<\frac{1}{c_1^2}\,\frac{1-a^2}{1-b^2}<1\,. \tag{C.5}$$

Since $|a| < 1$ and $|b| < 1$, (C.5) yields $c_1^2 > 1$ that contradicts the hypothesis $|c_1| < 1$. So, in this case no solution is possible.

Case 2. We suppose $\sigma > 0$ and that one of $\cos(\tau G)$, $\cos(\tau H)$, $\sin(\tau G)$, or $\sin(\tau H)$ vanishes. It is easy to remark from (C.2) that

$$\cos(\tau G) = 0 \iff \cos(\tau H) = 0\,, \tag{C.6}$$

$$\sin(\tau G) = 0 \iff \sin(\tau H) = 0\,. \tag{C.7}$$

If (C.6) holds then (C.2) becomes

$$\pm \sinh(\sigma H) = \pm c_1 \sinh(\sigma G)\,. \tag{C.8}$$

Since $\sinh x > 0$, $\forall x > 0$, the only possibility of a valid equation (C.8) is

$$\sinh(\sigma H) = |c_1| \sinh(\sigma G)\,. \tag{C.9}$$

However, sinh is an increasing function for positive arguments and since $G < H$ and $|c_1| < 1$, we have $\sinh(\sigma H) > \sinh(\sigma G) > |c_1| \sinh(\sigma G)$. Consequently, no solution is possible. If (C.7) holds then (C.2) becomes

$$\pm \cosh(\sigma H) = \pm c_1 \cosh(\sigma G)\,. \tag{C.10}$$

and with the same arguments we obtain that no solution is possible, either. From Case 1. and Case 2. it is obvious that σ must vanish. Then (C.1) reduces to the following equation

$$\cos(\tau H) = c_1 \cos(\tau G)\,. \tag{C.11}$$

One can demonstrate analogously that the equation corresponding to the denominator of (3.75)

$$(c+1)\sinh(\alpha H) + (1-c)\sinh(\alpha H - 2\alpha h) = 0\,, \tag{C.12}$$

has also only pure imaginary solutions and so, it reduces to

$$\sin(\tau H) = -c_1 \sin(\tau G)\,. \tag{C.13}$$

C.2 Localization of the zeros

In this Section a convenient form of the solution of (3.76) and (3.77) (or (C.11), (C.13), respectively) will be derived. We remark again that these equations are even in τ and we describe first the solutions in the positive domain. Since the sine and cosine functions are periodic, we expect that these solutions are periodic, too. In order to investigate this, we write from (C.11)

$$\cos(\tau H + 2m\pi) = c_1 \cos(\tau G + 2s\pi) \tag{C.14}$$

$$\Leftrightarrow \cos(\tau + \frac{2m\pi}{H})H = c_1 \cos(\tau G + \frac{2s\pi}{G})G\,, \tag{C.15}$$

where m, s are positive integers. If τ is a solution of (C.11) then $\tau' := \tau + \dfrac{2m\pi}{H} = \tau + \dfrac{2s\pi}{G}$ is a new solution of (C.11) provided that

$$\frac{m}{H} = \frac{s}{G}\,. \tag{C.16}$$

Writing $\dfrac{H}{G} = \dfrac{p}{q}$, where p, q are positive integers, $(p, q) = 1$, leads to

$$m = n\,p\,, \quad s = n\,q\,, \tag{C.17}$$

for $n = 1, 2, 3, ...$ So if τ is a solution of (C.11), then substituting (C.17) into (C.16) and then in τ' we find that $\tau + \dfrac{2np\pi}{H}$ is also a solution of (C.11). Since $\tau = 0$ is a solution of (C.11), we obtain that the principal interval of solution except 0 is $(0, 2p\pi/H]$. All these considerations hold also for (C.13).

We need to know how many roots of (C.11) and (C.13) exist in this interval. Let us denote by $f(\tau) = \cos(\tau H) - c_1 \cos(\tau G)$ and $g(\tau) = \sin(\tau H) + c_1 \sin(\tau G)$. First we remark that

$$\operatorname{sign}\left[f\left((l-1)\pi/H\right)\right] = (-1)^{l-1}\,, \tag{C.18}$$

$$\operatorname{sign}\left[g\left((2l-1)\pi/(2H)\right)\right] = (-1)^{l-1}\,, \tag{C.19}$$

for $l = 1, 2, 3, ...$ By use of Darboux' theorem it follows that f has at least one zero in each interval $((l-1)\pi/H, (l+1)\pi/H)$ and g has at least one zero in each interval $((2l-1)\pi/(2H), (2l+1)\pi/(2H))$. Consequently, the minimum number of the solutions of the equations (C.11) and (C.13) in the interval $(0, 2\pi/H]$ is $2p$. To prove that this is the exact number of the solutions one has to write (C.11) and (C.13) in the complex form. Using the formula $\cos x = (e^{ix} + e^{-ix})/2$ and denoting in (C.11)

$$z := e^{i\tau H/p}\,, \tag{C.20}$$

yield a polynomial equation of degree $2p$ in the variable z. The fundamental theorem of algebra states that over the complexes such an equation has as many roots (counting multiplicity) as the degree. Consequently (C.20) has $2p$ solutions. One can easily see that for each of these $2p$ values of z there is a unique τ in $(0, 2\pi p/H]$ that fulfills equation (C.20). In an analogous manner, one can demonstrate that (C.13) has no more than $2p$ solutions in $(0, 2\pi p/H]$, too. We note that 0 and $2\pi p/H$ are also solutions of (C.13).

Now we can write the complete solutions of (3.76) and (3.77) as $\tau = \pm\delta_{nl} = \pm(\delta_l + 2p\pi(n-1)/H)$ and $\tau = 0, \tau = \pm\gamma_{nl} = \pm(\gamma_l + 2p\pi(n-1)/H)$, respectively, $l = 1, 2, ... 2p$, $n = 1, 2, 3...$, where δ_l and γ_l are the solutions of these equations in the interval $(0, 2\pi p/H]$ and $(l-1)\pi/H < \delta_l < (l+1)\pi/H$, $(2l-1)\pi/(2H) < \gamma_l < (2l+1)\pi/(2H)$.

Appendix D

Pressure drop vs. volumetric flow rate - analytical formulas

Here we give analytical formulas for the pressure gradient vs. volumetric flow rate for Casson-like (4.31)-(4.32) and power-law fluids (4.29)-(4.30) flowing in a channel configuration with infinite electrodes (see Section 2.2.1). These formulas may be used to evaluate approximately the pressure drop in configurations with long finite electrodes when neglecting the end effects. Namely, on the electrode-free part of the channel walls, the pressure drop is calculated by applying the formula for a vanishing electric field while on the part where the electrodes are placed, the pressure drop is calculated by applying the formula for a constant electric field, where the value of the electric field is chosen to be the value established in the homogeneous region, in the middle of the electrodes, far from the electrode edges. The volumetric flow rate is given by

$$Q = \int_0^b \int_{-h}^{h} v_1(x_2) dx_2 dx_3 = b \int_{-h}^{h} v_1(x_2) dx_2 \,, \tag{D.1}$$

where b is the width of the channel.

D.1 The Casson-like model

From [28] we have the following formula that relates the pressure gradient $k = p_{,1}$ with the volumetric flow rate Q

$$\begin{aligned} Q = \frac{b}{120\,\eta_0^4 k^2} \{ & 40\sqrt{2}\,\eta_0\beta_1\beta_2^4 + 80\sqrt{2}\,\eta_0\beta_1^3 - 4\sqrt{2}\,\beta_2^6 - 30\sqrt{2}\,k^2(2h)^2\eta_0^3\beta_1 k^2 \\ & -120\sqrt{2}\,\eta_0^2\beta_1^2\beta_2^2 + 15\sqrt{2}\,k^2(2h)^2\eta_0^2\beta_2^2 + 10\,k^3(2h)^3\eta_0^3 - 2^{11/4} kh\sqrt{Z_1}\eta_0\beta_2^3 \\ & -12\,2^{1/4}\,k^2(2h)^2\sqrt{Z_1}\eta_0^2\beta_2 + 2^{10/4}\,kh\sqrt{Z_1}\eta_0^2\beta_1\beta_2 + 2^{9/4}\,\sqrt{Z_1}\beta_2^5 \\ & -2^{21/4}\,\sqrt{Z_1}\eta_0\beta_1\beta_2^3 + 2^{25/4}\,\sqrt{Z_1}\eta_0^2\beta_1^2\beta_2 \} \,, \end{aligned} \tag{D.2}$$

where $Z_1 := \sqrt{2}\,\beta_2^2 + 4\,kh\eta_0 - 4\sqrt{2}\,\eta_0\beta_1$. Equation (D.2) yields the volumetric flow rate of a Newtonian fluid, a Bingham fluid and a Casson fluid for $\beta_1 = \beta_2 = 0$, $\beta_2 = 0$ and $\beta_2 = 2\sqrt{\eta_0\beta_1}$, respectively. The pressure gradient for a vanishing electric field (when $\beta_1 = \beta_2 = 0$) is

$$k = 3Q/(2b\eta_0 h^3)\,, \tag{D.3}$$

and

$$Q = 4/3hbv_0\,, \tag{D.4}$$

where $v_0 = v_2(0)$ is the maximum velocity in the channel. Since we use Q as an input value in our procedure and we want to calculate the pressure drop as output, we have to invert formula (D.2) in order to obtain the pressure gradient for non-vanishing values of the electric fields. Analytically, this is not possible but using the software MATHEMATICA [91] we may obtain k as a function of the volumetric flow rate Q and of the uniform electric field E_u (for the definition of E_u, see Section 5.1.5). The pressure drop measured from $x_1 = -30$ on a distance of 60 mm for the configuration used in experiments (see Section 5.1.5) may be calculated approximately as

$$\Delta p = 3Q\eta_0/(2bh^3)\,(0.06 - 2l) + 2l\,k(Q, E_u)\,. \tag{D.5}$$

The non-dimensional pressure drop may be obtained easily as $\tilde{\Delta p} = \Delta p/p_0$, where $p_0 = \eta_0 v_0/h$ is defined in Subsection 4.3.1. We have

$$\Delta\tilde{p} = 2(0.06 - 2l)/h + 2lh\,k(Q, E_u)/(\eta_0 v_0)\,. \tag{D.6}$$

D.2 The power-law model

If we solve the problem (2.86)-(2.92) for a power-law fluid (4.29)-(4.30) we obtain (assuming $c_2 = 0$, $k < 0$) the following velocity field

$$v_1(x_2) = \frac{k_1 n}{n+1}(h^{(n+1)/n} - |x_2|^{(n+1)/n})\,, \tag{D.7}$$

where $k_1 = \left(\frac{-k}{m}\right)^{1/n}$. Now, calculating the volumetric flow rate yields

$$Q = \frac{2(n+1)}{2n+1}\,v_0 hb\,, \tag{D.8}$$

where

$$v_0 = v_1(0) = \frac{k_1 n}{n+1}\,h^{(n+1)/n}\,, \tag{D.9}$$

is the maximum velocity in the channel. Inverting this formula we obtain

$$k = -\left(\frac{Q(2+1/n)}{hb}\right)^n \frac{m}{h}\,. \tag{D.10}$$

The electrorheological effect (5.11) measured from $x_1 = -30$ on a distance of 60 mm for the configuration used in experiments (see Section 5.2.4) may be calculated approximately as

$$F_{\Delta p} = \frac{2l(k - k_0)}{0.06k_0}\,, \tag{D.11}$$

where

$$k_0 = \left(\frac{Q(2 + 1/n_0)}{hb}\right)^{n_0} \frac{m_0}{h}\,, \tag{D.12}$$

is the pressure gradient in the vanishing electric field.

Appendix E

Notation

Throughout the whole text the Einstein's summation convention on repeated indices is used.

$()_{,i}$ is used to abbreviate the partial derivative of the quantity $()$ with respect to x_i, i.e. $\frac{\partial()}{\partial x_i}$. If $()$ has one argument only then $()'$ and $()''$ denote the first order derivative of $()$ and the second order derivative of $()$, respectively.

$\frac{D()}{Dt}$ denotes the material derivative of the quantity $()$ which is defined by

$$\frac{D()}{Dt} := \frac{\partial()}{\partial t} + v_j \frac{\partial()}{\partial x_j} = \frac{\partial()}{\partial t} + v_j()_{,j} \, , \tag{E.1}$$

where v_j denotes the components of the velocity fields.

$\overset{*}{()}$ denotes the convective derivative which for a vector V_i is defined by

$$\overset{*}{V_i} = \frac{DV_i}{Dt} - v_{i,j}V_j + v_{j,j}V_i \, . \tag{E.2}$$

$\bigtriangledown^2$ denotes the Laplace operator.

In expressions like $f(\pm c^{\pm})$ the upper index "+" indicates the limit of the function f as x, the argument of f, tends to $\pm c$ from positive values of $(x \mp c)$ and the upper index "$-$" indicates the limit of f as x tends to $\pm c$ from negative values of $(x \mp c)$.

$\mathrm{Res}(f, z_0)$ denotes the residue of the function f in the point z_0 (see [89] for the definition of the residue).

We use the notation $f(x) = O(g(x))$ when x tends to some given limit, if the absolute value of the ratio $f(x)/g(x)$ is bounded by some given positive constant when x tends to its limit and we say that $f(x)$ is at most of the order of $g(x)$. If the ratio of the two functions $f(x)$ and $g(x)$ tends to unity when x tends to some given limit we write $f(x) \sim g(x)$ and we say that the functions $f(x)$ and $g(x)$ are asymptotically equivalent in the neighborhood of the limit point.

The symbol $\otimes$ denotes the outer (dyadic) product of two vectors which is a 2-tensor; if u, v are two vectors in $\mathbb{R}^3$ we have $(u \otimes v)_{ij} = u_i v_j$.

The second invariant of a 2-tensor A is denoted by $|A|$ i.e. $|A| := \sqrt{A_{ij}A_{ji}}$.

Bibliography

[1] M. Abramowitz and I. A. Stegun (eds.), *Handbook of Mathematical Functions*. New York: Dover Publications, Inc. (1965) 1046 pp. 30, 48, 111

[2] B. Abu-Jdayil and P. O. Brunn, Effects of nonuniform electric field on slit flow of an electrorheological fluid. *J. Rheol.* 39 (1995) 1327–1341. 14, 16

[3] B. Abu-Jdayil and P. O. Brunn, Effects of electrode morphology on the slit flow of an electrorheological fluid. *J. Non-Newtonian Fluid Mech.* 63 (1996) 45–61. 28

[4] B. Abu-Jdayil, *Electrorheological Fluids in Rotational Couette Flow, Slit Flow and Torsional Flow (Clutch)*. Aachen: Shaker Verlag, (1996) 137 pp. 16, 60, 64, 69, 73, 100

[5] B. Abu-Jdayil and P. O. Brunn, Study of the flow behaviour of electrorheological fluids at shear- and flow-mode. *Chem. Eng. and Process.* 36 (1997) 281–289. 28

[6] B. Abu-Jdayil and P. O. Brunn, Effects of coating on the behaviour of electrorheological fluids in torsional flow. *Smart Mater. and Struct.* 6(5) (1997) 509–520.

[7] B. Abu-Jdayil and P. O. Brunn, Effect of electrode morphology on the behaviour of electrorheological fluids in torsional flow. *J. Intel. Mat. Syst. Struct.* 13(1) (2002) 3–11. 14, 16

[8] H. Asoud, *Messugen von elektrorheologischen Flüssigkeiten in einem Flachkanal mit glatten, schrägen und geriffelten Elektroden.* Diplomarbeit, Univ. Erlangen-Nürenberg, Erlangen, (1999). 87

[9] R. J. Atkin, X. Shi and W. A. Bullough, Solutions of the constitutive equations for the flow of an electrorheological fluid in radial configurations. *J. Rheol.* 35(7) (1991) 1441–1461. 13, 15

[10] R. J. Atkin, X. Shi and W. A. Bullough, Effect of non-uniform field distribution on steady flows of an electro-rheological fluid. *J. Non-Newtonian Fluid Mech.* 86 (1999) 119–132. 13, 15

[11] H. A. Barnes and K. Walters, The yield stress myth?. *Rheol. Acta*, 24(4) (1985) 323–326. 66

[12] H. A. Barnes, The yield stress – a review or '$\pi\alpha\nu\tau\alpha$ $\rho\varepsilon\iota$' – everything flows?. *J. Non-Newtonian Fluid Mech.*, 81 (1999) 133–178. 65

[13] Bayer AG, *Sicherheitsdatenblatt*. Leverkusen, 6(1994). 73

[14] H. Block and J. P. Kelly, Electro-rheology. *J. Phys. D: Appl. Phys.* 21 (1988) 1661–1677. 12

[15] P. O. Brunn and B. Abu-Jdayil, Fluids with transverse isotropy as models for electrorheological fluids. *Z. angew. Math. Mech.* 78(2) (1998) 97–107. 13, 14

[16] P. O. Brunn and B. Abu-Jdayil, A phenomenological model of electrorheological fluids. *Rheol. Acta* 43 (2004) 62–67. 13

[17] V. Busuioc and D. Cioranescu, On the flow of a Bingham fluid passing through an electric field. *Int. J. Non-Linear Mech.*, 38 (2003) 287–304. 13, 63

[18] T. Butz and O. von Stryk, Modeling and Simulation of Electro- and magnetorheological Fluid Dampers. *Z. angew. Math. Mech.*, 82(1) (2002) 3–20. 14

[19] G. F. Carrier, M. Krook and C. E. Pearson, *Functions of a Complex Variable*. New York: McGraw-Hill (1966) 438 pp. 36, 118

[20] R. V. Churchill, *Complex Variables and Applications*. New York: McGraw-Hill (1960) 297 pp. 30

[21] Comsol AB, *Femlab*. Version 2.3.0.148 (2002). 53, 71

[22] CONDEA Chemie GmbH, *Sicherheitsdatenblatt*. Hamburg, 12(1996). 87

[23] C. R. Daubert, J. F. Steffe and A. K. Srivastava, Predicting the electrorheological behaviour of milk chocolate. *J. Food Process Eng.*, 21(3) (1998) 249–261. 13

[24] Y. F. Deinega and G. V. Vinogradov, Electric-fields in the rheology of disperse systems. *Rheol. Acta*, 23(6) (1984) 636–651. 12

[25] L. Diening, Maximal function on generaized Lebesgue spaces L-p(center dot). *Math. Inequal. Appl.*, 7(2) (2004) 245–253. 13

[26] R. Drouot, G. Napoli and G. Racineux, Continuum modeling of electrorheological fluids. *Int. J. of Modern Phys. B*, 16(17&18) (2002) 2649–2654. 13

[27] K. Edamura and Y. Otsubo, Electrorheology of dielectric liquids. *Rheol. Acta*, 43 (2004) 180–183. 13

[28] W. Eckart, Phenomenological modeling of electrorheological fluids with an extended CASSON-Model. *Continuum Mech. Thermodyn.*, 12(5) (2000) 341–362. 5, 7, 13, 15, 17, 22, 24, 28, 59, 60, 61, 62, 64, 69, 73, 127

[29] W. Eckart, *Theoretische Untersuchungen von elektrorheologischen Flüssigkeiten bei homogenen und inhomogenen elektrischen Feldern.* Aachen: Shaker Verlag (2000) 162 pp. 5, 7, 17, 20, 22, 23, 51, 73, 85

[30] W. Eckart and A. Sadiki, Polar theory for electrorheological fluids based on extended thermodynamics. *Int. J. of Applied Mechanics and Engineering*, 6(4) (2001) 969–998. 13

[31] B. Engelmann, R. Hiptmair, R. H. W. Hoppe and G. Mazurkevitch, Numerical simulation of electrorheological fluids based on an extended Bingham model. *Comput. Visual Sci.*, 2 (2000) 211–219. 13, 63

[32] D. Garg and G. Anderson, Structural Damping and Vibration Control via Smart Sensors and Actuators. *J. Vib. Control*, 9 (2003) 1421–1452. 14

[33] R. Hanaoka, M. Murakumo, H. Anzai and K. Sakurai, Effects of electrode surface morphology on electrical response of electrorheological fluids. *IEEE Trans. Dielect. Electr. In.* 9(1) (2002) 10–16. 14

[34] T. Hao, A. Kawai and F. Ikazaki, Dielectric Criteria for the Electrorheological Effect. *Langmuir*, 15 (1999) 918–921. 11

[35] T. Hao, Electrorheological fluids. *Adv. Mater.*, 13(24) (2001) 1847–1857. 11, 12, 14

[36] P. Hild, I. R. Ionescu, Th. Lachand-Robert and I. Rosca, The blocking of an inhomogeneous Bingham fluid. Applications to landslides. *M2AN*, 36(6) (2002) 1013–1026. 68

[37] Z. Huang and J. H. Spurk, Der elektroviskose Effekt als Folge elektrostatischer Kraft. *Rheol. Acta*, 29 (1990) 475–481. 13

[38] K. Hutter and A. A. F. van de Ven, *Field Matter Interactions in Thermoelastic Solids.* Berlin, Heidelberg: Springer Verlag, (1978) 231 pp. 17, 19, 20, 22

[39] K. Hutter, Time-dependent surface elevation of an ice slope. *J. Glaciology*, 25 (1980) 247–266. 68

[40] K. Hutter, The effect of longitudinal strain on the shear stress of an ice sheet. In defence of using stretched coordinates. *J. Glaciology*, 27 (1981) 39–66. 68

[41] K. Hutter, F. Legerer and U. Spring, First order stresses and deformations in glaciers and ice sheets. *J. Glaciology*, 27 (1981) 227–270. 68

[42] A. Inoue and S. Maniwa, Electrorheological effect of liquid crystalline polymers. *J. Appl. Polym. Sci.* 55 (1995) 113–118. 13

[43] P. Katsikopoulos and C. Zukoski, Effects of electrode morphology on the electrorheological response. *in Proceedings of the 4th Conference on Electrorheological Fluids* edited by R. Tao, World Scientific, Singapore, 1994. 14

[44] H. Kimura, K. Aikawa, Y. Masubuchi, J. Takimoto, K. Koyama and K. Minagawa, Phase structure change and ER-effect in liquid crystalline polymer/dimethylsiloxane blends. *Rheol. Acta* 37 (1998) 54–60. 13

[45] H. Kimura, K. Aikawa, Y. Masubuchi, J. Takimoto, K. Koyama and T. Uemura, 'Positive' and 'negative' electro-rheological effect of liquid blends. *J. Non-Newtonian Fluid Mech.* 76 (1998) 199–211. 13

[46] D. Klass and Th. Martinek, Electroviscous fluids. I. Rheological Properties. *J. Appl. Phys.* 38(1) (1967) 67–74. 12

[47] D. Klass and Th. Martinek, Electroviscous fluids. II. Electrical Properties. *J. Appl. Phys.* 38(1) (1967) 75–80. 12

[48] D. Klein, D. Rensink, H. Freimuth, G. J. Monkman, S. Egersdörfer, H. Böse and M. Baumann, Modeling the response of a tactile array using electrorheological fluids. *J. Phys. D: Appl. Phys.* 37 (2004) 794–803. 14

[49] C. Mavroidis, Y. Bar-Cohen and M. Bouzit, Haptic Interfaces Using Electrorheologica Fluids. In *Electroactive Polymer Actuators as Artificial Muscles: reality, potentials and challenges* SPIE Optical Engineering press (2001) 567–594. 14

[50] C. Mavroidis, Development of Advanced Actuators Using Shape Memory Alloys and Electrorheological Fluids. *Res. Nondestr. Eval.* 14 (2002) 1–32. 14

[51] G. J. Monkman, Addition of solid structures to electrorheological fluids. *J. Rheol.* 35 (1991) 1385–1392. 14

[52] N. Mellgren, *A combined viscoelastic plastic material in an oscillating pressure-driven plane channel flow.* Diplomarbeit, Technische Universität Darmstadt, 2002. 66

[53] I. Müller, *Thermodynamics.* Pitman Publishing, (1985) 521 pp. 21, 22

[54] B. Noble, *Methods Based on the Wiener-Hopf Technique for the Solution of Partial Differential Equations.* Oxford: Pergamon Press (1958) 246 pp. 30, 36, 111, 118, 119, 121

[55] Y. Otsubo, Effect of Electrode Pattern on the Column Structure and Yield Stress of Electrorheological Fluids. *J. Colloid Interface Sci.* 190 (1997) 466–471. 14

[56] Y. Otsubo and K. Edamura, Viscoelasticity of a dielectric fluid in nonuniform electric fields generated by electrodes with flocked fabrics. *Rheol. Acta*, 37 (1998) 500–507. 13

[57] Y. Otsubo and K. Edamura, Electric effect on the rehology of insulating oils in electrodes with flocked fabrics. *Rheol. Acta*, 38 (1999) 137–144. 13

[58] T. C. Papanastasiou, Flows of Materials with Yield. *J. Rheol.* 31(5) (1987) 385–404. 66

[59] M. Parthasarathy and D. J. Klingenberg, Electrorheology: Mechanisms and Models. *Mater. Sci. Eng.* 17 (1996) 57–103. 12, 60, 64

[60] J. Perlak and B. Vernescu, Constitutive equations for electrorheological fluids. *Rev. Roumaine Math. Pures Appl.* 45 (2000) 287–297. 13

[61] Ch. Pfeiffer, C. Mavroidis, Y. Bar-Cohen and B. Dolgin, Electrorheological Fluid Based Force Feedback Device. In *Proceedings of the 1999 SPIE Telemanipulator and Telepresence technologies VI Conference* SPIE Proc. 3840 (1999) 19–21. 14

[62] D. Pirck, *Homogene elektroviskose Flüssigkeiten.* Deutsches Patent, DE 41 39 065 A1 (1993). 87

[63] Y. Qi and W. Wen, Influence of geometry of particles on electrorheological fluids. *J. Phys. D: Appl. Phys.*, 35 (2002) 2231–2235. 12

[64] K. R. Rajagopal and A. S. Wineman, Flow of electro-rheological materials. *Acta Mechanica* 91 (1992) 57–75. 13, 57

[65] K. R. Rajagopal, R. C. Yalamanchili and A. S. Wineman, Modeling electro-rheological materials through mixture theory. *Int. J. Engng. Sci.*, 32(3) (1994) 481–500. 13

[66] K. R. Rajagopal and M. Růžička, Mathematical modeling of electrorheological materials. *Continuum Mech. Thermodyn.*, 13(1) (2001) 59–78. 13, 15, 58, 59, 60, 62

[67] L. Rejon, Electrorheological characterisation of suspensions of surface-modified ceramic hollow-sphere particles. *Oral presentation at Eurorheo 2002 Stuttgart.* 12

[68] E. J. Rhee, M. K. Park, R. Yamane and S. Oshima, A study on the relation between flow characteristics and cluster formation of electrorheological fluid using visualization. *Exp. in Fluids* 34 (2003) 316–323. 28, 64

[69] P. Riha, H. Kimura, K. Aikawa, Y. Masubuchi, J. Takimoto and K. Koyama, The shear-flow properties of electro-rheological liquid polymeric blends. *J. Non-Newtonian Fluid mech.* 85 (1999) 249–256. 13

[70] M. Růžička, *Electrorheological Fluids: Modeling and Mathematical Theory.* Berlin: Springer (2000) 176 pp. 13, 59

[71] B. W. Roos, *Analytic Functions and Distributions in Physics and Engineering.* New York: Wiley, (1969) 521 pp. 30, 36, 111, 112

[72] A. Sadiki and C. Balan, Rate-type Model for electro-rheological Material Behaviour consistent with Extended Thermodynamics: Application to a steady viscometric flow. *Proc. Appl. Math. Mech.* 2 (2003) 174–175. 13

[73] H. See, H. Tamura and M. Doi, The role of water capillary forces in electrorheological fluids. *J. Phys. D: Appl. Phys.* 26 (1993) 746–752. 12

[74] H. See, Advances in modeling the mechanisms and rheology of electrorheological fluids. *Korea-Australia Rheology J.* 11(3) (1999) 169–195. 12

[75] H. See, Constitutive equation for electrorheological fluids based on the chain model. *J. Phys. D: Appl. Phys.* 33 (2000) 1625–1633. 13

[76] U. Schindler, J. Schindler, R. Steger and P. O. Brunn, Optical studies (LDA) of an electrorheological fluid in slit flow. *Rheol. Acta* 34 (1995) 80–85. 11, 28

[77] N. D. Sims, R. Stanway, D. J. Peel, W. A. Bullough and A. R. Johnson, Controllable viscous damping: an experimental study of an electrorheological long-stroke damper under proportional feedback control. *Smart Mater. Struct.* 8 (1999) 601–615. 14

[78] A. J. M. Spencer, *Theory of Invariants.* Academic Press. Continuum Mechanics (A.C. Eringen, ed.), Vol.1. (1971) 57

[79] J. H. Spurk, *Fluid Mechanics.* Berlin, Heidelberg: Springer Verlag, (1997) 513 pp. 64

[80] J. E. Stangroom, Electrorheological fluids. *Phys. Technol.* 14 (1983) 290–296. 12

[81] J. E. Stangroom, Basic considerations in flowing electrorheological fluids. *J. Stat. Phys.* 64(5-6) (1991) 1059–1072. 12

[82] R. Stanway, J. L. Spronston and A. K. El-Wahed, Applications of electro-rheological fluids in vibration control: a survey. *Smart Mater. Struct.* 5 (1996) 464–482. 14, 15, 64, 66

[83] W. Y. Tam, G. Yi, W. Wen, H. Ma, M. M. T. Loy and P. Sheng, New Electrorheological Fluid: Theory and Experiment. *Phys. Rev. Lett.* 78 (1998) 2987–2990. 12

[84] H. Tamura, H. See and M. Doi, Model of porous particles containing water in electrorheological fluids. *J. Phys. D: Appl. Phys.* 26(8) (1993) 1181–1187. 12

[85] T. Tsukiji and S. Tanabe, ER effect of liquid crystal flowing between two parallel-plate electrodes. *Int. J. Mod. Phys. B* 16 (2002) 2569–2575. 13

[86] A. Ursescu, W. Eckart, H. Marschall and K. Hutter, Inhomogeneous electric field generated by two long electrodes placed along parallel infinite walls separating different dielectric media. *J. Engrg. Math.* 49 (2004) 57–75.

[87] B. Vernescu, Multiscale Analysis of Electrorheological Fluids. *Int. J. Mod. Phys. B* 16(17&18) (2002) 2643–2648. 13, 60

[88] B. Wang and Z. Xiao, A general constitutive equation of an ER suspension based on the internal variable theory. *Acta Mechanica* 163 (2003) 99–120. 13

[89] H. F. Weinberger, *A First Course in Partial Differential Equations*. New York: Dover Publications, Inc. (1995) 446 pp. 30, 44, 111, 131

[90] W. Winslow, Induced fibration of suspensions. *J. Appl. Phys.* 20 (1949) 1137–1140. 12

[91] Wolfram Research, Inc., *Mathematica*. Version 4.1.2.0 (2000). 40, 128

[92] Th. Wunderlich, *Der Einfluss der Elektrodenoberfläche und der Strömungsform auf den elektrorheologischen Effekt*. PhD thesis, Universität Erlangen-Nürnberg (2000) 160 pp. 14, 16, 60, 64, 69, 85, 87, 89, 93, 100

[93] Th. Wunderlich and P. O. Brunn, Pressure drop measurements inside a flat channel – with flush mounted and protruding electrodes of variable length – using an electrorheological fluid. *Exp. in Fluids* 28 (2000) 455–461. 14, 28, 60, 64, 73

[94] I. K. Yang and A. D Shine, Electrorheology of a nematic poly(n-hexyl isocyanate)solution. *J. Rheol.* 36(6) (1992) 1079–1104. 13

[95] H. Zhao, Z. Liu and Y. Liu, Mechanical properties of a new electrorheological fluid. *Solid State Commun.* 116 (2000) 321–325. 12

[96] X. Zhao and D. Gao, Structure evolution in Poiseuille flow of electrorheological fluids. *J. Phys. D: Apl. Phys.* 34 (2001) 2926–2931. 13

[97] X. Zhao, X. Y. Gao and D. J. Gao, Evolution of chain structure of electrorheological fluids in flow model. *Int. J. Mod. Phys. B* 16(17&18) (2002) 2697–2703. 13

Curriculum Vitae

Personal Data

Name:	Ana Ursescu
Address:	Hügelstr. 21, 64283, Darmstadt, Germany
Date and place of birth:	13.09.1975, Câmpina, Romania
Marital status:	Married since 26.12.2002, one child
Citizenship:	Romanian

Schools and Universities

Ph. D. student since 1 July 2001:	Department of Mechanics Darmstadt University of Technology, Germany
Diploma of Master Studies, 2000:	Department of Mathematics University of Bucharest, Romania (in Mathematics, Specialization: Fluid Mechanics and Solid Mechanics)
Bachelor's degree, 1998:	Department of Mathematics University of Bucharest, Romania (in Mathematics-Mechanics)
High School, 1994:	"N. Grigorescu" High School, Câmpina, Romania
Primary and Secondary School, 1990:	"I. Câmpineanu" School, Câmpina, Romania

Professional experience

Socrates fellowship 04/1999-06/1999:	Mathematics Department University of Ioaninna, Greece
assistant researcher 10/2000-to present:	Institute for Mathematical Statistics and Applied Mathematics Department of Applied Mathematics "Caius Iacob" Romanian Academy
visitor researcher 03/2001-04/2001:	Mathematics Department University of Ioaninna, Greece
PhD fellowship 07/2001-09/2004:	Graduiertenkolleg "Modellierung und numerische Beschreibung technischer Strömungen" der TU Darmstadt, Germany